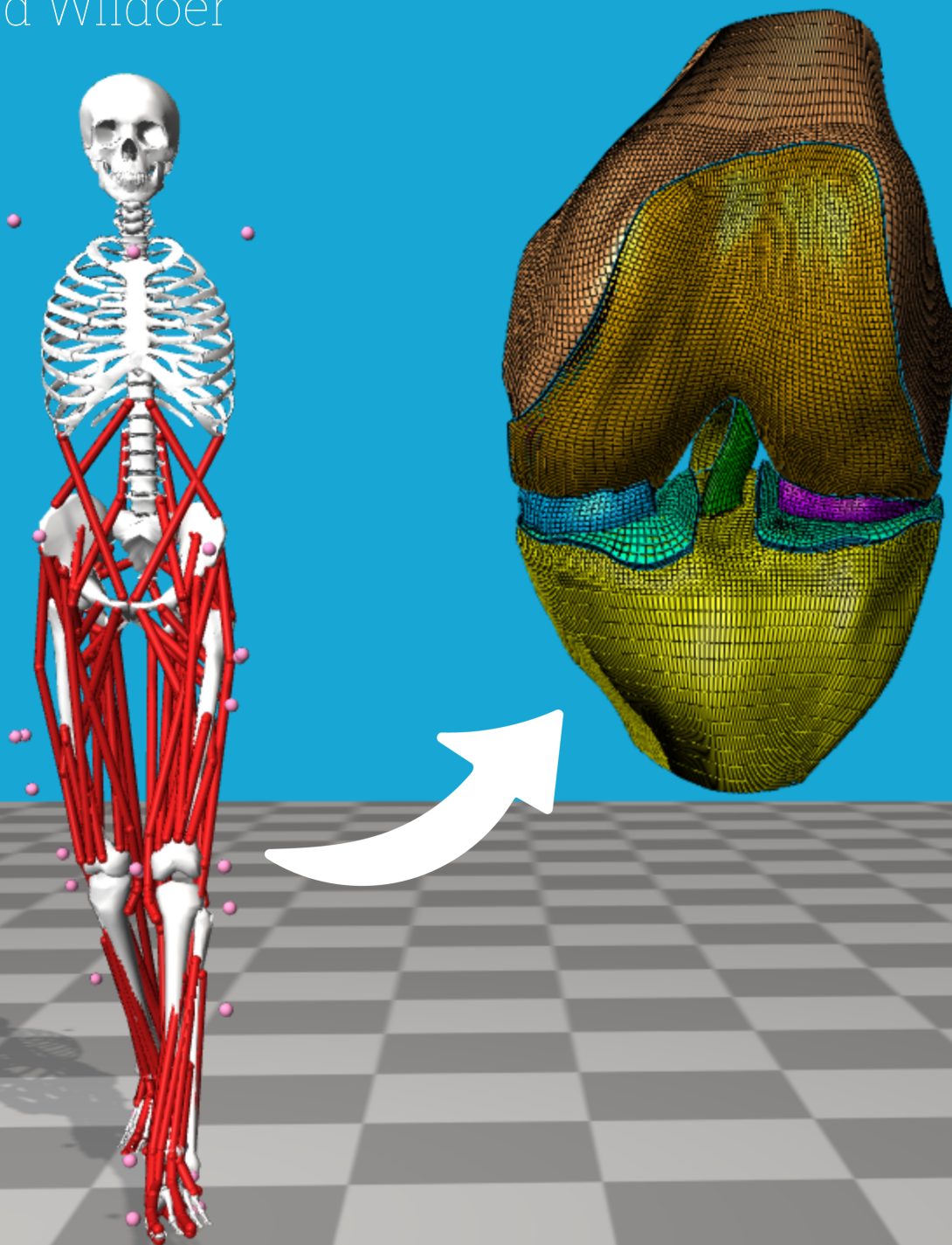


Sensitivity of a coupled modelling workflow to knee marker displacement

BM51035 BME Msc Thesis

David Wildöer



Sensitivity of a coupled modelling workflow to knee marker displacement

Determining the sensitivity of a
coupled modelling workflow to
variations in marker data retrieved
from gait analysis

by

David Wildöer

A thesis submitted to the Delft University of Technology in partial fulfillment of the requirements for the degree of Master of Science in BioMedical Engineering.

Thesis committee: Prof.dr.ir.J.Harlaar
N.Tümer
Dr.A.Seth
Institution: Delft University of Technology
Place: Faculty of Mechanical, Maritime and Materials Engineering (3ME)
Project Duration: March, 2022 - December, 2022

Preface

In March 2018 I tore the ACL of my left knee during a rugby match. I had never thought that a sport accident would have such an influence on my mental condition but also my future study career. Being stuck to your bed for weeks gives you a lot of time to think. At the time I had almost finished my bachelor in Technical Policy analysis and Management. However, I slowly realised, I was looking for another challenge.

I was looking for a challenge where I could combine my interest in health and the human body but also do more technical problem solving. Once I knew this, the decision to do a master in Biomedical engineering was made relatively quickly. I must say it was quite a turn around switching to a mechanical engineering master. It is interesting to see how four years later I have almost finished a graduation project on the knee joint, the same joint which was the instigator for my study switch.

This journey would have never been a success without the help of others. I would like to express my gratitude specifically to Mariska Wesseling for your guidance and daily supervision. You were always able to make time for me. Your directions and thorough feedback enabled me to ask the right questions and progress when I was stuck. When you were about to go on maternity leave you provided me with the right handles to continue my project. Additionally, I want to thank Nazli Tümer for your feedback during our biweekly meetings. Your pragmatic approach to problem solving helped me to make the right decisions when I was in doubt what to do. I would also like to acknowledge prof. Jaap Harlaar, although my presentations during your progress meetings were a bit brief. The meetings were a great moment to discuss with other peers and your feedback helped to relativize my situation. After the meetings I always had extra energy to continue working.

Finally, I would like to express my gratitude to my family and friends for your level-headedness and confidence that things would work out in the end. Eva, this thesis would be much less clear if it weren't for our english grammar sessions. Marlieke, thank you for your optimism and motivating me everyday. Lastly, Mam, Throughout my 7 years as a student your weekly calls and support were the thing that helped me out the most both personally and on study matters. Thank you!

*David Wildöer
Delft, December 2022*

Abstract

To better understand and predict osteoarthritis, researchers are developing so-called coupled modelling workflows. Coupled workflows convert data from gait analysis studies to subject-specific tissue mechanical response estimations through the use of musculoskeletal and finite element models. The tissue mechanical response inside the joint is thought to play an integral role in the onset and progression of osteoarthritis. To study this, the design of coupled workflow was proposed. This design contained subject-specific gait data which was processed by a musculoskeletal model with a single degree of freedom knee joint. Musculoskeletal output was transferred through an adjusted generic finite element model of the knee to calculate maximum principal stress and shear strain values in the tibial cartilage of the knee. Proper marker placement is crucial for making an accurate assessment of the patient's function in gait analysis studies. It has been claimed that marker misplacement is the main cause of measurement variability in gait analysis studies. It however remains unclear how potential marker misplacement propagates to the coupled modelling workflow results. To investigate this, in addition to the design of a coupled workflow, a sensitivity analysis was performed. With this sensitivity analysis we tried to answer the following question: *How does marker placement of knee joint markers in gait analysis influence the tissue mechanical response calculated by a coupled workflow?* For the sensitivity analysis, knee joint marker placements were virtually perturbed along anterior-posterior, proximal-distal and medial-lateral direction, to mimic marker misplacement. Corresponding knee biomechanics were estimated from the perturbed input data in the coupled workflow. Peak maximum principal stress values varied by up to 0.60MPa and peak shear strain varied by up to 0.08% as a result of perturbed knee marker placement. For cumulative stress levels, broader relative ranges were found. Moreover, the results showed that marker placement along the anterior-posterior direction had the greatest influence on corresponding tissue mechanical response estimations. In future studies a standard error of measurement margin is proposed in the assessment of coupled modelling workflow results. In conclusion, the proposed workflow was relatively easy to build and provided similar tissue mechanical response result to those as reported by more complex models which were more computationally intensive. This implies that in the future, coupled modelling processes may very well be incorporated into the clinical decision-making process for musculoskeletal disorders like osteoarthritis.

Contents

Preface	i
Abstract	ii
Nomenclature	v
1 Introduction	1
2 Research question	3
3 Methods	4
3.1 Data acquisition	5
3.2 Musculoskeletal model	6
3.2.1 OpenSim tools	7
3.3 Finite element model	10
3.3.1 Geometry	10
3.3.2 Contact	11
3.3.3 Boundary & loading conditions	12
3.3.4 Steps	14
3.4 The workflow	15
3.4.1 The workflow: OpenSim	15
3.4.2 The workflow: FEBio	16
3.4.3 Computer specifications and computational time	16
3.5 Post-processing of models' outcomes	17
3.5.1 Tissue mechanical response analysis	17
3.5.2 Statistics	17
4 Results	18
4.1 Influence of marker placement on MSM output	19
4.1.1 Comparison of MSM output	19
4.1.2 L.Knee marker placement	21
4.1.3 L.KneeMed marker placement	22
4.1.4 L.KneeFib marker placement	23
4.2 Influence of marker placements on FEM knee kinematics	24
4.2.1 Comparison of FEM knee kinematics	24
4.2.2 L.Knee marker	25
4.2.3 L.KneeMed marker	26
4.2.4 L.KneeFib marker	26
4.3 Influence of marker placements on tissue mechanical response	28
4.3.1 Comparison of stress/strain magnitude	28
4.3.2 Comparison of stress/strain accumulation	29
4.3.3 L.Knee marker	30
4.3.4 L.KneeMed marker	31
4.3.5 L.KneeFib marker	32
4.4 Influence of marker placements on regions of high tissue mechanical response	34
5 Discussion	36
5.1 Results interpretation	36
5.1.1 How does knee marker location influence musculoskeletal modelling results in a coupled workflow?	36
5.1.2 How does knee marker placement influence the finite element FEM knee kinematics in a coupled workflow?	37

5.1.3	How does knee marker placement influence the magnitude of the tissue mechanical response in the articular cartilage of the knee joint?	39
5.1.4	How does knee marker placement influence the location of the tissue mechanical response in the articular cartilage of the knee joint?	40
5.2	Limitations and recommendations for future research	41
5.2.1	Data acquisition	41
5.2.2	Musculoskeletal modelling	41
5.2.3	Finite element modelling	41
5.2.4	The workflow	42
5.3	How does this study move the field forward?	43
6	Conclusion	44
	References	45
A	BMM Lab Protocol	51
B	OpenSim Tools	53
C	Ligament insertion location	55
D	FEM supplementary material	58
E	Workflow supplementary material	60
F	Results supplementary material	62

Nomenclature

Abbreviations

Abbreviation	Definition
OA	Osteoarthritis
MSM	Musculoskeletal model
FEM	Finite element model
PF	Patellofemoral
TF	Tibiofemoral
PG	Proteoglycan
BMM	BioMechaMotion
DoF	Degree of freedom
IK	Inverse kinematics
SO	Static optimization
JRA	Joint reaction analysis
OK	OpenKnee
FE	Finite element
MCL	Medial collateral ligament
LCL	Lateral collateral ligament

1

Introduction

The number of people suffering from musculoskeletal disorders is increasing. From birth to old age, musculoskeletal disorders are relevant across all ages. Musculoskeletal disorders range from acute, transient diseases such as fractures, sprains, and strains, which cause pain and functional restrictions to chronic conditions like persistent lower back pain and osteoarthritis (OA) [1]. OA is a degenerative joint disease, in which cartilage degenerates as a result of wear and tear in the joint. It is the most prevalent musculoskeletal condition with over 100 million people worldwide suffering from the disease [2]. Age, sex, genetics, but also mechanical loading of a joint, have major roles in the onset and progression of musculoskeletal disorders like OA. Being weight-bearing joints, the knee, ankle and hip joint endure significant mechanical loading over the course of a person's life. Studies suggest that the progression of OA is associated with hyperphysiologic magnitudes of loading, and/or by the alteration of the normal loading pattern in the joint. Consequently, OA often develops in the knee, ankle or hip as a result of trauma, obesity, or overuse [3, 4]. Research on OA is especially important in the knee joint, as instability is a commonplace symptom in knee OA, with 72% of patients with knee OA reporting knee instability. Patients describe the instability as a sensation of buckling or giving away, causing them to lose confidence in their body which negatively influences a patient's quality of life [5, 6, 7, 8, 9]. Accurate knowledge of the mechanical loading of cartilage inside the knee during gait is required to properly understand the onset and progression of OA and develop therapeutic or preventative treatments [10]. Recent developments in instrumented knee implants have enabled the direct measurement of knee loads during daily activities [11, 12]. However, it is still not possible to non-invasively measure the tissue mechanical response of an intact knee during gait [13]. For that reason biocomputational models are used to estimate joint mechanics [13].

Biocomputational models use mathematics, physics, and computer science to enable researchers to simulate human biomechanics with the use of a computer. Musculoskeletal models (MSMs) allow for the modelling of human biomechanics. In a clinical setting, MSMs are part of gait analysis studies to assess the functioning of patients with motor disorders [14]. In practice, experimental motion is captured by applying reflective markers to the anatomical landmarks of a patient. During gait analysis the patient is asked to walk across an instrumented walkway equipped with force plates. During the analysis, reflective marker motion is captured with strategically placed cameras and external forces are measured using force plates. Afterwards, MSMs are used to estimate joint kinematics, kinetics, muscle forces, and joint contact forces. MSMs are able to estimate these outputs using user defined objective functions. This enables researchers to come up with modelling results which closely approximate a subject's biomechanics during gait [13, 15, 16, 17].

A biocomputational modelling method incorporated to analyse tissue biomechanics at cartilage level is finite element modelling. A finite element model (FEM) of the knee may include bony and soft tissue components of the patellofemoral (PF) and tibiofemoral (TF) aspects of the knee joint. These can be modelled with components with complex material properties to represent bone, ligaments, knee muscles, cartilage, and menisci. FEMs enable researchers to simulate the interaction of the components of the knee during daily activity and determine the tissue mechanical response estimates like stress and

strain. The interaction between the different knee components all contribute to the tissue mechanical response [18]. In FEM, gait analysis and MSM results can be applied as input in the form of boundary and loading conditions, to simulation knee motion during gait. These results include joint kinematics, muscle force, ligament forces, and joint contact forces. Research has shown that these factors play an essential role in the pathogenesis of OA [19, 20, 21, 22, 23]. Therefore, for full understanding of OA, information from both modelling techniques is required.

Here coupled workflows come into play. In coupled workflows joint kinematics and joint contact forces are estimated from gait analysis data using MSMs. This information is used to construct subject-specific boundary and loading conditions for a FEM. The FEM in turn calculates the corresponding subject-specific tissue mechanical response. The main objective of coupled workflows is to aid the clinical decision-making process. Coupled workflows are created to help clinicians predict the possible development of musculoskeletal disorders like OA.

Research suggests that altered joint biomechanics after injury and excessive stresses and strains experienced by articular cartilage are the main contributors to the development of OA [24, 25, 26]. Studies have linked high tensile stresses to collagen matrix degeneration of collagen fibrils, while high shear strains of the cartilage nonfibrillar matrix were linked to proteoglycan (PG) loss [27, 28, 29, 30]. In assessing the potential development of OA, a coupled workflow can be used to simulate the subject's knee biomechanics. Thus, the data arising from gait analysis needs to be reliable, and correctly simulate a person's motion during gait. The measurement system, skin movement artefacts, and marker placement have proven to be the main causes for variability in results in gait analysis studies [31, 32, 33, 34]. Of those factors marker placement has been identified as one of the largest sources of variability in gait analysis studies. Of all marker placements, knee marker placement is especially important as these markers are connecting the thigh and the shank segment in MSMs [35, 36]. Due to this characteristic knee markers have the potential to influence joint kinematics, kinetics, muscle forces and joint contact forces of the hip, ankle and most importantly the knee joint. [37, 14, 38].

Coupled workflows are still an emerging modelling technique. Thorough research on the mechanisms influencing coupled workflows is required for the method to be incorporated in the clinical decision making process. Until now research has mostly covered the material models and geometries adopted in the FEMs used for coupled workflows. These studies suggested that FEMs with simple material models and geometries are well able to estimate the proper tissue mechanical response and identify areas susceptible to the development of musculoskeletal disorders like OA [17, 39, 40]. To understand the influence that misplacement of knee markers has on the validity and reproducibility of the coupled workflow results, it is important to conduct a sensitivity analysis, as the uncertainty in marker placement can directly impact the classification of a subject's potential movement disorder. Sensitivity analyses have been performed on the impact of knee marker misplacement on MSM modelling outputs [14, 37, 41]. However, these results have not yet been integrated in research on coupled workflows. Such an analysis can offer important information on the impact of marker placement on the corresponding tissue mechanical response calculated by a coupled workflow. This information provides valuable insight into the possible error in model outcome due to marker misplacement and the confidence in general coupled workflow results. This has profound impact on the standardization of coupled workflows and the potential clinical decision making process.

2

Research question

To investigate the sensitivity of the coupled workflow to possible knee marker misplacements during gait analysis studies, a research question has been formulated:

How does marker placement of knee joint markers in gait analysis influence the tissue mechanical response calculated by a coupled workflow?

In order to organize this research study and, more significantly, to clarify the influence marker placement has on the elements that make up the coupled workflow, the research topic is separated into several sub-questions.

1. How does knee marker placement influence musculoskeletal modelling results in a coupled workflow?
2. How does knee marker placement influence the finite element model knee kinematics in a coupled workflow?
3. How does knee marker placement influence the magnitude of the tissue mechanical response in the articular cartilage of the knee joint?
4. How does knee marker placement influence the location of the tissue mechanical response in the articular cartilage of the knee joint?

3

Methods

To understand the influence of knee marker placement on the tissue mechanical response calculated in the cartilage of the knee joint, a sensitivity analysis was performed. A sensitivity analysis can give valuable insight into the possible error propagation in tissue mechanical response estimates which result from incorrect marker placement. This has important implications on reproducibility and the standardization of coupled modelling procedures. To answer the research question, the Monte-Carlo simulation method was used. The Monte-Carlo method offers a strategy for measuring the impact of a wide range of values of a particular independent variable on a specified dependent variable, without being familiar with the underlying mechanisms. It is important to note that the Monte-Carlo method can be used to measure the effects of changing multiple independent variables. Using a Latin Hypercube sampling method knee marker placements were altered. Altered marker locations will consequently change MSM output and influence the tissue mechanical response calculated by the FEM of the coupled modelling workflow. [42]. The sensitivity analysis will focus on the stance phase of gait as this period in the gait cycle induces the greatest loads on the cartilage of the knee and is therefore thought to be the main contributor in the progression of OA [43]. The following section will describe the components of the methods chronologically, as they were used during workflow setup and analysis. In the figure below, a general overview of the coupled modelling workflow developed for the simulations can be found.

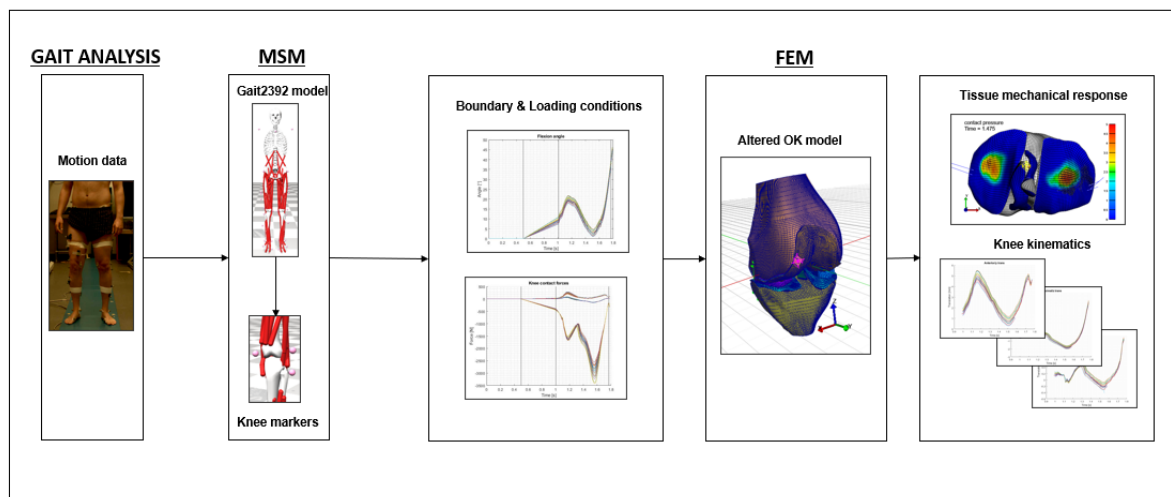


Figure 3.1: An overview of the coupled modelling workflow developed to investigate the influence of marker placement on tissue mechanical response in the knee joint, for a more detailed visualisation of the marker displacements see appendix E.

3.1. Data acquisition

Motion data was gathered from a single healthy subject (male, age: 27, height: 180cm, body mass: 80.5 kg), in the BioMechaMotion (BMM) laboratory at the faculty of Mechanical, Maritime and Materials Engineering (3mE) at the Delft University of Technology. Informed consent was obtained from the subject prior to the experiment. The subject was equipped with 40 reflective markers (\varnothing :12mm), on the anatomical landmarks of the foot, tibia, knee, femur, pelvis and torso on both the left and the right side (see Appendix A table A.2 and figure A.1).

BMM laboratory protocol was followed to ensure compatibility of the results. The protocol consisted of a static pose trial and a dynamic walking trial of 10 and 25 seconds respectively. During the static pose trial the subject was asked to stand in the anatomical position and step to the right with both legs onto an instrumented walkway. The static pose trial served as calibration of the marker model for all body segments, to facilitate marker tracking during the subsequent dynamic walking trial [44]. During the dynamic walking trial the subject was asked to walk across a seven meter long instrumented walkway which was equipped with four force plates to measure the ground reaction forces during gait. The force plates were positioned so that the forces of both the left and right leg could be measured for two consecutive steps. The subject's starting position was five meters in front of the force plates. The subject was asked to walk up and down the runway at a self-selected pace for 25 seconds with normal foot positioning. If each foot did not touch one force plate the trial was repeated until a dynamic walking trial was measured in which each foot of the right and left leg landed on a subsequent force plate during walking.

During the experiment, motion data was recorded using twelve Oqus 700 motion capture cameras at 100 Hz (Qualisys, Gothenburg, Sweden). Ground reaction forces were recorded at 1000 Hz using four Kistler type 9260AA force plates (Kistler, Winterthur, Switzerland) See figure 3.2 for visualisation of experimental setup. Both marker motion and force plate data were filtered using a Butterworth low-pass filter at 6Hz and 25Hz respectively. Retrospectively ground reaction force data was additionally edited in MATLAB (MATLAB and Statistics Toolbox Release 2020b, The MathWorks, Inc., Natick, Massachusetts, United States) by excluding forces which had an axial force component lower than 20 Newtons, to account for possible noise and measurement inaccuracies in the force plates [45]. The orientation of the motion data marker files were transformed using Mokka (Mokka, Biomechanical ToolKit (BTK), Arnaud Barré, 2011-2013) to meet the coordinate system of the musculoskeletal modelling software [46]. A total of three dynamic walking trials were performed of which one trial with the least interference and noise was used as input for the musculoskeletal modelling software.

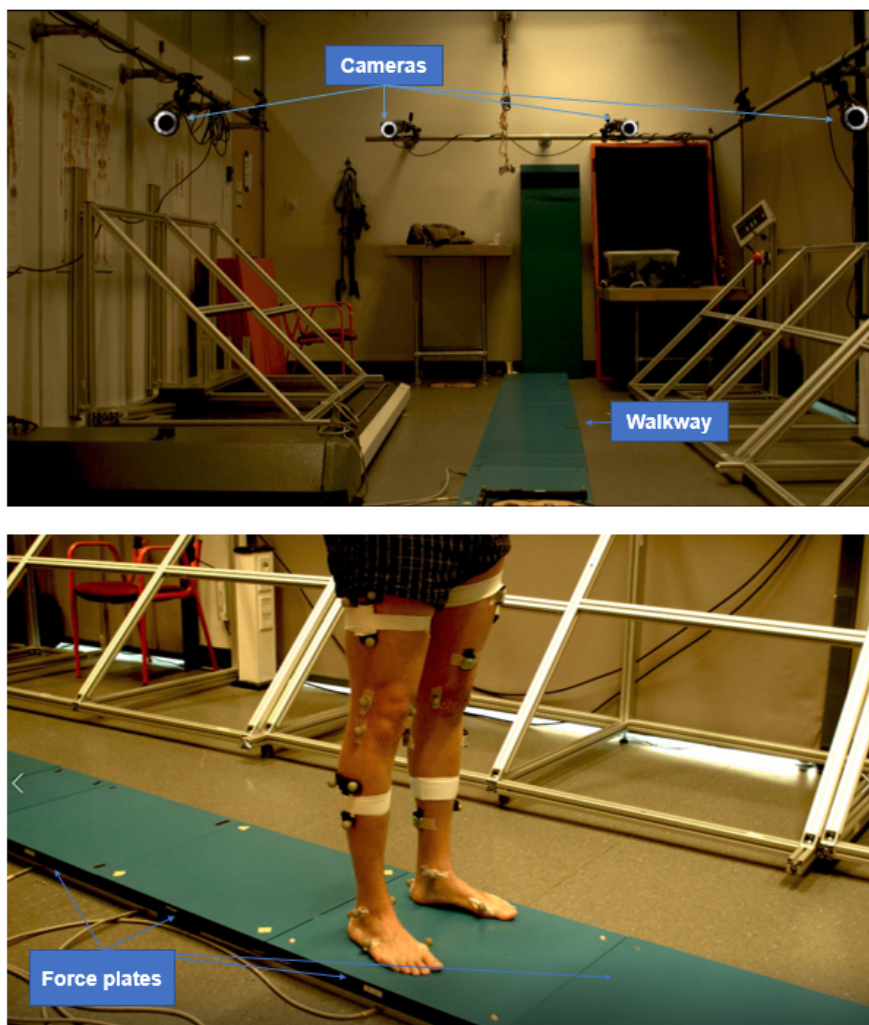


Figure 3.2: An overview of the experimental setup in the BioMechaMotion Laboratory at the TU Delft.

3.2. Musculoskeletal model

OpenSim 4.3 was used as a musculoskeletal modelling software (NCSRR, National Center for Simulation in Rehabilitation Research, Stanford, CA, USA). OpenSim allows for modelling, simulating, controlling, and analyzing the neuromusculoskeletal system [47]. For biomechanics analysis in OpenSim the Gait2392 model was used (developed by Darryl Thelen (University of Wisconsin-Madison) and Ajay Seth, Frank C. Anderson, and Scott L. Delp (Stanford University)) [48]. The Gait2392 model is a three-dimensional, 23-degree-of freedom (DoF) model of the human musculoskeletal system. The model features 92 musculotendon actuators to represent 76 muscles in the lower extremities and the torso. The model's virtual markerset was adjusted to match the markers as used in the BMM laboratory protocol. A figure of this model can be found below (figure 3.3).

Gait2392 knee joint

As the knee joint is the joint of interest for this study it is critical to have a distinct understanding of the representation of the knee joint in the MSM model. In the knee joint, the determination of the quadriceps muscles' moment arm provides a challenge because of the knee's three-bone, multi-ligamented structure. In previous research a simplified model of the knee was created to calculate the extensor moment arm of the knee in a computationally efficient manner [49]. In this model the patellar levering mechanism, as well as the kinematics of the TF and the PF in the sagittal plane, are all taken into account by the single DoF. The transformations between the femoral, tibial, and patellar reference frames are all given as functions of the knee angle [50]. The developers of the Gait2392 model implemented

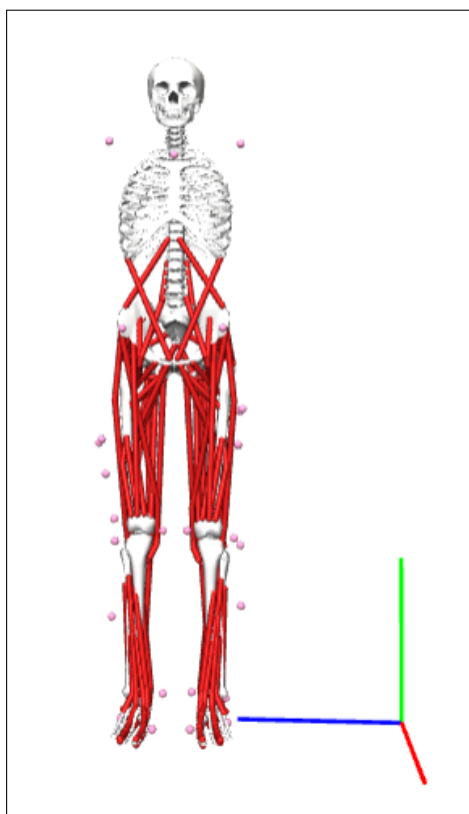


Figure 3.3: **Gait2392** is a 23 DoF model of the human musculoskeletal system. The model features 92 musculotendon actuators to represent 76 muscles in the lower extremities and the torso. The model's marker set was adjusted to match the markers as used in the BMM lab protocol. The coloured axis show the global coordinate system the red axis (x) correspond to anterior-posterior direction, green to proximal-distal/axial (y) and blue to medial-lateral directions (z). **Note:** not all markers from the gait analysis (see appendix A) are represented in this figure as not all were used in the OpenSim analysis.

this knee model and simplified it further by removing the patella from the model, to avoid kinematic constraints. To account for the patella the insertions of the quadriceps on the tibia are modeled as moving points in the tibial frame [48].

3.2.1. OpenSim tools

In order for OpenSim to calculate knee kinematics, muscle forces and joint contact forces as a series of analysis had to be performed. In the following section these are introduced.

Scaling

In order to generate the proper anthropometrics based on the subject's characteristics, scaling was performed. In scaling the experimental marker data were compared to virtual markers on the unscaled Gait2392 model. From the 40 markers affixed during the gait analysis experiment 32 markers were used during the OpenSim analysis. The dimensions of each segment in the model were scaled so that the distance between the virtual markers matched the distance between the experimental markers. Details on the scale factors can be found in appendix B (Table B.1 and B.2). Looking at the scale factors used, it can be observed that for the Z-dimensions of both the torso and the pelvis segment an alternative scale factor was chosen which corresponded with the scale factor used for the left femur (FemurL). This was done as this scale factor resulted in a musculoskeletal model which visually best represented the subject's dimensions.

After scaling, the model's virtual marker positions were moved to match the experimental marker positions in the static pose trial. The virtual marker locations corresponding to the static pose were computed by averaging the marker positions from the motion capture data in between 4.8 and 5 seconds of the static trial, as this time range showed exemplary marker data. Relative marker weights were used to determine how strongly the static pose algorithm should match the experimental marker

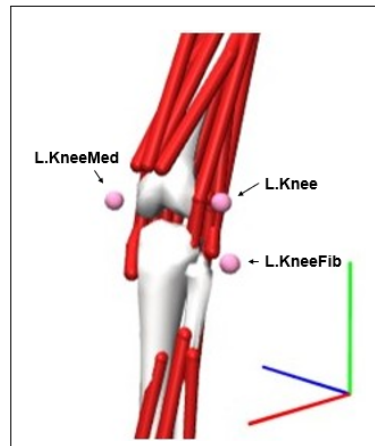


Figure 3.4: Gait2392 left knee joint, including the three knee markers (L.Knee, L.KneeMed and L.KneeFib). The coloured axis show the global coordinate system the red axis (x) correspond to anterior-posterior direction, green to proximal-distal/axial (y) and blue to medial-lateral directions (z).

positions. Weights used varied from 0.1 to 25 with the anatomical markers of the anterior superior iliac spine, shoulder, and knee getting the highest weights and the cluster markers on the femur and tibia getting the lowest weight (see appendix B, table B.3). Once the static pose was computed all model markers were moved to the averaged "static pose" positions of the experimental markers.

Inverse kinematics

After scaling, inverse kinematics (IK) was performed with all joints unlocked. The scaled Gait2392 model was used as input together with the marker data from the dynamic trial and a IK setup file. For the IK trial the time range was set in between 5.84 and 6.62 seconds, as this time frame showed the subject during stance phase with the most reliable marker data and ground force registration (ground force will be considered later on). In the IK setup file the relative weights of each marker are registered. The IK tool goes through each time frame of motion and computes the associated joint angles which positions the model in a pose that best matches the experimental markers from the dynamic walking trial. The IK tool does this by solving a weighted least squares problem (see appendix B.1). The weight associated with each marker specifies how strongly that marker's error term should be minimised. For the purpose of our analysis the anatomical landmarks of the pelvis and knee were given the highest weights, while the ankle and shoulder markers were given lower weights (see appendix B.4). The output file of the IK tool was a motion file (.mot) containing the generalised coordinate trajectories (joint angles) over time.

Static optimization

The static optimization (SO) tool was used to estimate muscle activation level and the muscle forces at each time instant. The SO tool uses the known motion of the model to solve the equations of motion for the unknown forces. Here muscle forces are estimated by minimizing the sum of squared muscle activations (see appendix B.2). The SO tool used the following files as input: the scaled Gait2392 model, the motion file calculated by the IK tool which was filtered using a standard 5 Hz filter, a residual and reserve actuators file, external load data as measured by the force plates, and a SO setup file. The residual and reserve actuators file is attached to correct for dynamic inconsistencies between the estimated joint accelerations and the external forces in the free joints of the model. In the residual and reserve actuators file every DoF can be corrected with one actuator. The external loads file consists of the components of force and torque as measured by the force plates. During heel-strike the calcaneus bone makes initial contact with the force plates. Therefore, the registered forces and torques were applied to the calcaneus bone in the Gait2392 model. Torque data as measured by force plate 4 on contact with the right leg was not incorporated in the external loads file as this measurement showed to be corrupted. The SO setup file also described the exponent for the activation-based cost function to be minimised, which was set to 2. The SO output file consisted of both muscle forces and activation estimations.

Joint reaction analysis

Afterwards, a joint reaction analysis (JRA) was performed. JRA is a tool to calculate resultant forces and moments at the joints. Specifically, it calculates the joint contact forces and moments transferred between the femur and the tibia as a result of all loads acting on the model. These forces and moments correspond to the internal loads carried by the joint structure. The reaction loads calculated by the JRA tool show the contributions of any structures which have not been represented in the MSM, but would result in the desired joint kinematics. Structures can include cartilage contact and left out ligaments. The reaction loads act at the joint centers of both the tibia and the femur. The input files for the JRA are identical to those of the SO tool. Additionally, a list of the joint names of interest, a list of the body on which the reactions occur, a list of frames in which the corresponding reaction is expressed and the muscle forces file as calculated by the SO tool has to be provided. In the list of joints all joints were checked. For both the list of bodies and frames the "child" representation was chosen. This implies that the 3D vectors of the contact forces in the knee were set to apply on the tibia and expressed in the tibia frame (which corresponds to the global frame) [51]. The JRA output consists of forces in the anterior-posterior (x), proximal-distal/axial (y) and medial-lateral (z) directions (see figure 3.4 for reference directions).

3.3. Finite element model

For finite element (FE) simulations the FE modelling tool FEBio was used (FEBio, Jeff Weiss and Gerard Ateshian, Colaboration between the Universities of Utah and Colombia, United States)[52]. FEBio is a software tool for nonlinear finite element analysis in biomechanics and biophysics. To simulate the human knee, the Open Knee (OK) model was used. The OK model is a free access virtual biomechanics representation of the TF knee joint [53]. The OK model is based on the MRI of the right leg of a female donor (age: 70, height: 168cm, body mass: 77.1kg) without a medical history of knee injury. The OK model works with a different axis system than the MSM. The next chapters will therefore primarily use the anatomical direction names to prevent confusion. According to movement science terminology the OK model represents a 6 DoF knee joint. These 6 DoF refer to the rotation and translations along the three perpendicular planes of the FEM. The OK model models the knee joint by connecting the femur and the tibia using three rigid joint connectors, each representing a different femur bone movement on the tibia. Rigid joint connectors connect two rigid bodies by producing non-linear constraints between them and allowing motion only along the joint's DoFs. These constraints can be conceptualized as linear/torsional springs with a specified stiffness (penalty factors in the rigid connectors determines this stiffness) that prevents relative translations/rotations of the femur along DoFs that must remain constrained [54]. Due to the rigid joint connectors the femur could rotate around the x-axis (flexion–extension), y-axis (abduction–adduction movement) and z-axis (external–internal). Moreover the rigid joint connectors also allowed for translation of the femur across the x-axis (lateral), y-axis (anterior), and z-axis (axial). Lastly, the tibia was fully constrained. The additional movement freedom of the OK model in comparison to the Gait2392 knee joint (only allows for flexion–extension estimations) allowed for more intricate estimations of the biomechanics of the knee during gait, and consequently for more detailed tissue mechanical response estimations. For the OK model to be able to simulate gait as during the dynamic walking trial adjustments had to be made to the original OK model. These are described in the following section.

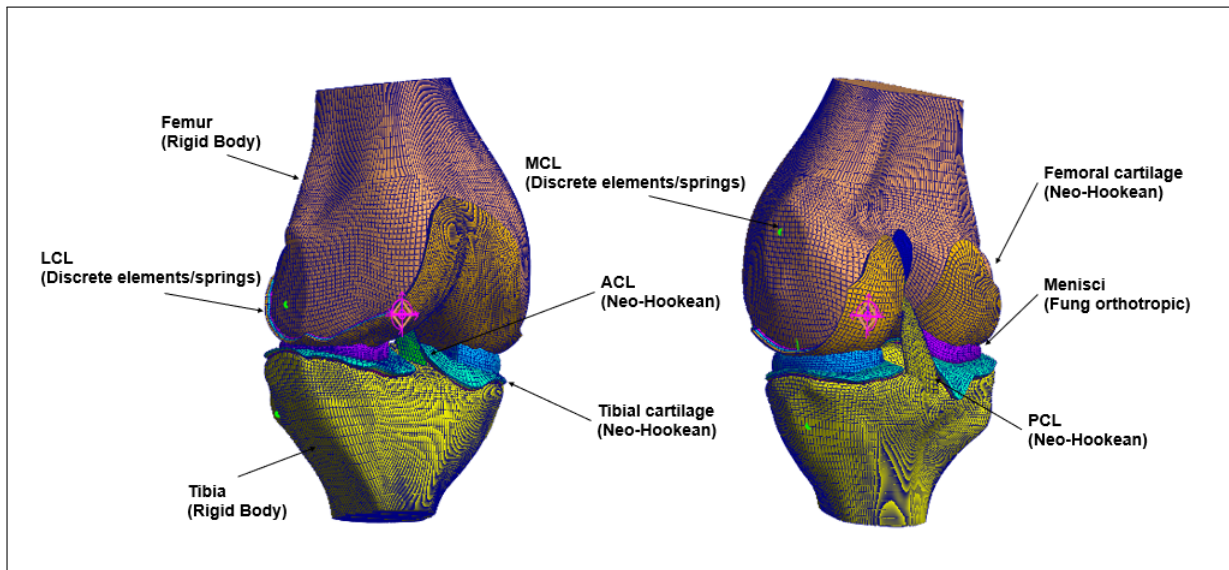


Figure 3.5: Altered OK model and its components, for additional view on model see Appendix D.1.

3.3.1. Geometry

MCL and LCL ligaments

A recent study showed that knee joint models with ligaments modeled as springs produce comparable results to models with more complex ligament representations [55]. Therefore, the 3D representation of the medial collateral ligament (MCL) and lateral collateral ligament (LCL) were replaced with spring elements [56]. This was done to reduce the chance for convergence issues and decrease the computational burden imposed by using the MCL and LCL representations from the original OK model. Both the MCL and LCL were modelled as linear springs with a tensile stiffness of $k = 100 \text{ N/mm}$ [57] and

a pre-strain of 4% [58, 17]. FEBio is not able to account for pre-strain using linear springs, hence a non-linear spring representation had to be implemented. Non-linear spring characteristics in FEBio are described using a force vs. displacement curve. Therefore, to implement the appropriate stiffness and pre-strain both MCL and LCL dimensions were measured from the original OK model. The corresponding force vs. displacement curve was generated using a custom script in MATLAB.

According to previous studies, ligament forces are an essential part of total joint force [17]. In changing to a spring representation for the MCL and LCL, the insertion locations of the springs have converged to a single node on the medial and lateral side of the tibia and femur. This increases the possible risk of incorrect MCL and LCL insertion location, which could influence knee behaviour during gait simulation. Therefore, to determine the optimal insertion locations of both the MCL and LCL, an additional experiment was set up. This experiment included a passive knee flexion simulation in which the OK model was put under a 100N compressive axial load while being flexed to 45°. In the experiment passive knee flexion was simulated using four evenly spaced ligament insertion orientations on both the medial and lateral side of the knee joint. Insertion locations were picked according to the boundaries set by the 3D ligament representation (see appendix C.1 for visualisation of ligament insertion). This resulted in $4 \times 4 = 16$ models, these models represented 16 distinct ligament orientations with varying MCL and LCL insertion locations. The models were run individually to determine the optimal orientation. Knee kinematics of the FEM were tracked for the different ligament insertion locations, results were compared using a custom script in MATLAB. For the optimal solution an orientation was chosen which represented a mid-range of all possible knee kinematics given the 16 ligament orientations.

The optimal ligament orientation was the orientation which most closely resembled the mean of the kinematics for all tested ligaments orientations (see appendix C figures C.2, C.3, C.4, C.5 for DoF plots).

Meniscal horn attachment

In the original OK model meniscal horn attachments are defined using linear springs attaching each node on the meniscal horn faces to the appropriate node on the tibia. In the original model FEBio had difficulty finding a converging solution when a compressive force load was applied to the menisci, due to excessive sliding of the menisci in between the femoral and tibial cartilage. To solve this issue the linear springs were replaced with a fixed displacement boundary condition applied to the meniscal horns, connecting the meniscal horns to the tibia. The fixed displacement boundary condition was set at the location where the meniscal roots would typically attach [59, 60, 61].

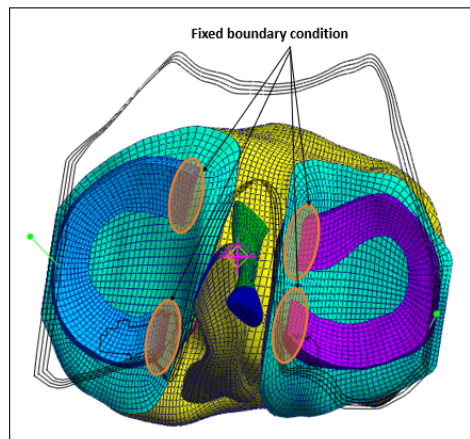


Figure 3.6: Fixed meniscal horns, marked area represents location of fixed boundary condition application.

3.3.2. Contact

The original OK model has a frictionless contact between the tibial cartilage and the menisci, however, in the physiological knee there should be some friction between the tibial cartilage and the menisci. In the psychological knee peripheral attachments are present to connect the menisci to the tibia and restrain meniscal motion [62, 63]. To restrain meniscal motion during simulation a sliding-elastic interface was

incorporated in the altered model. A friction coefficient of 0.5 was allocated for the contact between the menisci and tibial cartilage. The friction coefficient was chosen based on trial and error, as simulations which incorporated this coefficient showed results in the same order of magnitudes as results from literature.

3.3.3. Boundary & loading conditions

In the altered OK model, boundary and loading conditions were applied to simulate knee biomechanics during the stance phase of gait. Boundary and loading conditions included:

- The flexion-extension angle as calculated by the IK tool in OpenSim (see figure 3.9a).
- The knee joint contact forces in the proximal-distal/axial, anterior-posterior and medial-lateral direction, calculated by the JRA tool in OpenSim (see figure 3.9).

The tissue mechanical response and remaining knee kinematics (5 DoF) of the OK model were estimated due to the interactions of the components of the OK model as a result of the application of the boundary and loading conditions from the MSM. During the beginning of the stance phase the flexion angle and knee joint contact forces showed considerable noise. The knee was extended during the high noise time interval, which resulted in a high relative movement of the moving point, which stood in for the link between the quadriceps muscle and the patella. The brief fluctuation in knee flexion angle and joint contact forces was observed as a result of this high relative movement. To smoothen the data and improve FEM simulations both the flexion angle and the knee joint contact forces were smoothed in their respective direction using a Gaussian-weighted moving average filter in MATLAB. This filter made it possible to remove the noisy data portions without affecting the remaining data. See figure 3.7 for the filter effect

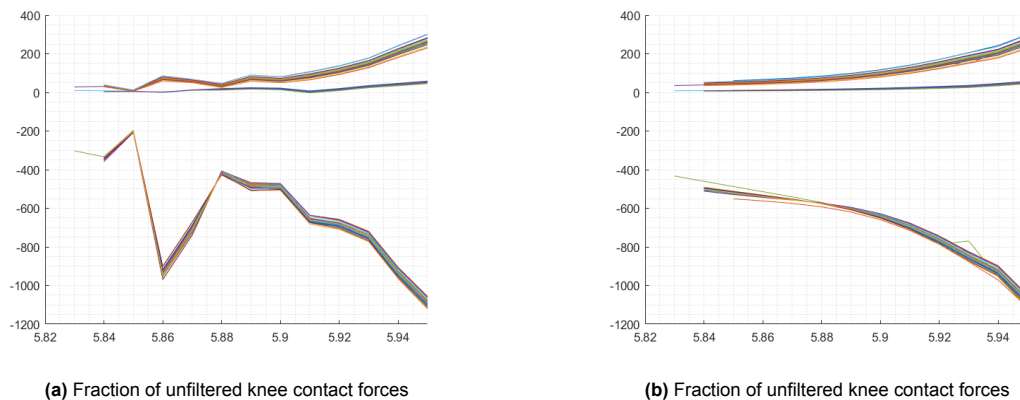


Figure 3.7: Unfiltered and filtered knee contact force curves

In the MSM the joint contact forces act at the joint centers (mobilizer frames) of both the femur and the tibia. This location corresponds with the point of boundary and loading condition application in the OK model, which was also located in the joint centers of both the femur and tibia. In the OK model for both the femur and tibia, rigid body reference points coincide with the origin of the model coordinate system. All loading and boundary conditions for the bones, tibiofemoral joint loading, and kinematics were defined at these points in model's coordinate system [48, 53]. The boundary and loading conditions were applied as time dependent load curves to their respective components. The flexion angle was applied to the Femur-ImgLnk rigid cylindrical joint, as this rigid connector is responsible for medial-lateral translation and flexion-extension across the OK model (for a more extensive explanation on the joint coordinate system see appendix D.2). The knee joint contact forces were applied as time dependent rigid forces to the femur in their corresponding direction, thus the anterior-posterior force was applied along the y-axis, the axial force along the z-axis, and the medial-lateral force along the x-axis (see figure 3.8). The OK model has been developed based on a right knee joint. For the purpose of our simulations we are interested in the left knee. To resolve this, the force direction along the medial-lateral axis was inverted. In models of the knee the patella and tendons mainly controls the anterior-posterior translation. As a result force and moment driven models that lack the patella may

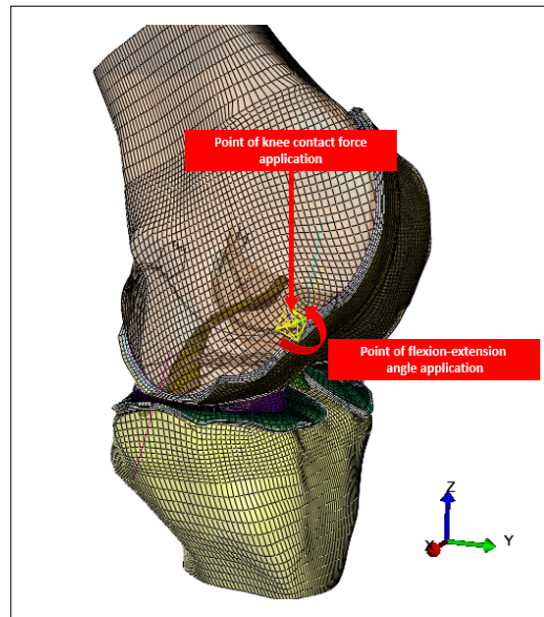
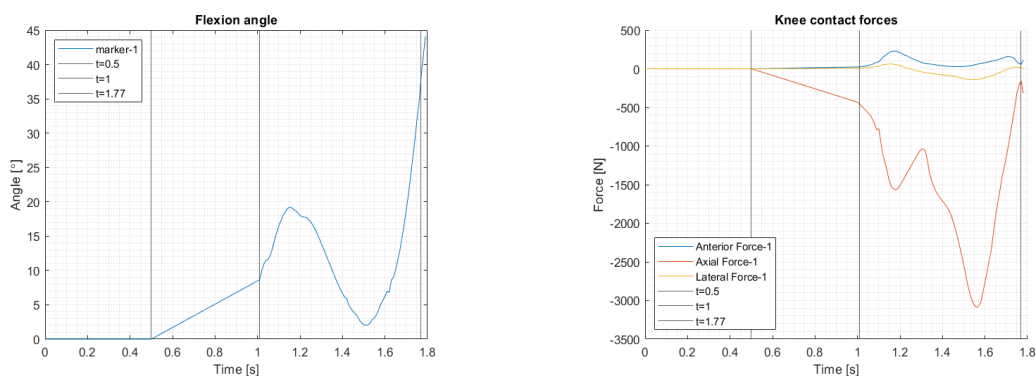


Figure 3.8: Points of application of flexion-extension rotation and knee contact forces

overestimate the femoral translations in the anterior-posterior direction [58]. As the OK model does not include the PF joint, the anterior-posterior joint contact force was scaled by 50%. This factor was determined by running multiple simulations with varying scaling factors for anterior-posterior joint contact force. Scaling the anterior-posterior joint contact force to 50% resulted in knee kinematics which best represented anterior-posterior knee translations from literature.

In applying these boundary and loading conditions, the simulation was divided into two steps. First, A displacement step from $t=0$ to $t=0.5$ seconds which moved the femur distally 0.6mm along the axis (axially) of the knee, to ensure proper contact between the femur, menisci and tibia. Good contact between these parts resulted in improved load distribution estimations and minimised possible convergence problems during FEM simulations [64]. In the second step from $t=0.5$ to $t=1.77$ the load curves were linearly ramped up from $t=0.5$ until $t=1$ at which the FEM was in starting position to simulate the stance phase. This meant both the flexion-extension angle and the knee contact forces were at their respective values corresponding to the start of the stance phase (see figure 3.9a and figure 3.9b at $t=1$) Afterwards, the stance phase simulation was realised from $t=1$ to $t=1.77$ seconds.



(a) input curve representing the flexion angle during stance phase of gait. **(b)** load curves representing the joint contact forces during stance phase of gait. [0,0.5] refers to displacement step. [0.5, 1] = linear flexion and force ramp up. [1, 1.77] = stance phase simulation.

Figure 3.9: Boundary & loading conditions used as input for the OK model

3.3.4. Steps

The simulation was divided into two steps as discussed in the previous section. Both the time settings and nonlinear solver had to be altered to account for the simulation of gait (see appendix D.1 and D.2 for details on step settings). Both steps were simulated as static and utilised the full Newton Method (by setting max updates to 0).

As Step 2 simulated more complex conditions a safety condition was built in. When a time step fails, FEBio will try the step again with a smaller time step size. As a result the maximum and minimum step sizes for step 2 were set lower than in step 1. An additional safety margin was set by increasing the number of maximum retries to 200. The maximum retries parameter determines how many times a time step may be retried before FEBio terminates. These step setting improvements warrant successful simulation of the stance phase of the dynamic walking trial during the sensitivity analysis.

3.4. The workflow

For the sensitivity analysis, a Monte Carlo simulation was performed. To analyse the sensitivity of the FEBio model to marker misplacements, the knee marker data from both the static pose and dynamic walking trial had to be displaced over the knee joint. Consequently the altered marker data had to be imported into OpenSim and processed through scaling, IK, SO, and JRA. The results of these analyses were to be used as input for the OK model. Lastly FEBio simulation results had to be extracted for post-processing. To automate this process, a workflow was set up. The workflow consists of a series of scripts which enabled for automated marker displacement, OpenSim and FEBio analysis, and post-processing of results. The workflow was created in MATLAB using the OpenSim's application programming interface (API) and the GIBBON toolbox (GIBBON, Kevin M Moerman, United States), which allowed for interaction between MATLAB and FEBio [65].

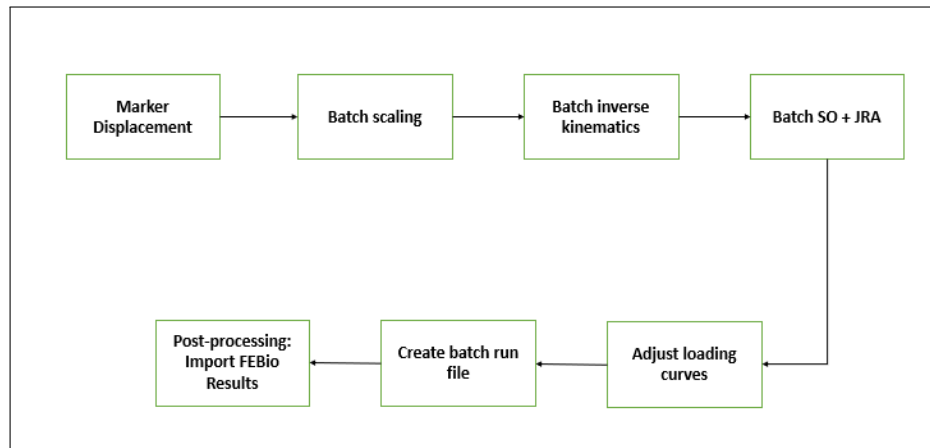


Figure 3.10: Schematic of the semi-automated coupled workflow: Containing a series of Matlab scripts designed to apply marker displacement and consequently scale a model, perform IK, SO, JRA, adjust the boundary and loading condition load curves, create a batch run file and post-processing of the results from the FEBio simulations.

3.4.1. The workflow: OpenSim

In the marker displacement script, 20 marker displacements were applied to the three knee markers defining the knee joint. This was done to the static pose and dynamic trial marker data (.trc) for the L.KneeMarker, LKneeMed-Marker and the L.KneeFibMarker. The displacements for the Monte Carlo simulation were generated using a Latin hypercube sampling method. Latin hypercube sampling is a near-random sampling method which takes into account previously taken samples in order to reduce sample size required to achieve an evenly spread distribution of marker placements [66]. To account for marker misplacement the broadest possible range of marker displacements found in literature was chosen. The original marker position from the BMM laboratory experiment was taken as the anatomical landmark, which corresponded to the anatomical landmark at the knee joint. Subsequently marker displacements were placed around this anatomical landmark.

- Displacements were applied across the anterior-posterior (red) and proximal-distal (green) direction. Along these axes a circle with a radius of 30mm was plotted in which the Latin Hypercube sampling method would pick samples [14, 67]. For a visualisation of the sampling see figure 3.11 and appendix E.2a.
- Additionally samples were taken across the medial-lateral (blue) axis in a range of 10mm. This corresponds to samples being placed 5mm medially and 5mm laterally from the anatomical landmark. Medial-lateral marker displacements were applied to simulate misplacement

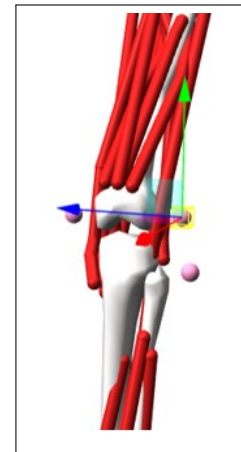


Figure 3.11: Knee marker placement

in the medial-lateral plane [68]. For a visualisation of the marker placements across the medial-lateral plane, see figure 3.11 and appendix E.2.

Subsequently, the batch scaling script would scale the Gait2392 model 20 times according to the 20 static pose trials with altered knee marker placement, resulting in 20 scaled Gait2392 models. Afterwards, the 20 scaled models would go through the batch inverse kinematics script, using the corresponding 20 displaced dynamic trial marker files (identical displacements were applied to the static pose and dynamic walking trial) resulting in 20 motion files containing the joint angles during stance phase. Lastly, the results from the scaling and inverse kinematics would be used to calculate the batch static optimization and joint reaction analysis. The OpenSim segment of the coupled workflow would result in 20 scaled models, 20 motion files, and 20 knee contact forces files all corresponding to a specific marker displacement, to be used as input for the load curve adjustment script.

3.4.2. The workflow: FEBio

Considering each marker position, the OK model was run with loads & boundary conditions based on the updated load curves. In this step 20 FEBio files were created all with identical settings except for the load curves, which consisted of the corresponding flexion angle and knee contact forces. A batch run file was created which would sequentially call for the simulation of the 20 FEBio models, The batch file was created in order to speed up the simulation process. Calling on the FEBio models automatically will reduce the off time due to manual labor by the programmer. Simultaneously, a log file would be created containing the kinematics, stresses and strains, estimated by the FEM. Lastly, the workflow consists of a script enabling for the automated input of FEBio log files in MATLAB, to be used for post-processing.

3.4.3. Computer specifications and computational time

Table 3.1: Estimated computational time for each workflow process for displacements of a single marker

Process	Marker displacement	Batch scaling	Batch inverse kinematics	Batch SO +JRA	Adjust loading curves	Create batch run	Run Batch file	Import results from FEBio	Handling time	Total
Time	3.5 min	1.5 min	2.5 min	60 min	50 min	0.5 min	1200 min	2 min	10 min	1328 min (22.2) hours

Marker displacements and batch OpenSim analysis of the workflow were performed using a HP Zbook laptop (8-core processor, 64 GB RAM, NVIDIA QUADRO RTX5000, Gen 3 x4 NVMe SSD TLC). Batch FEBio analysis was performed using a remote desktop connected to the CBL1 computer located at the faculty of Mechanical, Maritime and Material Engineering at the TU Delft (16-core processor, 32GB RAM, GeForce RTX 2080, Samsung NVMe 1 TB SSD hard drive) which allowed for parallelised finite element calculations, cutting down on computational time due to the multiple core processor. Due to the parallelised finite element calculations, the run time of a single FEM could be reduced to approximately 60 minutes. In table 3.1 an overview can be found of the workflow processes and the corresponding time required to complete each process. **Note:** This section and table cover the simulation of a single knee marker being adjusted. In total all three knee markers (L.Knee, L.KneeMed and L.KneeFib) of the left leg were processed by the workflow.

3.5. Post-processing of models' outcomes

3.5.1. Tissue mechanical response analysis

As the aim of coupled workflows is to aid the clinical decision making process, it is important that the workflow can discern changes in key factors responsible for the onset and progression of musculoskeletal disorders like OA. Considerable research has been done on the factors influencing the cartilage degeneration in OA:

- Research suggests that maximum principal stress (tensile) above a threshold of 7MPa is assumed to trigger collagen network degeneration in cartilage [29, 69, 70].
- Furthermore, experiments and computer simulations linked tissue strains above 30% to chondrocyte apoptosis and subsequent Proteoglycan (PG) loss. In these findings shear strains above 32% were assumed to lead to PG loss [71, 72, 73].

Therefore, for the purpose of this study peak values of both maximum principal stress (tensile) and shear strain were analysed. Moreover, regions of high stress and strain were tracked to identify locations prone to possible collagen network damage and/or PG loss. Elements were labelled as high stress or high strain when their respective maximum principal stress or shear strain values exceeded the threshold values stated above. Peak stresses and strains were evaluated for the elements of the the medial and lateral side of the tibial cartilage for all three knee markers.

Besides excessive joint loading which results in high peak maximum principal stress and shear strain values also stress accumulation can cause OA to develop in a joint. Cumulative excessive stress leads to OA results from post-traumatic joint incongruity, joint dysplasia and instability. However stress accumulation can also cause OA in patients without known joint abnormalities [74]. To account for this accumulation in the post-processing of the models' outcomes. The total number of elements exceeding the predetermined stress and strain thresholds throughout the stance phase were registered for the various marker placements in output variables that were generated. The medial and lateral sides of the tibial cartilage were distinguished here as well.

3.5.2. Statistics

Pearson's correlation coefficient was used to quantify the strength of a relationship between marker placement and workflow output in question. It is important to note here that a distinction was made between marker placement along the three different directions (Corresponding to the OpenSim global coordinate system):

- Anterior(+)-posterior(-)
- Proximal(+)-distal(-)/Axial
- Medial(+)-lateral(-)

x, y and z coordinates of markers were determined. The signs behind the directions describe the positive and negative direction. Subsequently correlations were calculated between the marker placement directions and coupled workflow outputs. The correlation coefficients were calculated in MATLAB as a number between -1 and 1. One being the strongest positive correlation and -1 being the strongest possible negative correlation [75]. If there is a positive correlation, then markers are placed further along the positive direction, increasing the corresponding workflow output. For a negative correlation, it means that if markers are placed further along the positive axis, the corresponding workflow output decreases.

The Pearson's correlation coefficient was complemented by the corresponding p-value. P-values evaluate how well your data rejects the null hypothesis, which states that there is no relationship between marker placement and the workflow output in question. The p-value was used as a measure of confidence in the found relationship. Successfully rejecting the null hypothesis implies that the results are statistically significant. The p-value quantifies the probability the observed effect would have occurred by chance. The threshold for considering a statistically significant relationship was set at $p = 0.05$. In case $p < 0.05$ the null hypothesis was rejected and the assumption that there is a significant relationship between the marker placement and the corresponding workflow output was accepted.

4

Results

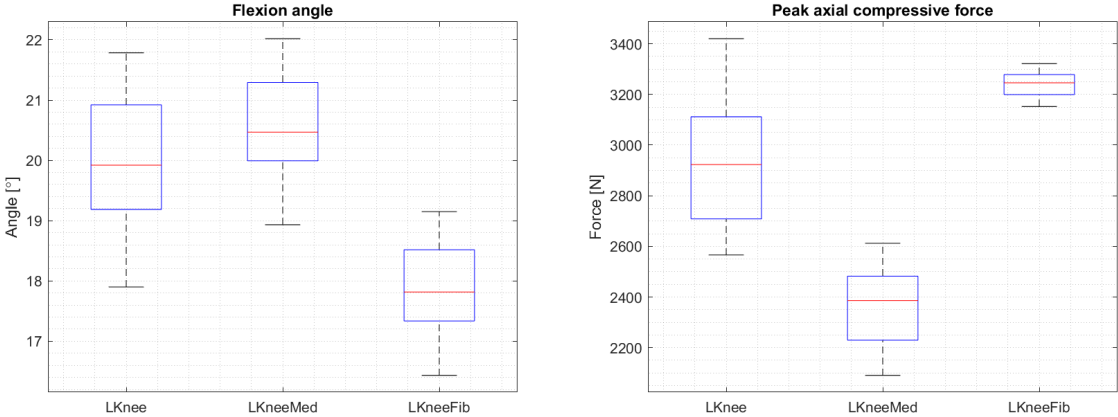
The research question and its sub-questions were used to guide the presentation of the results. First, results were presented addressing how marker placement affects the MSM output regarding knee kinematics and knee joint contact forces as determined by the coupled workflow's MSM. (4.1). Second, the influences of knee marker placement on the coupled workflow's FEM's knee joint kinematics were shown (4.2). The influence of marker placement on the peak magnitude of stresses and strains estimated in the articular cartilage of the knee joint as a result of varied marker placements was presented afterwards (4.3). Lastly, in addition to presenting the magnitude, the location of high stress and strain regions due to varying marker placements were also displayed 4.4.

4.1. Influence of marker placement on MSM output

First, the influence of knee marker placement on MSM output was analysed. The flexion angle of the knee joint as well as the contact forces acting on the knee joint in the axial (proximal-distal), anterior-posterior, and medial-lateral directions were of importance here. These MSM outputs formed the input for the FEM in the coupled workflow. The range of MSM outputs as a result of different knee marker placements were provided in the next section, broken down per knee marker. First, magnitudes of the respective MSM outputs were compared. This was followed by a visualisation of flexion angle and knee contact forces curves over time for the displaced knee markers. Afterwards, correlation coefficients and p-values were calculated to quantify the relationship between the different marker placements and the magnitudes of the MSM output.

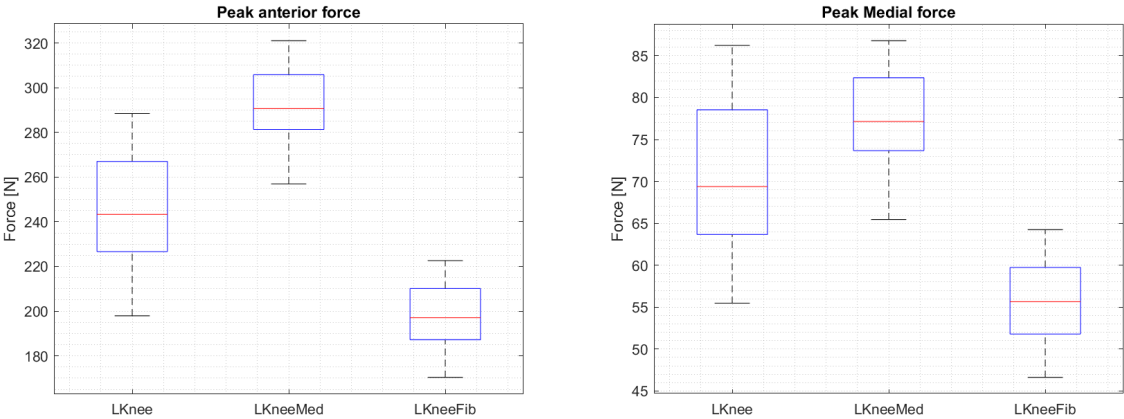
4.1.1. Comparison of MSM output

Figure 4.1 shows the variability in the maximum values as estimated by the MSM for the knee markers. MSM outputs included flexion angle, axial force, anterior-posterior force, and medial-lateral force. Figure 4.1 shows the MSM results found for the 20 different marker placements of each knee marker. Specific points from the flexion and force curves were picked for the comparison of the MSM outputs. For flexion-extension, maximum knee flexion angle was assessed. The peak compressive force was chosen for the axial force. The maximum value of the peak in anterior force was selected for the anterior-posterior joint contact force in the knee. Lastly, the largest value of the medial peak in force output was picked for the medial force comparison. Figure 4.1 describes the distribution of maximum MSM outputs and data skewness through displaying the data quartiles (or percentiles) and median. Figure 4.1a demonstrates that by varying knee marker placement maximum knee flexion angles were estimated in between 22.018° and 16.434° . The L.Knee marker was responsible for the greatest range of maximum knee flexion angles, whereas a different placement site for the L.KneeMed marker produced the narrowest range of maximum knee flexion estimations. The L.KneeFib marker typically showed the lowest maximum knee flexion angles during the stance phase of gait. Peak axial compressive forces were found ranging from 2057.570N to 3419.000N (figure 4.1b). The L.Knee marker was responsible for the largest variety in peak axial compressive force. The L.Knee marker also showed the largest range of possible peak axial compressive forces due to varying marker placements. Generally, the L.KneeMed marker showed the lowest peak axial compressive forces, while the L.KneeFib showed the smallest range in possible output. Peak anterior forces for the various knee indicators ranged from 167.957N to 320.989N. Due to different marker placements, the L.KneeFib marker often displayed the lowest peak anterior forces, whereas the L.KneeMed marker displayed the maximum peak anterior forces. Lastly, both the L.Knee and L.KneeMed marker showed maximum peak medial forces around 86N. The L.KneeFib generally showed the lowest peak medial forces.



(a) Bar plot showing the range, Q1, median and Q3 of maximum flexion angles produced by varying marker placement of the knee markers.

(b) Bar plot showing the range, Q1, median and Q3 of maximum compressive axial force as a result of varied marker placements of the knee markers.



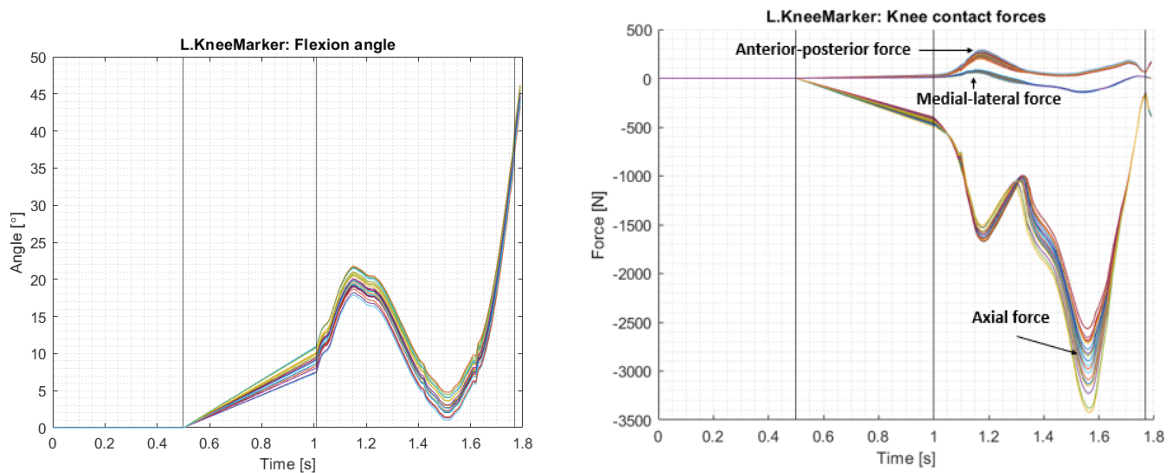
(c) Bar plot showing the range, Q1, median and Q3 of maximum anterior force as a result of varied marker placement of the knee markers.

(d) Bar plot showing the range, Q1, median and Q3 of maximum medial force as a result of varied marker placement of the knee markers

Figure 4.1: Bar plot of peak MSM outputs for the different markers given the altered marker placement.

4.1.2. L.Knee marker placement

For L.Knee marker the range of load curves due to altered marker placements are presented in the figure below (figure 4.2). The flexion (figure 4.2a) and force curves (figure 4.2b) revealed comparable profiles for the various L.Knee marker locations. The profiles, however, appear to have varying maximum and minimum magnitudes.



(a) Load curves each representing an angle input during stance phase of gait as calculated through different L.Knee marker placements. A positive angle corresponds to knee flexion. (b) Load curves representing 20 joint contact forces inputs during stance phase of gait as calculated through different L.Knee marker placements. From top to bottom these are the anterior-posterior knee contact force, the medial-lateral knee contact force and lastly the axial contact force.

Figure 4.2: MSM output as a result of altered L.Knee marker placement. MSM output will be used as input in the form of boundary & loading conditions for the FEM.

Table 4.1 shows the correlation coefficients and the corresponding confidence values for the relationships between marker placement directions and MSM output for the three knee markers. For comparison the same points which defined the ranges of MSM outputs in the previous section were chosen for the correlation calculations of the different marker placements. Marker placements were split up into three marker placement directions which together define the location of the marker (Ant-post, Prox-dist and Med-lat).

To illustrate how these correlation coefficients were estimated an example will be provided for the relationship between marker placement and knee flexion angles. Figure 4.3 shows the relationship between marker placements along the different directions and the maximum flexion angle. Correlation coefficients and p-values were calculated for every relationship. The p-values were used here to determine the probability an effect would have occurred by chance. For the following correlations only relationships with a p-value lower than 0.05 (significant) were considered. These correlation coefficients showed a strong positive relationship between anterior-posterior marker placement and maximum knee flexion angle. The strong positive correlation was illustrated with the orange line in the left figure. For the other remaining marker placement directions no significant relationship could be determined, hence the low confidence and correlation coefficient closer to 0 (These relationships can also be seen in table 4.1). The same method of defining relationships between marker placement direction and coupled workflow results was also applied for the rest of the relationships and throughout the whole study.

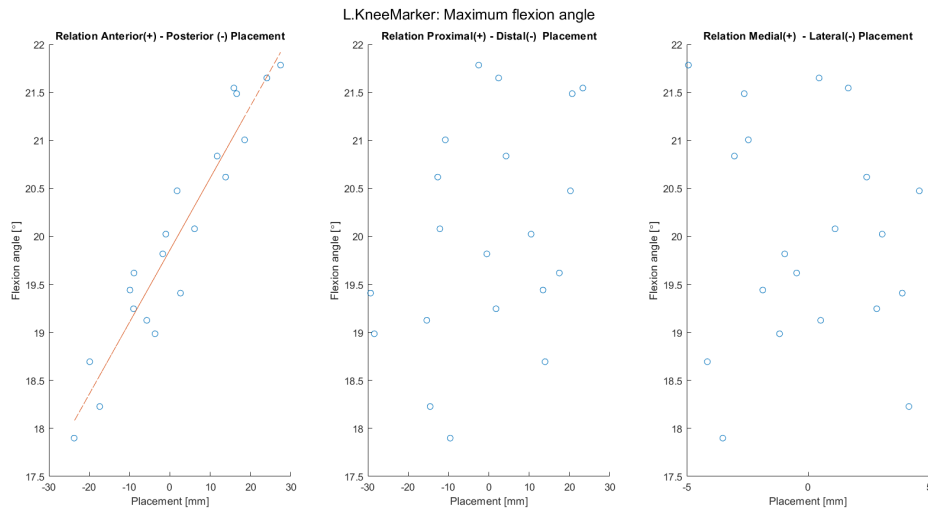


Figure 4.3: Example: Relationships marker placement with respect to direction and MSM output for the L.Knee marker.

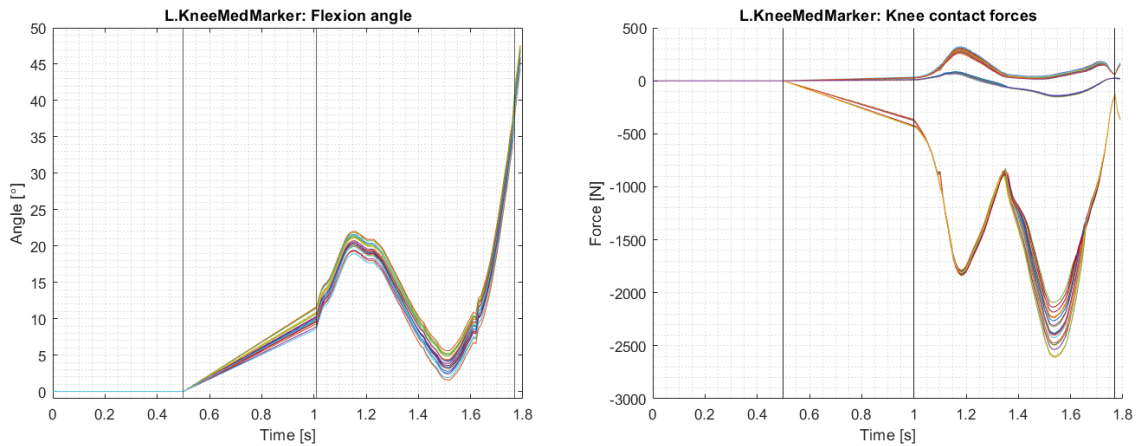
A strong positive significant correlation was found for L.Knee marker placement in the anterior direction and the maximum flexion angle ($r=0.953$, $p=0.000$). This relationship implies that when the L.Knee marker is placed anterior to the anatomical landmark this results in an increase in maximum flexion angle. Figure 4.2 shows that for the simulated L.Knee marker displacements a higher maximum flexion angle also corresponds with higher maximum extension during the stance phase of gait. The relationship between anterior-posterior marker placement was negative for axial compressive force ($r=-0.987$, $p=0.000$, see table 4.1), while a positive relationship was found between anterior-posterior marker placement and anterior-posterior ($r=0.995$, $p=0.000$) and medial-lateral force ($r=0.955$, $p=0.000$). This relationship implies that L.Knee markers placed anteriorly to the anatomical landmark resulted in an perceived decrease in axial compressive force and an increase in peak anterior force and peak medial force.

	Knee flexion angle		Axial compressive force		Anterior-posterior force		Medial-lateral force	
	<i>r</i>	<i>p</i>	<i>r</i>	<i>p</i>	<i>r</i>	<i>p</i>	<i>r</i>	<i>p</i>
L.Knee								
Ant-post	0.953	0.000	-0.987	0.000	0.955	0.000	0.955	0.000
Prox-dist	0.377	0.101	0.002	0.995	0.373	0.106	0.357	0.122
Med-lat	-0.116	0.627	-0.047	0.843	-0.116	0.626	-0.206	0.384
L.KneeMed								
Ant-post	0.992	0.000	-0.995	0.000	0.953	0.000	0.937	0.000
Prox-dist	0.191	0.420	0.022	0.926	0.369	0.109	0.419	0.066
Med-lat	-0.050	0.835	0.074	0.757	-0.045	0.849	-0.098	0.682
L.KneeFib								
Ant-post	0.956	0.000	-0.972	0.000	0.948	0.000	0.908	0.000
Prox-dist	0.368	0.111	0.060	0.802	0.383	0.096	0.431	0.058
Med-lat	-0.095	0.692	0.066	0.781	-0.083	0.729	-0.137	0.565

Table 4.1: Pearson's correlation coefficient and the corresponding p-values for the relationship between marker placement and corresponding MSM output. Values in bold highlight the significant relationships (p -value<0.05).

4.1.3. L.KneeMed marker placement

For the L.KneeMed markers the range of load curves due to altered marker placements were presented in the figure below (figure 4.4). Here, the flexion angles and knee contact forces showed similar patterns with varying magnitudes of flexion and force for the load curves. For the L.KneeMed marker a strong positive significant relationship was found for anterior-posterior marker placement and maximum knee flexion angle ($r=0.992$, $p=0.000$). Additionally, the same applied to anterior-posterior marker placement and anterior-posterior force ($r=0.953$, $p=0.000$), and for anterior-posterior marker placement and medial-lateral force ($r=0.937$, $p=0.000$). As for the L.Knee marker, axial compressive force showed a strong negative relationship with anterior-posterior marker placement ($r=-0.995$, $p=0.000$).

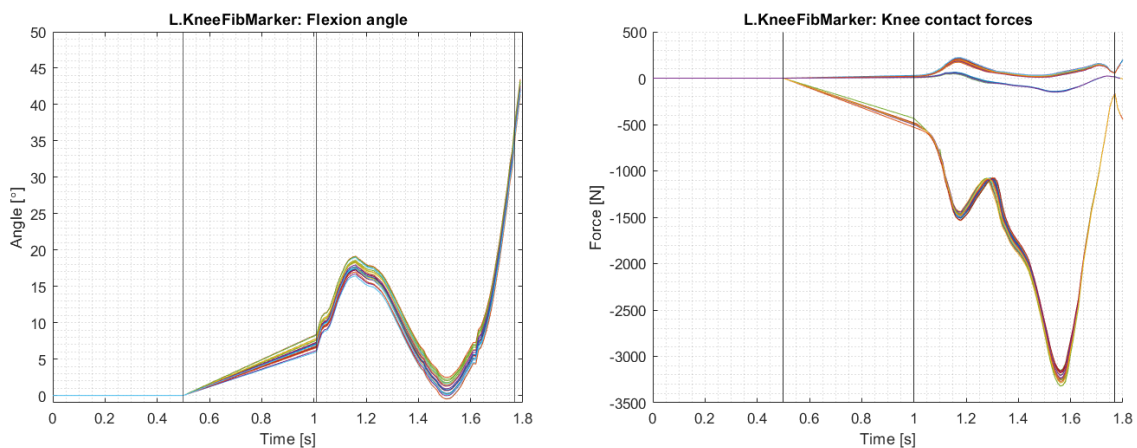


(a) load curve representing 20 flexion angle inputs during stance phase of gait as calculated through different L.KneeMed marker placements. A positive angle corresponds to knee flexion. (b) Load curves representing 20 joint contact forces inputs during stance phase of gait as calculated through different L.KneeMed marker placements. From top to bottom these are the anterior-posterior knee contact force, the medial-lateral knee contact force and lastly the axial contact force.

Figure 4.4: MSM output as a result of altered L.KneeMed marker placement. MSM output will be used as input in the form of boundary & loading conditions for the OK model.

4.1.4. L.KneeFib marker placement

For L.KneeFib marker the range of load curves due to altered marker placements are presented in the figure below (figure 4.5). The flexion angle curve as a result of varying L.KneeFib marker placements showed minor hyper extension around $t \approx 1.5$ (figure 4.5). Besides the slight hyper extension, similar load curves were found for the different flexion angles and knee contact forces, however all with varying magnitudes. In quantifying the relationship between L.KneeFib marker placement and MSM output, once again a strong negative significant relationship was found for anterior-posterior marker placement and knee flexion angle ($r = -0.982$, $p = 0.000$). A positive relationship was found for anterior-posterior marker placement and the knee joint contact forces (axial compressive force, $r = 0.972$, $p = 0.000$, anterior-posterior force $r = 0.948$, $p = 0.000$ and medial-lateral force $r = 0.908$, $p = 0.000$, see table 4.1).



(a) load curve representing 20 flexion angle inputs during stance phase of gait as calculated through different L.KneeFib marker placements. A positive angle corresponds to knee flexion. (b) Load curves representing 20 joint contact forces inputs during stance phase of gait as calculated through different L.KneeFib marker placements. From top to bottom these are the anterior-posterior knee contact force, the medial-lateral knee contact force and lastly the axial contact force.

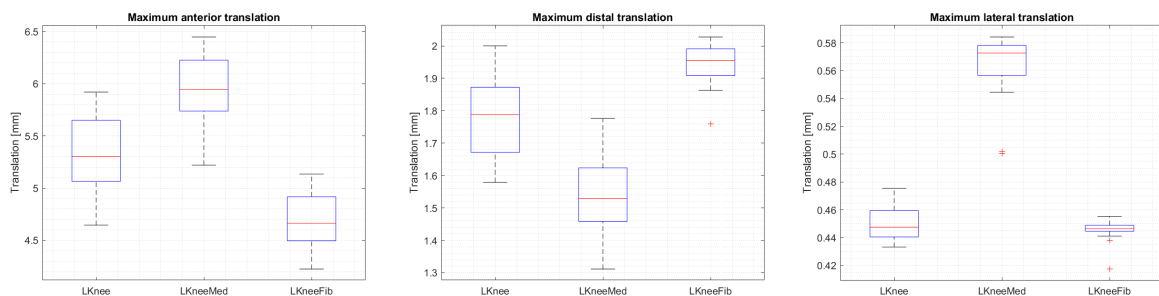
Figure 4.5: MSM output as a result of altered L.KneeFib marker placement. MSM output will be used as input in the form of boundary & loading conditions for the OK model.

4.2. Influence of marker placements on FEM knee kinematics

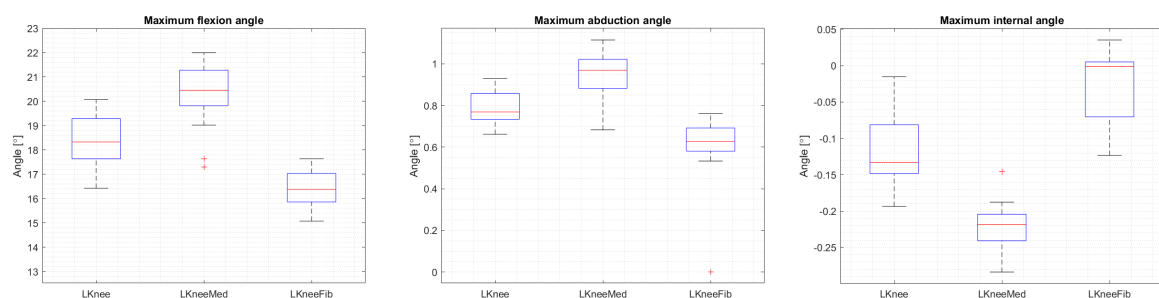
The results of incorporating the MSM outputs from the previous section as boundary and loading conditions are displayed in the following section. In order to quantify the relationship between marker placements and the corresponding FEM knee kinematics, knee kinematics results included both figures of the FEM knee translations and rotations. FEM knee translations and rotations resulted from simulations with different knee marker placements. Additional figures showed the knee kinematics along all 6 DoF during the stance phase of gait. A table containing correlation coefficients and confidence results was also included. For structure sake, only the relationships that had p-values lower than 0.05 were mentioned in the following sections.

4.2.1. Comparison of FEM knee kinematics

Figure 4.6 shows the variability in the maximum knee kinematic values as estimated by the FEM for the various knee markers. Knee kinematics include knee anterior-posterior, proximal-distal, medial-lateral translation, flexion-extension angle, abduction-adduction angle, and internal-external rotation angle. The ranges in figure 4.6 correspond to the outcomes of the 20 different marker placements of the three knee markers. Specific points from the kinematics predictions curves were picked for the comparison of the FEM predictions. For anterior-posterior translation, maximum anterior translation was used. Proximal-distal translation used maximum distal translation for comparison. Maximum lateral translation was used for the comparison of marker placement along the medial-lateral direction. For the rotational DoFs maximum flexion was chosen to compare the various flexion angles. Maximum adduction angle was picked to analyse abduction-adduction rotations and maximum internal angle was chosen for the comparison of internal-external rotations. Figure 4.6 describes the distribution of the maximum knee kinematics values and data skewness through displaying the data quartiles (or percentiles) and median.



(a) Range of maximum anterior translation as a result of varying marker placement for the three knee markers. (b) Range of maximum distal translation as a result of varying marker placement for the three knee markers. (c) Range of maximum lateral translation as a result of varying marker placement for the three knee markers.



(d) Range of maximum flexion angle as a result of varying marker placement for the three knee markers. (e) Range of maximum adduction angle as a result of varying marker placement for the three knee markers. (f) Range of maximum external angle as a result of varying marker placement for the three knee markers.

Figure 4.6: Comparison of maximum knee kinematic values of the FEM knee.

Figure 5.2a shows that maximum anterior translations varied between 6.45mm and 4.22mm for varying marker placements. In this instance, the maximal anterior translation was often highest for the L.KneeMed marker and lowest for the L.KneeFib marker. The different knee markers' maximum distal

translations, which ranged from 1.31mm to 2.03mm, closely matched one another (figure 5.2b). The L.Knee and L.KneeFib marker's maximal lateral translation had similar magnitudes. The maximum lateral translations for these markers were between 0.42mm and 0.48mm. The L.KneeMed marker's lateral translation revealed to have the highest potential values (ranging from 0.5mm to 0.59mm, see figure 5.2c). Due to different marker placements, maximum flexion angles ranged from 15.050° to 22.002° . The L.Knee marker displayed the widest variety of potential outcomes in this instance (figure 5.2d). The range of maximum abduction angles was 0.534° to 1.115° . The L.Knee and L.KneeMed markers' various marker placements led to the highest rise in abduction angle magnitude. Finally, the maximum internal rotation angle varied between 0.015° and -0.283° . The positioning of the L.Knee and L.KneeMed markers was responsible for the lower maximum internal rotation angles, whereas the displacement of the L.KneeFib marker produced the highest internal rotation angles.

4.2.2. L.Knee marker

In FEM simulations from the L.Knee marker displacement, 5/20 simulations failed before reaching the time step which corresponded to the second peak of axial compressive force of the stance phase (t \approx 1.55s) (see 4.1). For the L.Knee marker, the range of FEM knee translational and rotational kinematics are presented in the figures below (simulations which prematurely failed included).

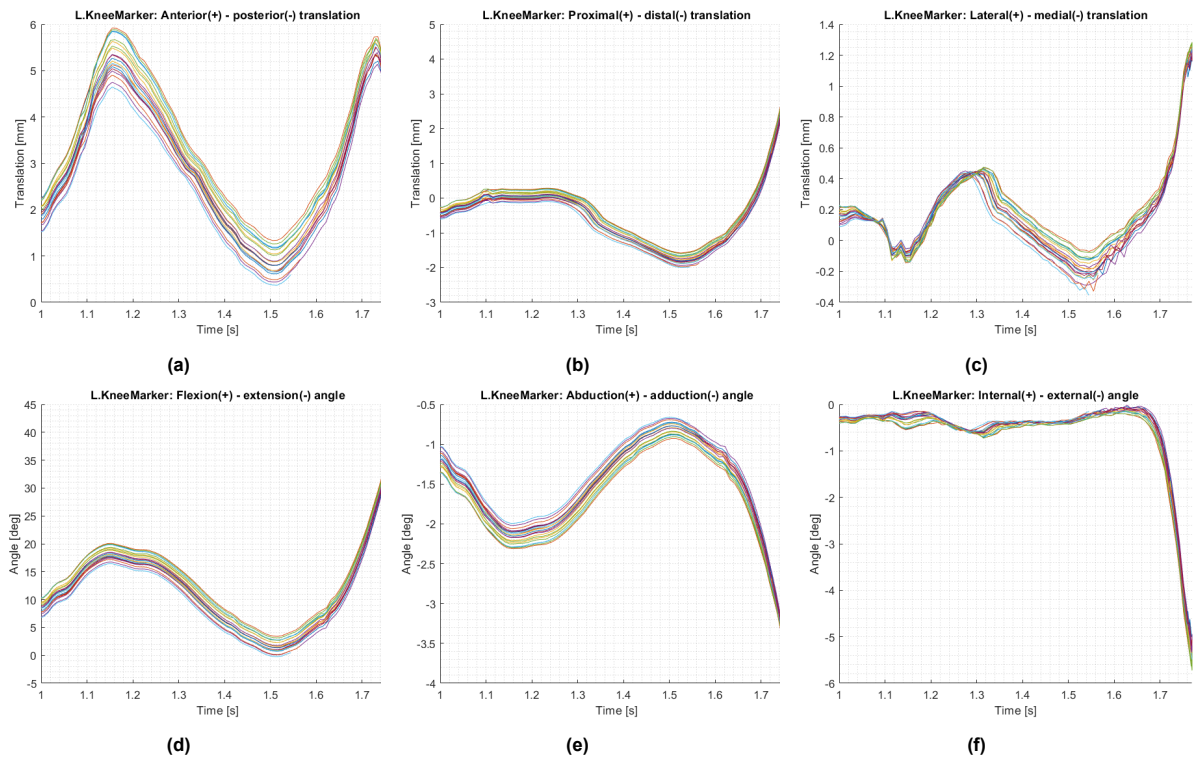


Figure 4.7: Knee joint rotations as a result of altered L.KneeMarker placements

The patterns of the knee kinematics as a result of altered L.Knee marker placements were relatively similar to one another, with varying magnitudes. Only the lateral knee translation showed inconsistencies for some simulations in between t=1.5 and t=1.7. As explained in the Methods section, the left knee of the subject was the knee of interest. The FEM knee however represents the right knee. In order to account for this the sign convention of the medial-lateral force application has been switched. As a result of this discrepancy, lateral translations are considered positive when analyzing the FEM knee kinematics. For L.Knee marker displacements a positive correlation was found between anterior-posterior marker placement and anterior translation ($r=0.950$, $p=0.000$), proximal translation ($r=0.999$, $p=0.000$), and lateral translation ($r=0.845$, $p=0.000$). These relationships imply that when the L.Knee marker is placed anteriorly to the anatomical landmark, the FEM of the coupled workflow showed greater peak anterior translations during the stance phase of gait. For the rotational kinematics a positive correlation was found for anterior-posterior translation and the maximum flexion angle ($r=0.951$, $p=0.000$). The cor-

relation coefficient for abduction-adduction ($r=-0.987$, $p=0.000$) and internal-external rotation ($r=-0.531$, $p=0.016$) showed to have a negative relationship with anterior-posterior marker placement.

4.2.3. L.KneeMed marker

For varying simulations with L.KneeMed marker placements, 6/20 FEM simulations failed before reaching the time step which corresponded to the second peak of axial compressive force of the stance phase ($t \approx 1.55$ s). The following figures show the range of FEM knee translational and rotational kinematics for the L.KneeMed markers (simulations which prematurely failed included).

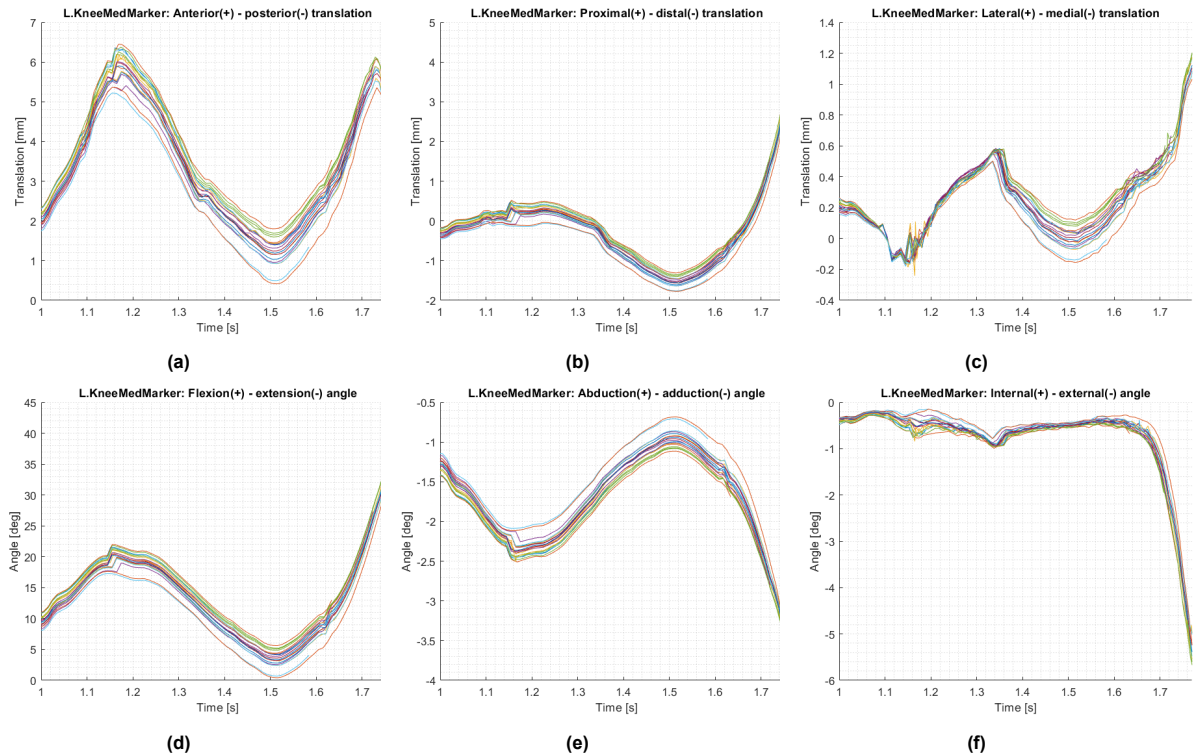


Figure 4.8: Knee joint rotations as a result of altered L.KneeMed marker placements

Again, positive relationships were found for anterior-posterior marker placement and peak anterior ($r=0.972$, 0.000), proximal ($r=0.956$, 0.000), and lateral ($r=0.760$, 0.000) translations. Maximum flexion angle positively correlated with anterior-posterior marker placement ($r=0.949$, 0.000). Abduction-adduction ($r=-0.907$, 0.000) and internal-external ($r=-0.962$, 0.000) rotations both negatively correlated with anterior marker placement.

4.2.4. L.KneeFib marker

6/20 simulations failed before reaching the time step which corresponded to the second peak of axial compressive force of the stance phase ($t \approx 1.55$ s). The following figures show the range of FEM knee translational and rotational kinematics for the L.KneeFib marker (simulations which prematurely failed included). Results for the different knee kinematics showed similar patterns except for some of the results of the lateral-medial translations. These showed high relative noise when simulating the latter part of the stance phase (figure 4.9c). For L.KneeFib marker displacements a positive relationship was found for anterior-posterior marker placement and peak anterior translation ($r=0.954$, 0.000). The same applied for the relationship between anterior-posterior marker placement and peak proximal translation ($r=0.978$, 0.000). Contrary to the other knee marker results, a negative relationship was found for anterior-posterior marker placement and lateral-medial translation ($r=-0.479$, 0.038).

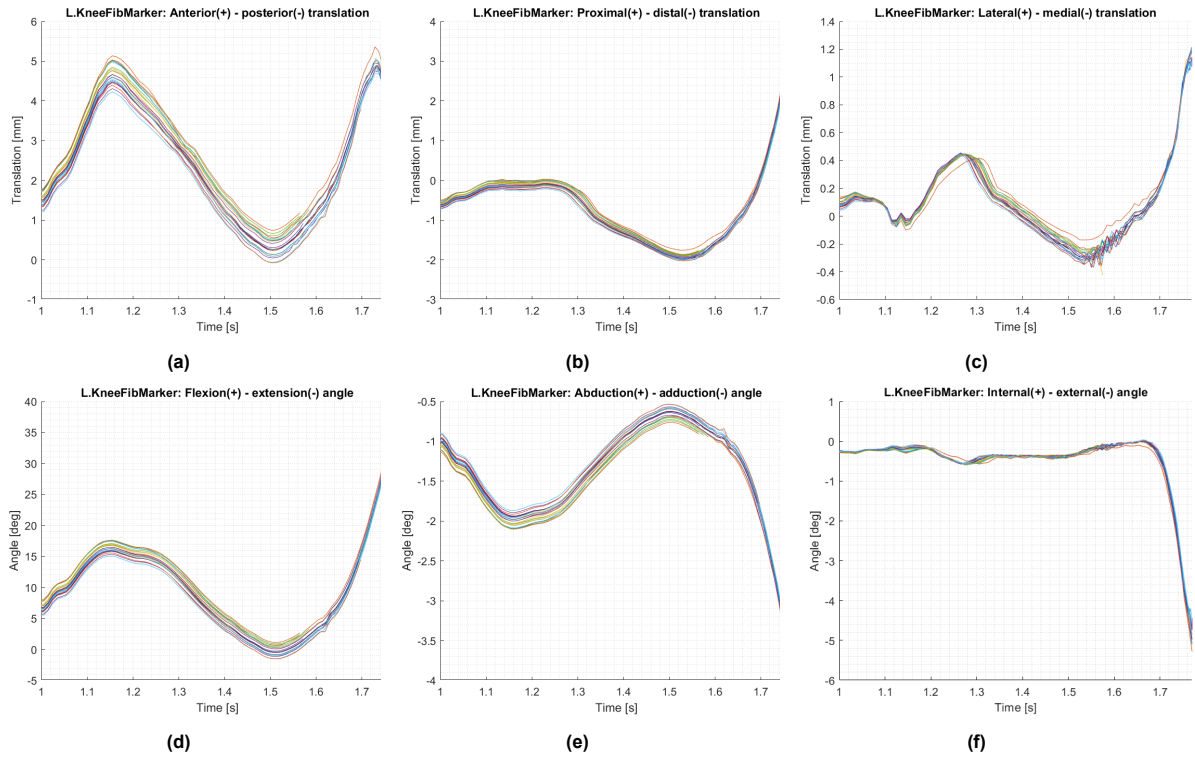


Figure 4.9: Knee joint rotations as a result of altered L.KneeFibMarker placements

	Anterior-poster		Proximal-distal		Lateral-medial	
L.Knee	r	p	r	p	r	p
Ant-post	0.950	0.000	0.999	0.000	0.845	0.000
Prox-dist	0.387	0.092	0.083	0.829	0.129	0.588
Med-lat	-0.124	0.601	-0.052	0.728	0.010	0.965
L.KneeMed	r	p	r	p	r	p
Ant-post	0.972	0.000	0.956	0.000	0.760	0.000
Prox-dist	0.245	0.297	-0.186	0.431	-0.126	0.596
Med-lat	0.005	0.982	0.015	0.951	0.412	0.071
L.KneeFib	r	p	r	p	r	p
Ant-post	0.954	0.000	0.978	0.000	-0.479	0.038
Prox-dist	0.387	0.102	-0.113	0.645	-0.343	0.150
Med-lat	-0.073	0.768	-0.103	0.674	0.458	0.048

Table 4.2: Correlation coefficient and corresponding p-value for marker placement and FEM translational knee kinematics

	Flexion-extension		Abduction-adduction		Internal-external	
L.Knee	r	p	r	p	r	p
Ant-post	0.951	0.000	-0.987	0.000	-0.531	0.016
Prox-dist	0.383	0.096	-0.219	0.354	-0.359	0.120
Med-lat	-0.119	0.617	0.176	0.458	0.604	0.005
L.KneeMed	r	p	r	p	r	p
Ant-post	0.949	0.000	-0.907	0.000	-0.962	0.000
Prox-dist	0.123	0.605	0.247	0.294	-0.138	0.561
Med-lat	0.119	0.617	-0.121	0.611	-0.044	0.854
L.KneeFib	r	p	r	p	r	p
Ant-post	0.962	0.000	-0.986	0.000	-0.670	0.002
Prox-dist	0.362	0.128	0.071	0.772	0.310	0.196
Med-lat	-0.068	0.782	0.110	0.655	0.171	0.484

Table 4.3: Correlation coefficient and corresponding p-value for marker placement and FEM rotational knee kinematics

4.3. Influence of marker placements on tissue mechanical response

The following section shows how marker placements influenced the magnitude and range of the peak maximum principal stress and peak shear strain inside the cartilage of the knee during the stance phase of gait. Firstly, an overview was provided comparing the magnitudes and ranges of the peak maximum principal stresses and shear strains. Afterwards, an overview was provided comparing the total number of elements exceeding the predetermined threshold throughout the stance phase per knee marker simulation. This is followed up by a visualisation of the peak maximum principal stresses and peak shear strains over time for the varying marker placements. Lastly, the correlation results are presented in order to quantify any potential relationship between the position of the marker placement and the magnitude of the estimated tissue mechanical response. An example of the visualisation from the both the maximum principal stress and shear strain is provided in figure 4.10

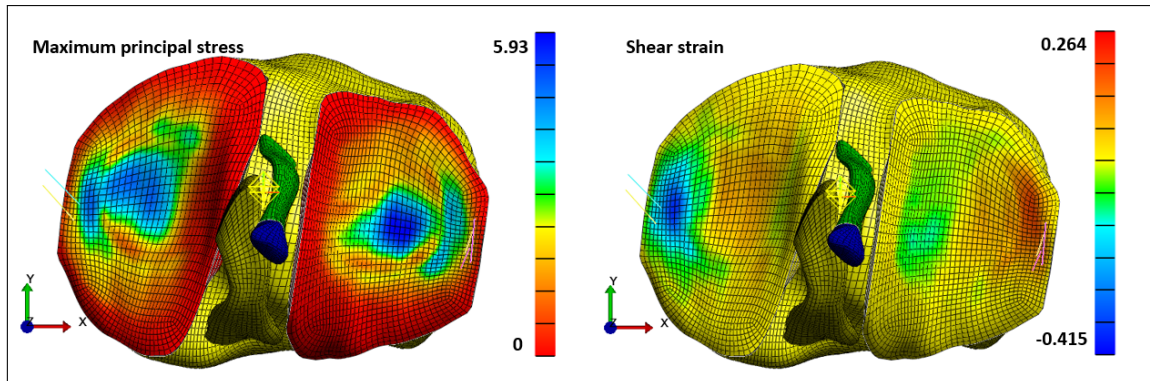


Figure 4.10: Visualisation of the maximum principal stress (left) and maximum shear strain (right) at arbitrary time $t=1.545$. Legends have been adjusted for better conformity with report.

4.3.1. Comparison of stress/strain magnitude

For the comparison of tissue mechanical response, peak magnitude and range of maximum principal stresses and shear strains were measured during gait. This was done for the 20 simulations of every perturbed knee marker. Peak maximum principal stress and peak shear strain values in figure 4.11 corresponded to the greatest stress/strain value during a single stance phase simulation. Figure 4.11 describes the distribution of the maximum principal stress, shear strain and corresponding data skewness through displaying the data quartiles (or percentiles) and median.

For the medial tibial cartilage, peak maximum principal stress values ranged from 5.299 to 6.148 MPa. The peak maximum principal stress measured for varying L.KneeMed marker placements was the highest (6.148MPa), whereas the peak maximum principal stress measured for the L.Knee marker was the lowest (5.299 MPa). While the L.KneeFib exhibited the smallest range of potential peak stress values, the L.Knee marker showed the greatest range of peak maximum principal stress values (see figure 4.11a). Peak maximum principal stress values on the lateral side of the tibial cartilage were generally higher than on the medial side and varied between 7.047MPa and 5.951MPa. L.KneeFib marker displacements showed peak maximum principal stress around 7MPa while the highest peak maximum principal stress value for the L.KneeMed marker was registered at 6.378 MPa (see figure 4.11b). Peak shear strain estimations for the medial tibial cartilage ranged from 0.525 to 0.436. On the lateral side lower cartilage shear strains were estimated. Peak shear strain estimations on the lateral side of the tibial cartilage ranged from 0.240 to 0.299 (see figures 4.16c and 4.16d).

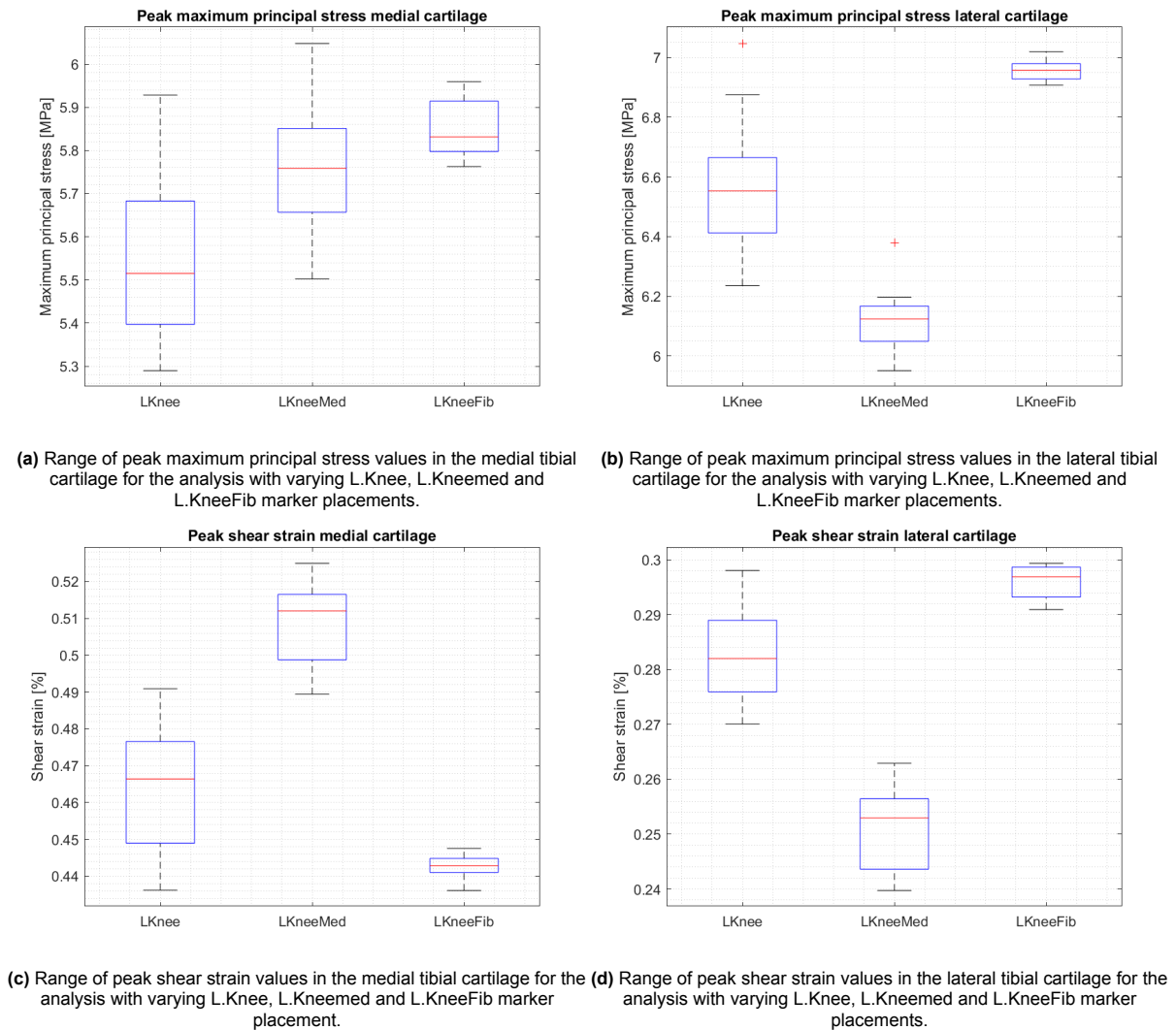


Figure 4.11: Demonstrates the range and size of peak maximum principal stress and peak shear strain in the medial and lateral cartilage of the knee for the three knee markers.

4.3.2. Comparison of stress/strain accumulation

Cartilage degeneration is thought to be the result of prolonged exposure to high stress and strains. Therefore, it is also of importance to take into account cumulative stresses and strains. To quantify the influence of marker placement on stress/strain accumulation during the stance phase of gait, the number of elements which exceeded the stress and strain threshold were recorded. This was done for all 20 altered knee marker placements of the L.Knee, L.KneeMed, and L.KneeFib markers. Threshold values for these variables were 5MPa and 0.32% respectively. The number of elements which exceeded the specified thresholds in every simulation were compared to one another and presented in figure 4.12. Figure 4.12 describes the distribution of the elements surpassing the threshold and data skewness through displaying the data quartiles (or percentiles) and median. The largest number of total elements reported over the stress threshold during the stance phase was 1127 elements. This value was obtained by moving the location of the L. KneeFib marker in the medial cartilage (figure 4.12a). The maximum number of elements with stress values exceeding the threshold during the stance phase of gait, 2087, was caused by the fluctuation in L. KneeFib marker placement. The L.KneeMed marker alteration caused the medial and lateral tibial cartilage to experience the least amount of stress values above the predetermined thresholds. Variations in L.KneeFib marker placements caused the greatest shear strain accumulation (figure 4.12c). Shear strains in the lateral tibial cartilage did not exceed the threshold, therefore lateral tibial cartilage shear strain results were omitted.

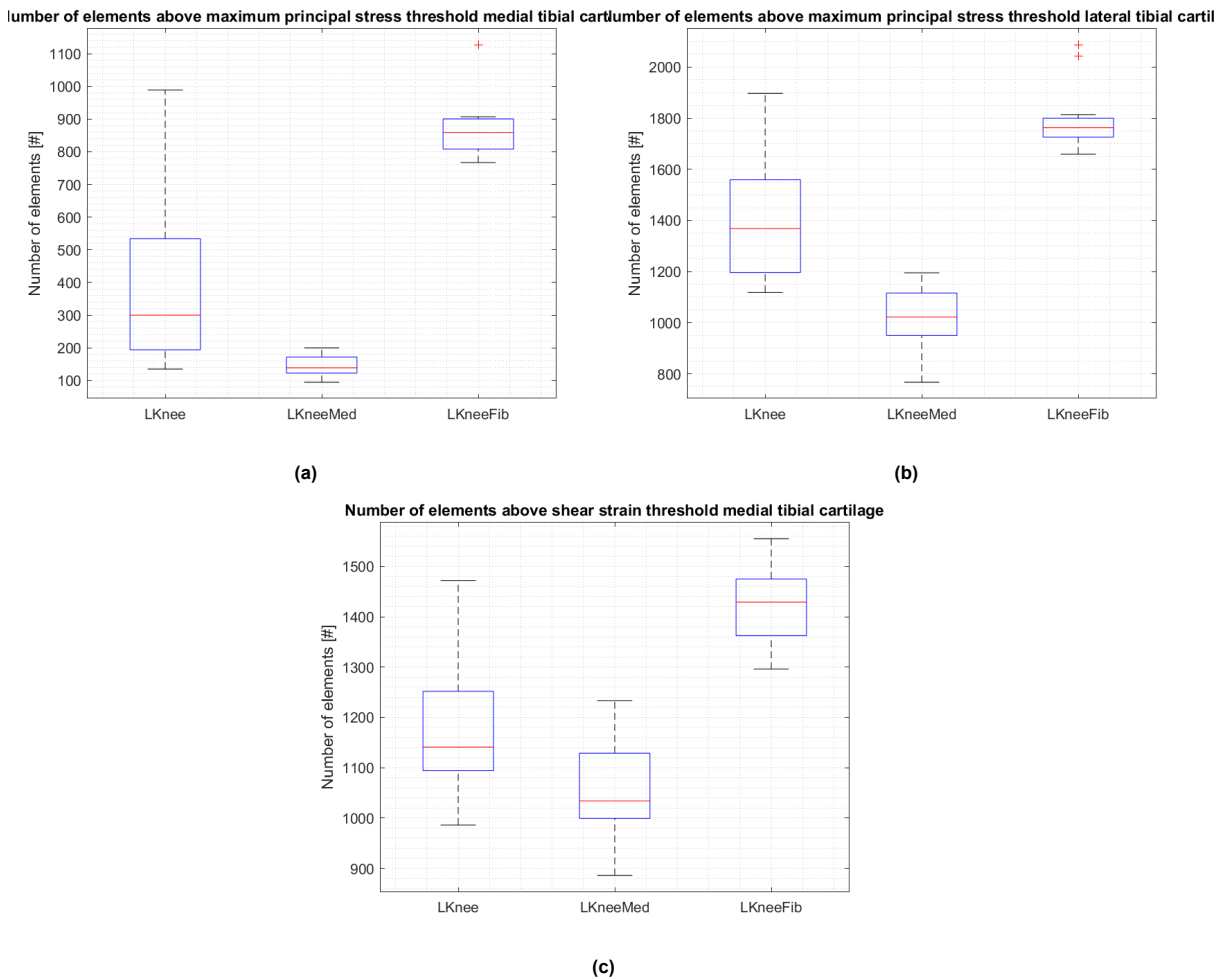


Figure 4.12: Number of elements exceeding the degeneration threshold (maximum principal stress > 5MPa shear strain > 0.32) in the medial and lateral tibial cartilage throughout the stance phase of gait, for the different marker placements of the L.Knee, L.KneeMed, and L.KneeFib markers. As shear strain in the lateral tibial cartilage did not exceed the specified threshold, this figure is omitted.

4.3.3. L.Knee marker

Visualisations of the peak maximum principal stresses and maximum shear strains throughout the stance phase of gait for varying locations of the L.Knee marker are found in figure 4.13. A two peaked stress and strain curve was found for all tissue mechanical response figures. The medial and lateral cartilage's peak maximum principal stress response and the tibial cartilage's peak shear strain all exceeded their respective degeneration thresholds across higher portions of their peaked curves. The lateral tibial cartilage's maximum shear strain values, however, did not exceed the predetermined threshold.

Correlations between marker placement and peak maximum principal stresses were computed to quantify the relationship between the two variables (table 4.4). For L.Knee marker displacements a negative correlation was found between anterior-posterior marker placement and peak maximal principal stress in the medial ($r=-0.947$, $p=0.000$) and lateral ($r=-0.959$, $p=0.000$) cartilage. No other significant relationship was found for L.Knee marker placement and peak maximum principal stresses in either the medial or lateral cartilage of the knee. The relationship between peak shear strain and marker displacement of the L.Knee saw a positive relationship between anterior-posterior marker placement and peak shear strain in the medial cartilage ($r=0.914$, $p=0.000$). A negative correlation was found for the relationship between anterior-posterior marker placement and peak shear strain in the lateral cartilage of the knee ($r=-0.972$, $p=0.000$). These relationships imply that in case a marker is placed anteriorly to the anatomical landmark, perceived peak shear strains in the medial cartilage increase while they decrease in the lateral cartilage. Proximal-distal marker placement also correlated positively

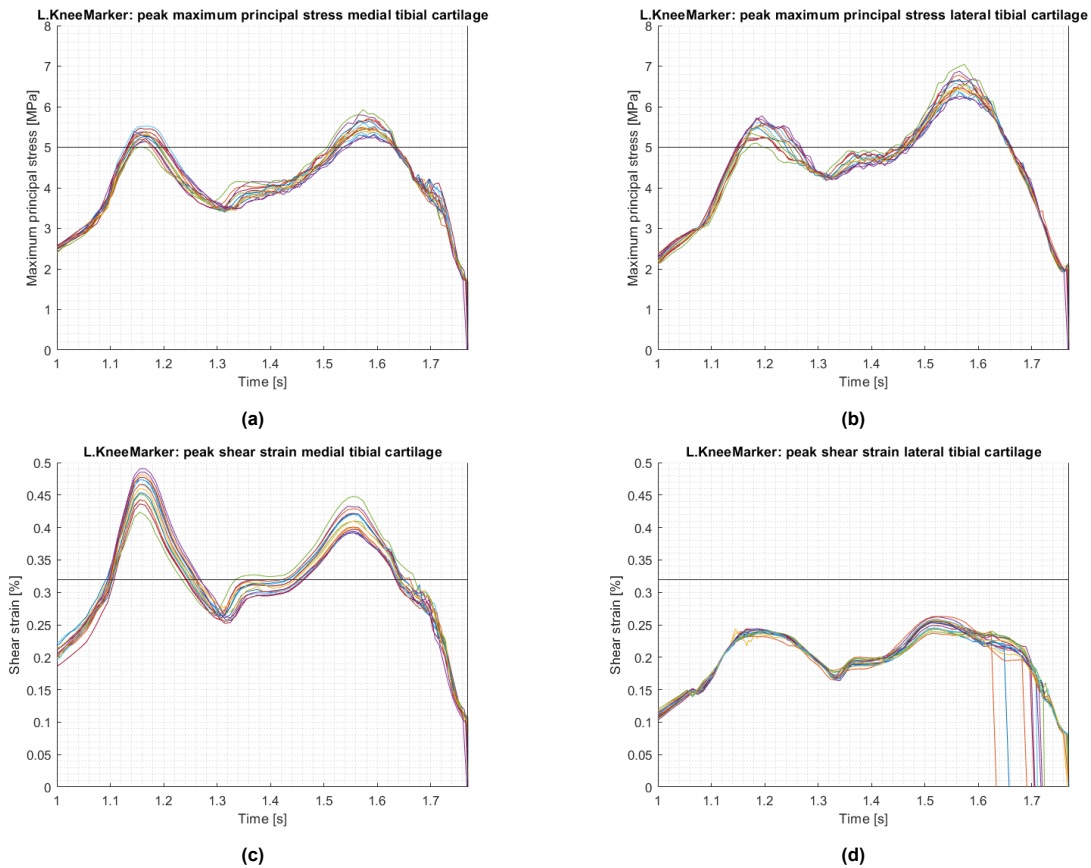


Figure 4.13: Peak maximum principal stress and shear strain in the medial tibial cartilage due to altered marker placement of the L.Knee marker. Vertical lines represent respective stress and strain threshold, responsible for cartilage degeneration.

with both peak shear strain in the medial ($r=0.521$, $p=0.047$) and lateral ($r=0.543$, $p=0.037$) cartilage (table 4.5). Moreover, negative correlation coefficients were encountered for the relationship between anterior-posterior marker placement and the cumulative number of elements above the stress threshold in the medial ($r=-0.942$, $p=0.000$) and lateral ($r=-0.943$, $p=0.000$) cartilage (table 4.6). Lastly, a negative correlation coefficient was calculated for the relationship between anterior-posterior marker placement and the number of elements surpassing the strain threshold throughout the stance phase in the medial cartilage ($r=-0.746$, $p=0.001$). No element strain values exceeded the strain threshold on the lateral side of the cartilage, therefore correlation coefficients could not be constructed (figure 4.7).

4.3.4. L.KneeMed marker

When examining the tissue mechanical responses of the analysis for different L.KneeMed marker placements, a similar two peaked curve pattern was found (figure 4.14). The 7 vertical lines on the curves' right side represent simulations that failed before the analysis was fully completed ($t=1.77$). Their results were nonetheless taken into account in the analysis because their simulations went beyond the time step which corresponded to the second peak in the tissue mechanical response curves.

No significant correlations were found for marker placement directions of the L.KneeMed marker along the three different directions and the peak maximum principal stress during simulation of the stance phase. A positive correlation coefficient was calculated for the relationship between anterior-posterior marker placement and peak shear strain in the medial cartilage ($r=0.822$, $p=0.000$). For the same marker direction in the lateral cartilage a negative correlation coefficient was calculated ($r=-0.988$, $p=0.000$). Moreover, anteriorly placed L.KneeMed markers saw both an increase in the number of elements above the stress threshold ($r=0.891$, $p=0.000$) and the number of elements above the strain threshold ($r=0.739$, $p=0.000$) in the medial cartilage.

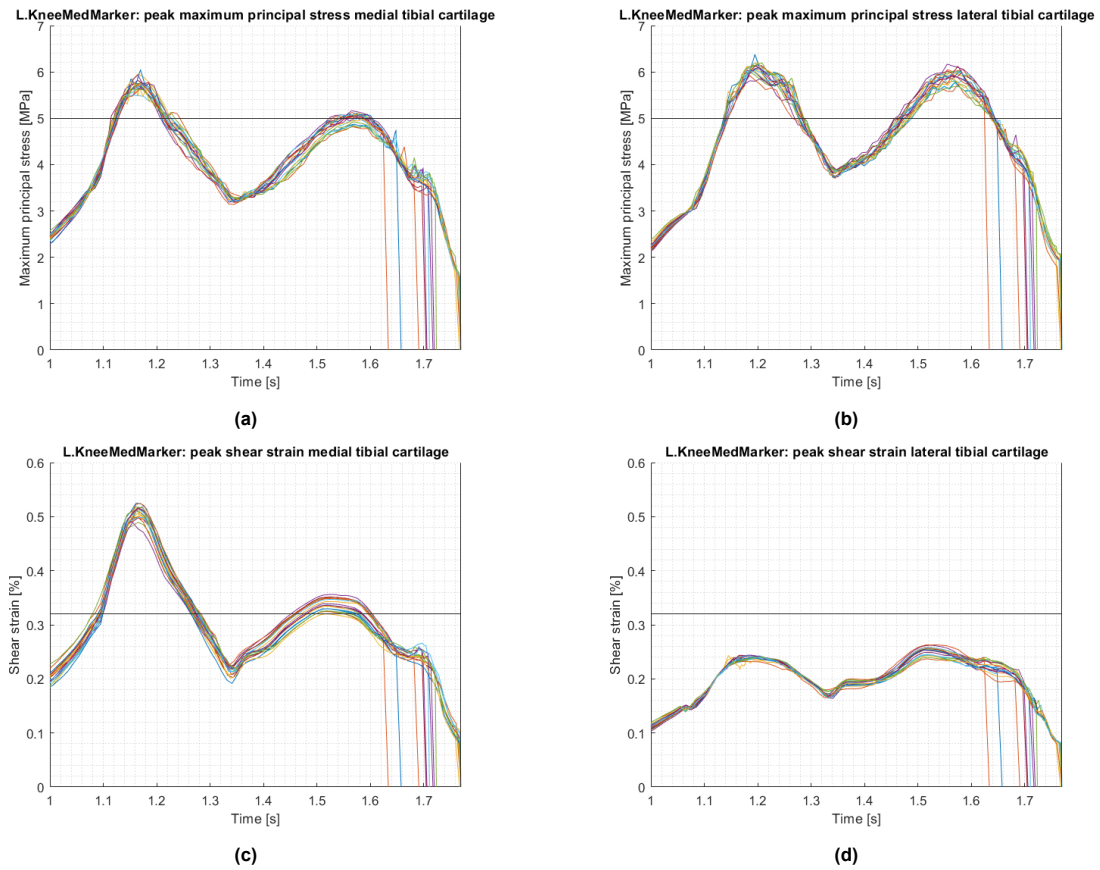


Figure 4.14: Peak maximum principal stress and shear strain in the medial tibial cartilage due to altered marker placement of the L.KneeMed marker. Vertical lines represent respective stress and strain threshold, responsible for cartilage degeneration.

4.3.5. L.KneeFib marker

Lastly, when inspecting the tissue mechanical response due to different L.KneeFib marker placements, the same two peaked curve was found for the peak maximum principal stress and maximum shear strain values of the medial and lateral tibial cartilage. For different L.KneeFib marker locations, 5/20 simulations did not reach full completion ($t=1.77$), but were still included (figure 4.15).

For the varied L.KneeFib marker placements a positive correlation was found for anterior-posterior marker placement and estimated peak maximum principal stress in the medial ($r=0.750$, $p=0.005$) and lateral cartilage ($r=0.613$, $p=0.026$). The same positive relationship was calculated for anterior-posterior marker placement and peak shear strains in the medial ($r=0.595$, $p=0.032$) and lateral cartilage ($r=0.902$, $p=0.000$). For the relationships between the individual marker placement directions and the number of elements above the stress and strain threshold throughout the stance phase, no significant relationships were found.

Peak maximum principal stress	L.Knee				L.KneeMed				L.KneeFib			
	Medial		Lateral		Medial		Lateral		Medial		Lateral	
Marker placement direction	<i>r</i>	<i>p</i>	<i>r</i>	<i>p</i>	<i>r</i>	<i>p</i>	<i>r</i>	<i>p</i>	<i>r</i>	<i>p</i>	<i>r</i>	<i>p</i>
Ant-post	-0.947	0.000	-0.959	0.000	-0.228	0.364	0.384	0.105	0.750	0.005	0.613	0.026
Prox-dist	-0.310	0.281	-0.213	0.446	0.051	0.899	0.040	0.870	0.066	0.838	0.470	0.105
Med-lat	0.463	0.095	0.488	0.065	0.032	0.840	-0.271	0.888	0.009	0.978	0.232	0.445

Table 4.4: Illustrates the relationship between marker placement direction and the peak maximum principal stress of the medial and lateral cartilage. *r* values are presented to quantify the possible relationship between marker placement direction and change in corresponding peak maximum principal stress. The probability that the observed effect would have happened by chance is expressed using the *p*-value (significance level).

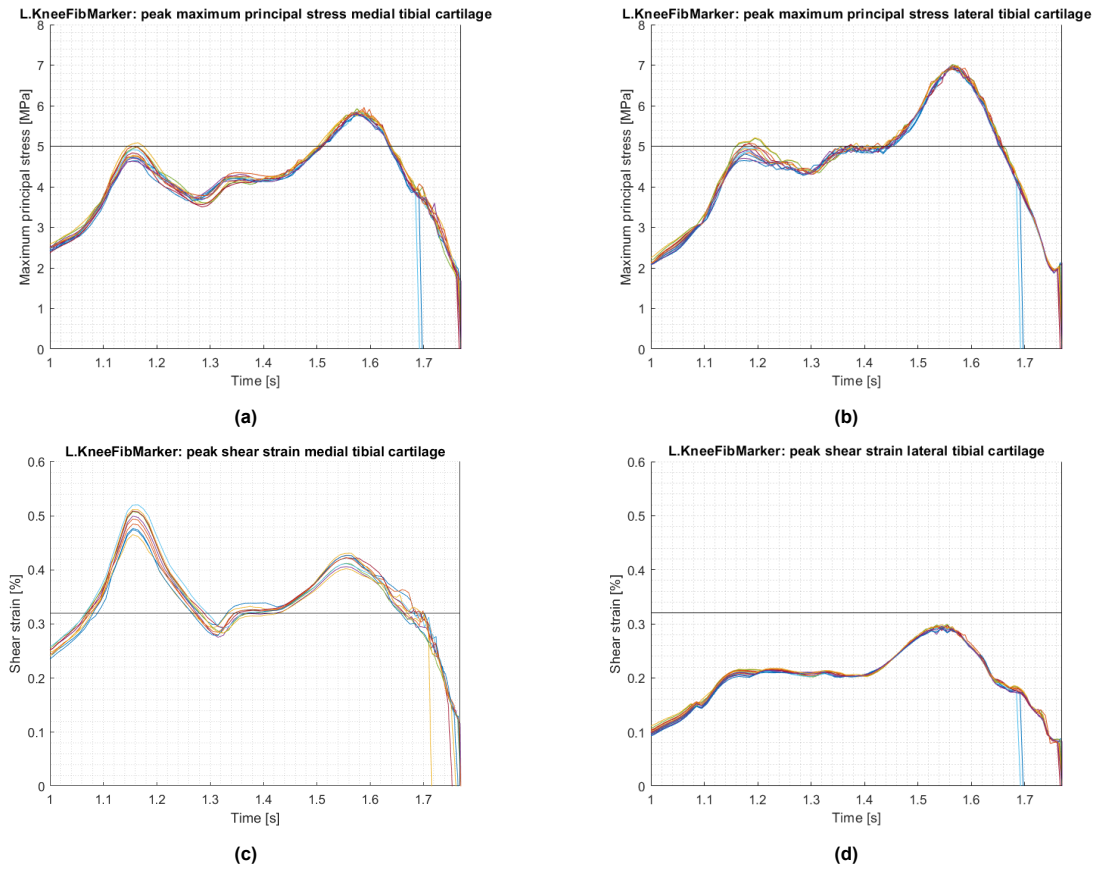


Figure 4.15: Peak maximum principal stress and shear strain in the medial tibial cartilage due to altered marker placement of the L.KneeFib marker. Vertical lines represent respective stress and strain threshold, responsible for cartilage degeneration.

Peak shear strain Cartilage	L.Knee				L.KneeMed				L.KneeFib			
	Medial		Lateral		Medial		Lateral		Medial		Lateral	
Marker placement direction	<i>r</i>	<i>p</i>	<i>r</i>	<i>p</i>	<i>r</i>	<i>p</i>	<i>r</i>	<i>p</i>	<i>r</i>	<i>p</i>	<i>r</i>	<i>p</i>
Ant-post	0.914	0.000	-0.972	0.000	0.822	0.000	-0.988	0.000	0.595	0.032	0.902	0.000
Prox-dist	0.521	0.047	0.543	0.037	0.346	0.147	-0.023	0.324	0.056	0.857	-0.002	0.096
Med-lat	-0.439	0.102	-0.219	0.433	-0.060	0.807	0.292	0.925	-0.335	0.263	0.482	0.995

Table 4.5: Illustrates the relationship between marker placement direction and the peaks shear strain of the medial and lateral cartilage. *r* values are presented to quantify the possible relationship between marker placement direction and change in corresponding peak shear strain. The probability that the observed effect would have happened by chance is expressed using the *p*-value (significance level).

Number of elements above stress threshold (5MPa) Cartilage	L.Knee				L.KneeMed				L.KneeFib			
	Medial		Lateral		Medial		Lateral		Medial		Lateral	
Marker placement direction	<i>r</i>	<i>p</i>	<i>r</i>	<i>p</i>	<i>r</i>	<i>p</i>	<i>r</i>	<i>p</i>	<i>r</i>	<i>p</i>	<i>r</i>	<i>p</i>
Ant-post	-0.942	0.000	-0.943	0.000	0.891	0.000	-0.271	0.261	0.186	0.563	-0.004	0.989
Prox-dist	-0.310	0.319	-0.274	0.323	0.335	0.175	0.069	0.778	-0.416	0.179	-0.222	0.466
Med-lat	0.504	0.066	0.465	0.080	-0.117	0.644	0.228	0.348	0.085	0.793	0.255	0.400

Table 4.6: Illustrates the relationship between marker placement direction and the average number of elements with a maximum principal stress value higher than the threshold stress (5 MPa). To quantify the potential correlation between marker placement direction and change in corresponding number of elements above the threshold stress value, *r* values are reported. The probability that the observed effect would have happened by chance is expressed using the *p*-value (significance level).

Number of elements above strain threshold (0.32%) Cartilage	L.Knee				L.KneeMed				L.KneeFib			
	Medial		Lateral		Medial		Lateral		Medial		Lateral	
Marker placement direction	<i>r</i>	<i>p</i>	<i>r</i>	<i>p</i>	<i>r</i>	<i>p</i>	<i>r</i>	<i>p</i>	<i>r</i>	<i>p</i>	<i>r</i>	<i>p</i>
Ant-post	-0.746	0.001	0	-	0.739	0.000	0	-	0.443	0.129	0	-
Prox-dist	-0.190	0.498	0	-	0.443	0.058	0	-	0.034	0.912	0	-
Med-lat	0.625	0.013	0	-	-0.265	0.272	0	-	-0.004	0.990	0	-

Table 4.7: Illustrates the relationship between marker placement direction and the average number of elements with shear strains higher than the threshold strain (0.32%) . To quantify the potential correlation between marker placement direction and change in corresponding number of elements above the threshold strain value, *r* values are reported. The probability that the observed effect would have happened by chance is expressed using the *p*-value (significance level).

4.4. Influence of marker placements on regions of high tissue mechanical response

The location of high stress and strain regions determines where cartilage degeneration takes place. Average locations of high stress and strain regions throughout the stance phase have been determined for the varying marker placements of the knee markers. Figure 4.16 represents the visualisation of the average high stress and strain regions inside both the medial and the lateral tibial cartilage. Results show that average high stress regions are located closely together varying only a few millimeters from one another.

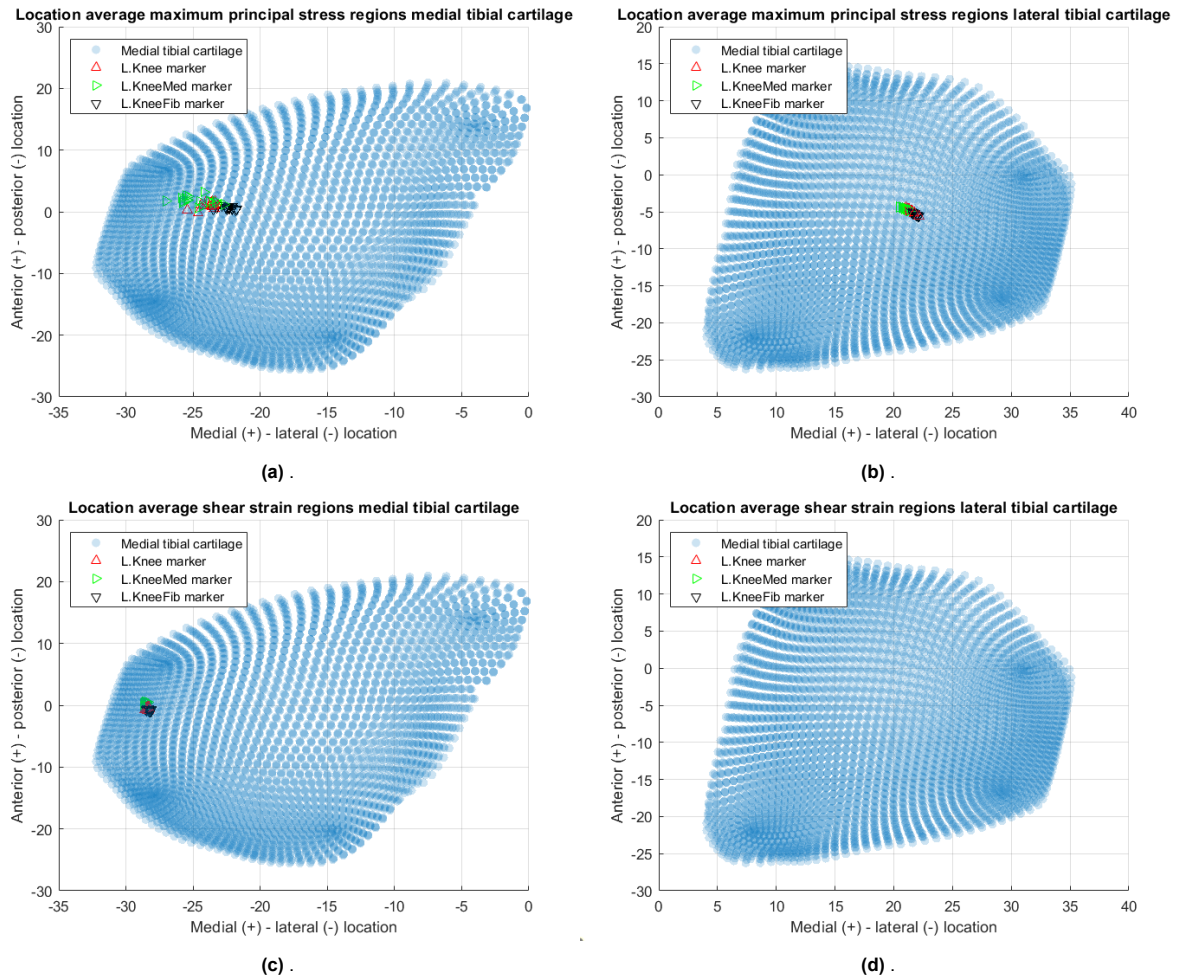


Figure 4.16: Average location of high stress/strain regions in the medial and lateral tibial cartilage.

To quantify the influence of knee marker placements on the corresponding location of high stress and strain regions, correlation coefficients were calculated. The results of this analysis can be found in the Appendix F, table F.1 and table F.2.

Anterior-posterior marker placement positively correlated with a change in location of the high stress region in the anterior direction for all knee markers. This relationship implies that a knee marker placed anteriorly to the anatomical landmark will result in a high stress region appearing more anteriorly in both the medial and lateral cartilage (see tab F.1 for correlation coefficients and p-values). Additionally, a negative correlation was calculated for the relationship between medial-lateral marker placement and anterior-posterior translation of the high stress region in both the medial and lateral tibial cartilage. Moreover, for the lateral cartilage a positive relationship was found for proximal-distal L.KneeFib marker placement and anterior-posterior translation of the high stress regions. Anterior-posterior marker placement positively correlated with a change in location of the high stress region in the proximal direction of

the medial cartilage for all knee markers. Additionally, anterior-posterior marker placement correlated negatively with proximal-distal translation of the high stress regions for L.Knee marker placements. For the L.KneeFib marker, proximal marker placement correlated negatively with proximal-distal translation of the high stress regions inside the lateral cartilage. A negative correlation was found for lateral medial translation of high stress regions and anterior-posterior marker placement of the knee markers in the medial and lateral cartilage. Additionally, a negative relationship was found between proximal-distal marker placement and lateral-medial translation of high stress regions for the L.KneeFib marker.

For mean locations of maximum shear strains a positive relationship was calculated for anterior-posterior marker placement and anterior-posterior translation of high strain regions for all knee markers in the medial cartilage. A negative relationship was found for anterior-posterior marker placement and proximal-distal translation of the high shear strain region for the L.Knee and L.KneeFib marker. For the L.KneeMed marker a positive relationship was calculated between anterior-posterior marker placement and proximal-distal translation of high shear regions. Additionally medial marker placement saw a positive correlation with proximal-distal translation of the high strain region. A positive relationship was seen for anterior-posterior marker placement and lateral-medial translation of the high shear region for the L.KneeMed marker. For the L.Knee and L.KneeFib marker a negative relationship was found between anterior-posterior marker placement and the lateral-medial translation of the high shear region. Medial translation of the L.Knee marker also resulted in lateral translation of the high strain region. Since the strain values in the components of the lateral tibial cartilage did not reach the threshold value, no relationship between marker placement position and the location of high strain regions could be detected for the lateral cartilage.

5

Discussion

Coupled workflows couple MSMs and FEMs together to calculate subject-specific tissue mechanical responses from gait analysis data. Coupled workflows may prove to be an effective technique for predicting the onset and progression of musculoskeletal disorders like OA. Coupled workflows that include the knee joint in particular could be useful because OA frequently develops in this joint, leading to discomfort, instability, and a general decline in quality of life. In gait analysis studies, marker placement forms one of the major sources of variability. Variability in marker placement thus forms one of the major sources of uncertainty in coupled workflow results. This uncertainty can directly impact the classification of patients musculoskeletal disorder based on severity (or existence) of the disorder. How this variability in gait analysis propagates in the musculoskeletal modelling and consequently the tissue mechanical response estimations of the FEM in a coupled workflow is currently unknown.

5.1. Results interpretation

To determine the influence of different knee marker placements on the tissue mechanical response computed in a coupled workflow, a sensitivity analysis was conducted. The sensitivity analysis was performed to answer the following research question:

How does marker placement of knee joint markers in gait analysis influence the tissue mechanical response calculated by a coupled workflow?

A number of sub-questions were created to assist in answering this question. The coupled workflow and the tissue mechanical response data were divided and examined separately in order to assess the influence of marker placements. The section that follows will provide the answers to the sub-questions.

5.1.1. How does knee marker location influence musculoskeletal modelling results in a coupled workflow?

Results on the influence of marker placement on musculoskeletal modelling results showed similar relationships between marker placement direction and corresponding musculoskeletal modelling results for all knee markers. According to this relationship, when knee markers were placed anteriorly to the anatomical landmark, MSM output saw an increase in maximum flexion angle during the stance phase of gait. A decrease in maximum axial compressive force and an increase in maximum anterior force and maximum medial force was also registered for these simulations. MSM output however was relatively unaffected for proximal-distal and medial lateral marker placement. The relationship between marker placement and knee flexion angle was similar to relationships found in literature [14, 37, 41]. The results indicate that anteriorly placed markers most certainly contribute to an overall increase in flexion angle during the stance phase of gait. This can be explained by the fact that changes in the anterior-posterior positions of knee markers cause misalignment of the primary and secondary axis of the femur and shank segments of the MSM. These alterations create a rotational offset in the flexion angle, while also resulting in cross-talk between segment axes [76, 77]. The negative relationship between anterior marker placement and the increase in maximum knee flexion during gait can also

explain the perceived increase in peak reaction force estimated for the knee joint. Figure 5.1 illustrates what muscles are responsible for contact forces in the knee during gait. The gastrocnemius muscle is responsible for a large deal of reaction force estimation [78]. The gastrocnemius muscle functions to plantar flex the foot at the ankle and flex the lower extremities at the knee [79]. When sprinting and walking straight, both roles are crucial for supporting the knee joint. The decrease in knee flexion due to posteriorly placed markers leads to an increase in gastrocnemius activation and subsequent force production, in order to successfully push off the foot during gait. As a result of this force production, the knee is compressed causing the increase in overall joint reaction forces. The variability is so prevalent in the second peak in axial compressive force, as in this phase of gait the gastrocnemius muscle is the dominant muscle in determining the size of the knee contact/reaction forces.

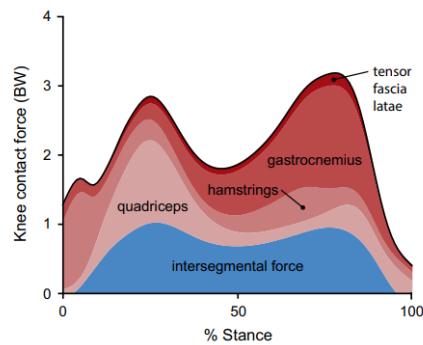


Figure 5.1: Contribution to knee contact/reaction forces during walking [78]

5.1.2. How does knee marker placement influence the finite element FEM knee kinematics in a coupled workflow?

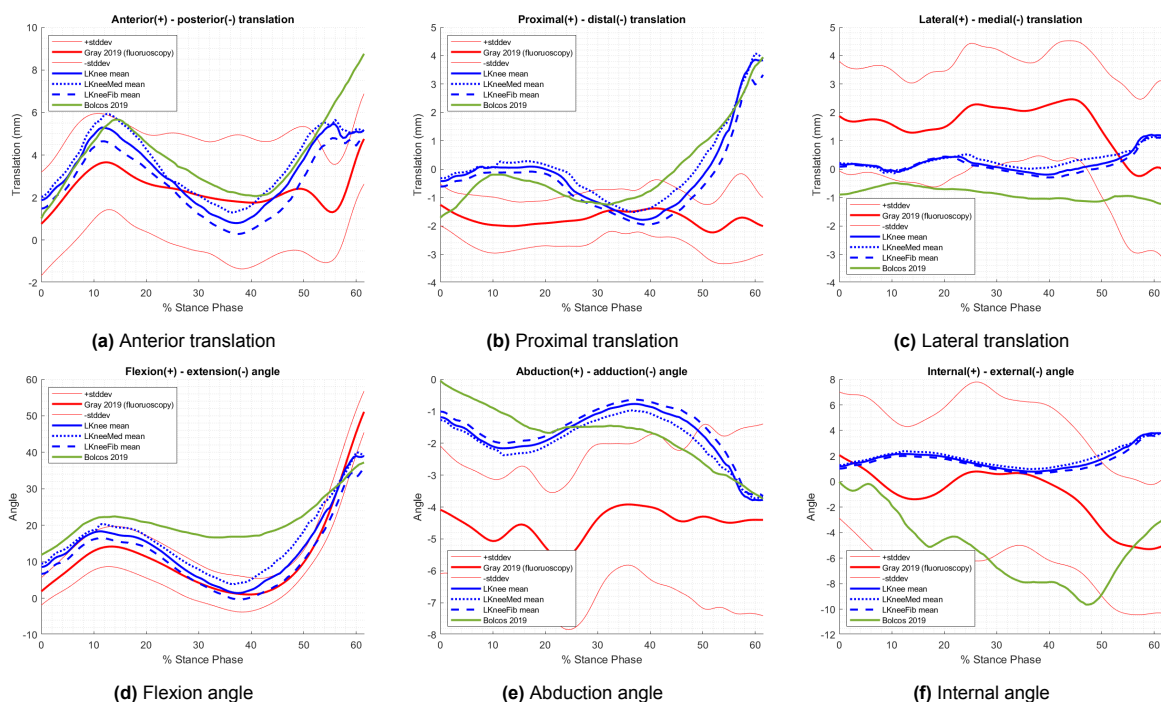


Figure 5.2: FEM kinematics of the knee joint in comparison with experimental measurements [80] and other coupled workflow results [17]. Curves show the mean translations and rotations for the displaced knee markers.

For simulations of different marker placements, the FEM knee's overall kinematics varied. Both translational and rotational kinematics were in the same order of magnitude as the kinematics found

in computational biomechanics studies [17, 81] and fluoroscopy data [80, 82] from literature (For a visualisation, figure 5.2). Nonetheless, the variations between the estimated kinematics, fluoroscopy results and coupled workflows from literature could be due to differences in applied boundary and loading conditions, knee orientations, gait style, FEM components or FEM material parameters.

Distal translation decreased with a decrease in axial compressive force for anterior marker placement. The peak anterior knee joint contact forces rose as a result of anterior marker placement in the knee, and translations also increased in the anterior direction. Though contradictory, the findings of lateral-medial translation, brought on by anteriorly positioned knee markers, demonstrated a negative correlation between the L. KneeFib marker. In turn, it showed a positive correlation between the anterior marker placement and lateral femur translation for the L. Knee and L. KneeMed markers. According to the literature, increased flexion angles are associated with an increase in lateral translation [83, 84, 85], which is consistent with the findings of the L.Knee and L.KneeMed marker variations. For now, the simulations of the L.KneeFib marker displacements generally generated rather high axial compressive forces (between 3150N and 3350N) and lower flexion angles (between 15.1 and 17.6), which appears to be the cause for the negative correlation between lateral-medial translation and anterior marker placement in comparison to simulations of the other markers. To provide additional context only individual peak values from the medial-lateral translation profile were compared to the directions of marker placement for the correlation coefficients. This increases the risk of including undesirable side effects because it's possible to choose the incorrect point for establishing correlations. Therefore, it's crucial to avoid being overly focused on the statistics results. For all knee marker perturbations, medial-lateral force and medial-lateral translation appear to be in the same order of magnitude and have similar patterns to values found in the literature.

For the rotational kinematics of the knee joint, no inconsistencies were found for relationships between marker placement direction and rotational kinematics. An anteriorly placed marker resulted in an increase in flexion angle as was the case for the MSM results. As the flexion-extension angle was the only angle directly applied as a boundary condition to the FEM, abduction-adduction and external-internal rotation were estimated as a result of component interactions of the FEM model. As abduction-adduction and external-internal rotation angles are difficult to capture from gait analysis data, having them originate from the tissue interactions is an advantage. This does however come with the cost of an increase in computational time, due to the added number of interactions. In FEBio free and prescribed rotations can not be combined for a single rigid body. To solve this inconvenience the femur and tibia were connected using three rigid cylindrical joints (as explained in Chapter 3). This way, only flexion-extension rotations could be applied while having abduction-adduction and external-internal rotation derive from interaction of the components of the knee joint. These constraints produce reaction forces and moments that are enforced with penalty parameters. The penalty parameters can be conceptualised as stiffnesses of linear/torsional springs that prevent relative translations/rotations of the rigid bodies (femur and tibia) along DoFs that must remain constrained for that joint. In the FEM, penalty parameters were automatically adjusted to an appropriate value [86, 54]. Due to penalty parameter adjustments, the flexion rotations in the FEM deviated slightly from the input flexion angles calculated in the MSM. The FEM model estimated median values of the maximum flexion angle of the L.Knee and L.KneeFib marker displacements were approximately 8% lower for the FEM estimations than for the MSM.

Not all simulations involving various marker placements were able to run their full course with success. FEM simulations can fail for a variety of reasons. The majority of the simulations that ended prematurely had higher axial compressive force values ($\approx 3100\text{N}$). As a result, the FEM might have not been able to handle the imposed forces. A reason for this could be that the mesh quality deteriorates under too much compression. Using a refined mesh in this case would solve the problem. Another solution would be to strengthen the FEM component's material parameters, although doing so reduces the FEM's accuracy to the physiological knee. Another reason for the failed simulations could be that FEBio was not able to find a converging solution for the given time settings. In general in FEBio static FEM simulation results are independent of time step. However, in this case time dependency was built into the model by including load curves for flexion and knee contact force application. As a result the FEM software can have difficulty finding a solution. This can happen when the solution is too far from the initial model configuration. To test this, a series of failed and successfully completed marker placements were re-run using a smaller time step setting. This method improved simulations for some of the failed marker placements, while inducing errors for other previously successfully running simulations.

Table 5.1: Average standard error of the estimate describing the error associated with predicting knee kinematics from skin marker derived kinematic from the study by Benoit *et al.* [35] and the maximum differences in knee kinematics results due to variation of knee marker placement.

Translations (mm)	Average standard error	L.Knee	L.KneeMed	L.KneeFib
Anterior-posterior	5.9	1.3	1.2	0.9
Proximal-distal	6.8	0.4	0.5	0.3
Lateral-medial	2.7	0.1	0.1	0.1
Rotations (°)				
Flexion-extension	2.5	3.6	4.7	2.6
Abduction-adduction	3.6	0.3	0.4	0.2
Internal-external	2.9	0.2	0.1	0.2

This was presumably the case because in some cases a simulation with a smaller time step caused load curves to be imposed on the FEM which cause instability. Building in an automatic re-run option that restarts simulations with a smaller time step in case a simulation fails prematurely is one way to address this issue in future coupled workflows. However, this significantly lengthens the workflow's run time, hence it was omitted from this study. Additionally, the aim was to develop a workflow to investigate the influence of marker placements on the tissue mechanical response calculated, rather than to develop a workflow that could perform 100% of the simulations successfully.

Whether the findings on the relationship between marker movement and corresponding knee kinematics estimations can be fully explained by altered marker placement is another issue. A study performed by Benoit *et al.* tried to quantify the error caused by skin movement artifacts when reporting the kinematics of the knee joint. This was done by comparing kinematics from gait analysis from subject's equipped with skin mounted markers versus subject's where markers were directly attached to the anatomical landmarks using bone pins [35]. Results showed considerable differences between the measurement techniques. Skin movement may even be large enough to conceal the actual movements of the knee joint, thus making reporting of knee joint kinematics using skin markers potentially uncertain. For this study this might also be the case as ranges in kinematics results due to different knee marker placements in all cases (except for flexion-extension angle) showed to be within the estimated standard error due to skin marker movement as estimated by Benoit *et al.* (see table 5.1). In analysing coupled workflow results it remains unclear whether perceived behaviour was caused by marker placement or skin movement artefacts.

5.1.3. How does knee marker placement influence the magnitude of the tissue mechanical response in the articular cartilage of the knee joint?

Peaks in maximum principal stress and shear strains coincided with the two peaked curve of axial compressive force. This load curve represents the largest force during the stance phase. As the elements of the cartilage experience the highest stresses and strains for simulations with high axial compressive force, it is assumed that the axial compressive force is predominantly responsible for the high stresses/strains of the cartilage elements.

When comparing the correlations between marker placement, peak maximum principal stress, and peak shear strain values, dissimilar relations were found for the different markers. For example, for perturbations of L.Knee markers, anterior placement of the L.Knee marker resulted in a decrease in peak maximum principal stress for the medial and lateral cartilage. In contrast for the L.KneeFib marker an increase in peak maximum principal stress is perceived in the lateral cartilage for anterior marker placement of the knee. This discrepancy in results could be caused by the fact that for calculating correlation coefficients, marker placements along different directions were compared to peak (maximum) points throughout the maximum principal stress and shear strain curves. Therefore, errors in peak value estimations due to noise in the tissue mechanical response curves of the FEM could have had great impact on the calculation of correlation coefficients. A coefficient estimation containing more simulation results should improve correlation estimations. Another option would be to decrease the time step of the FEM simulations in order to generate smoother stress and strain profiles. This however comes with an increase in computational time. An alternative solution for future research would be to interpolate the noisy tissue mechanical responses to generate smooth stress and strain profiles.

To accommodate for the limits of looking only at peak values of stress and strain, a measure that counted the number of elements that surpassed the stress or strain threshold during the stance phase

of gait for the marker perturbations was added. Here, once again, correlation results showed different results for the relationships between marker placement direction and cumulative stress and strain for the different knee markers. Although correlation values showed to be contradicting (having different sign conventions for the same marker displacement direction for different markers), the simulations of altered L.KneeFib markers generally showed the highest number of elements above the maximum principal stress threshold in the medial and lateral cartilage. The L.KneeFib marker was followed by the L.Knee marker and generally the L.KneeMed marker showed the smallest number of elements exceeding the stress threshold in the medial and lateral cartilage. This corresponds with the theory that an increase in axial compressive force causes an increase in perceived maximum principal stress. For the number of elements exceeding the shear strain threshold, different behaviour was found in which the L.Knee marker perturbations showed the lowest number of elements exceeding the shear strain threshold. More research is necessary to demonstrate whether this is an exception or whether there is an underlying mechanism dictating shear strain throughout the tibial cartilage.

Tissue mechanical response values varied considerably throughout literature. In a study by Bolcos *et al.* maximum principal stress values in the tibial cartilage were found varying inbetween 0 and 4 MPa during the stance phase of gait [17]. In another study of Bolcos, maximum principal stress values varied between 0 and 15 MPa for the stance phase of gait. In the same study, maximum shear strain values varied up to 20% using the same workflow for different patients [39]. A study performed by Esrafilian *et al.* found maximum principal stress values range from 0 to 4MPa for the stance phase of gait [81]. Looking at the tissue mechanical response values in this study it can be concluded that the maximum principal stress and shear strain values showed a pattern and magnitude similar to the results found in the literature [17, 81, 39].

Numerous factors can contribute to the heterogeneity in tissue mechanical response that was observed in comparison to values found in literature. These can be categorised roughly into three groups: boundary & loading conditions, model components, and material models. A study performed by Bolcos *et al.* [17] which compared kinetic and kinetic-kinematic driven knee joint finite element models, showed variations in FEM knee kinematics and maximum principal stress using different input loading and boundary conditions. The same study also did research on the tissue mechanical response calculated by models including and excluding the PF joint. While all results showed similar patterns and orders of magnitude, differences of up to 50% could still be found for output parameters like maximum principal stress due to differences in boundary & loading conditions and model components. One of the reasons for the difference in results could be the material models used in the FEM. The adjusted OK model used for this coupled workflow used a Neo-Hookean hyperelastic and Fung orthotropic representation for the cartilage and the menisci in the model. Models in literature often incorporate more complex poroviscoelastic or fibril-reinforced poroviscoelastic material properties [17, 81], which are able to simulate the time dependent behaviour of cartilage [87]. Research comparing different material models for cartilage show that the Neo-Hookean model overpredicts stress at high strain values and underpredicts stress at low strain values [87]. However, when the results were evaluated over the entire range of strains, average contact stress, contact area, and qualitative contact, patterns were indistinguishable between the relatively simple Neo-Hookean and more complex cartilage representations [87]. This study therefore concluded that a simple Neo-Hookean model is sufficient to provide predictions that were in reasonable agreement with experimental measurements.

5.1.4. How does knee marker placement influence the location of the tissue mechanical response in the articular cartilage of the knee joint?

Not only hyperphysiologic magnitudes of loading but also stress and shear strain accumulation in altered regions of cartilage add to the degeneration of OA [74]. In the last analysis, mean locations of high stresses and strains were compared to marker placement directions of the knee markers. The association between marker placement direction and the location of high stress regions revealed comparable relationships for the various knee markers. Generally, anteriorly placed markers resulted in a high stress region being placed more anteriorly, proximal, and medial to the original location for the medial cartilage. While the high stress regions shifted anteriorly, distal, and medially in the lateral cartilage.

For the location of high shear strain regions dissimilar relationships were found for the shift in high strain location and marker placement direction for the different knee markers. A possible reason for this dissimilarity could be the role of outliers of high stress/strain elements throughout the analysis.

Outliers could contain elements with sub-optimal shape which therefore experience high stress and strain values which are not present in the physiological knee. To mitigate this problem in future studies an extra condition could be set to analyse the location of high stress/strain regions. This condition could impose an additional requirement that the area of high stress and strain regions should exceed a specific size before being taken into account.

There were no records of studies looking into how marker placement affected the location of high stress and strain regions for coupled workflows. In this study, a measure for the mean location of high stress/strain regions throughout the stance phase was derived. FEM studies in literature on tissue mechanical response results in the knee looked at the stress or strain profile at a given time point. Choosing an alternative method made it difficult to compare results to stresses and strains from established literature. However, comparing the mean locations of high stress/strain regions is an advantage over other methods because cartilage degeneration results from not only excessive stress and strain but also from the accumulation of stress and strain [74].

5.2. Limitations and recommendations for future research

The following section contains limitations and recommendations for future research. These are handled in accordance with the section of the coupled workflow to which they belong.

5.2.1. Data acquisition

Only a single run from one subject was used to gather gait data, which may not represent kinematics and kinetics of different subjects [56]. Especially as the subject, had ACL reconstruction surgery on his right leg. This however will mostly influence the size of the tissue mechanical response estimations and not so much influence the differences in model behaviour due to knee marker misplacement. Nevertheless, it would be beneficial to include a variety of subjects in future research. Additionally, a postdoctoral researcher and master student with no prior clinical experience in gait analysis studies planted markers in a university lab environment. The lack of clinical experience suggests that there could be some sort of inaccuracy in determining the location of the anatomical landmark. This could have negatively affected the joint coordinate system definition in the Gait2392 model. However, knee marker locations were virtually displaced while other knee marker locations did not vary in assessing the effect of knee marker placement. Therefore, we concluded that this inherent error has low impact on the results of this study. In addition, there were only 20 marker displacements per knee marker ($3 \times 20 = 60$ in total). While 20 marker placements within the predetermined area should explain the relationship between marker placement and subsequent tissue mechanical response, using only a limited number of markers increases the chances of biased results. Increasing the sample size could be a valid solution to mitigate the effect of failed simulations, reduce possible errors in simulations, and increase confidence in statistics results. Furthermore, the subject of the construction and the analysis of the coupled modelling workflow did not have an instrumented prosthesis, therefore direct validation of simulation results was not possible.

5.2.2. Musculoskeletal modelling

Moreover, the MSM model included only a single DoF. Some sources claim that only one rotational DoF for the knee works well to assess overall walking parameters, but is less well suited for a detailed study of the knee [88, 89]. The accuracy of muscle force and joint contact force estimations which were crucial in coupled workflow behavior can be improved by expanding the MSM's DoF.

It would be beneficial to compare different MSM outputs from several MSM models with different knee joint DoFs in later studies. The OpenSim JAM model would be a good starting point. In this model, the knee joint is represented as a 12 DoF (6 DoF PF and 6 DoF TF) joint [90]. This enables for direct application of all rotational and translational DoFs as boundary & loading conditions in the FEM of a coupled workflow.

5.2.3. Finite element modelling

The OK model is a generic knee model based on a 70 year old (77.2 kg) female donor. The knee joint's geometry therefore does not correspond to the geometry of the subject's knee joint. For the estimation of subject-specific tissue mechanical responses in future studies, it is important to not only include subject-specific gait data but also a FEM knee which is based on the subject's knee geometry

[91].

The adjusted version of the OK generation 1 model which was utilised in this study did not include the PF joint. The primary purpose of the PF joint is to increase the extensor mechanism's lever arm, hence boosting the quadriceps' efficiency. Additionally, force and moment driven models overestimate femoral translations in the anterior-posterior direction when the PF joint is not included. For this reason, in order to generate a functional FEM and match experimental translation values, the estimated anterior-posterior force had to be scaled to 50%. Manually scaling muscle forces, however, carries the possibility of unintentional bias on the part of the researcher. To lessen the possibility that this will affect upcoming modelling outcomes, a FEM which takes the PF joint into account would be well worth looking into. The PF joint is included in the generation 2 OK model, although simulations using this model have shown to be substantially more time consuming, making it less suitable for fast analyses of knee biomechanics.

For quick examination of knee biomechanics in the OK model, material models have been kept quite simple as described earlier in this chapter. However, the time-dependent material behavior of cartilage cannot be simulated by the material models currently employed. Follow-up studies should examine whether this simplification would impact coupled workflow estimations. Comparing the modelling outcomes of research that makes use of material models that more accurately reflect the physiological cartilage of the knee can accomplish this.

Since the MCL and LCL components kept on failing during simulation, the original OK model's 3D representation of the ligaments was changed to linear springs for the MCL and LCL. For the spring stiffness literature was consulted. However, in literature, ligament stiffness values are frequently derived from cadaveric research. Moreover, literature shows a wide variety of potential stiffness levels which do not necessarily comply with the ligament characteristics [17, 59, 64, 57, 92]. The force generated by the springs also originated from a single node on the femur and tibia when the MCL and LCL are represented as springs. For this reason, an analysis was conducted to determine how the insertion location affected the kinematics of the knee. This analysis showed that knee's external rotation is exceptionally sensitive to insertion location. This finding may be of great importance in follow-up research. Literature showed that external rotation is not so much responsible for the magnitude of the tissue mechanical response but rather for the location of the application [17]. Therefore, it is a crucial factor in research on OA and other degenerative joint diseases. To ensure that the ligaments are accurately modeled, additional research on ligament representation and insertion position is needed. An alternative solution would be to directly apply external-internal rotations from a MSM, like the OpenSim JAM model as described earlier.

Lastly, in the knee, menisci and tibial cartilage are joined by peripheral attachments. In some studies, springs have been inserted between the menisci and the tibial cartilage to mimic these attachments [93]. However in most studies, the peripheral attachments were completely ignored and the contact was modeled as a smooth surface. This contact definition is only effective in simple load scenarios that do not involve femur anterior-posterior and medial-lateral translations. Therefore, in order to simulate the peripheral attachment, a friction coefficient of 0.5 was assigned for the contact between the menisci and tibial cartilage. This friction coefficient was picked so that FEM knee kinematics would approximate the values found in literature. It would be advisable to do an additional sensitivity analysis of the influence of the friction coefficient on knee biomechanics results for the model in future investigations.

5.2.4. The workflow

In the design of the workflow, the focus was on marker displacement. Skin movement artefacts were not considered among the different positions of the knee markers. Studies on skin movement artefacts reported that these could vary in between 10–30mm on the shank and thigh [68], and up to 40mm dependent upon the specific body segment [94, 95]. This range coincides with the range taken for the marker displacement of the workflow. As a result, when analysing the influence of marker placement, it remained unclear whether the perceived coupled workflow behaviour could be attributed to marker placement or skin movement artefacts. This question can be answered by redoing the experiment using gait data obtained in a fluoroscopic imaging system [82]. This way, the actual anatomical landmarks can be tracked throughout gait. By using this setup it is possible to discern between errors induced by altered marker placement and skin movement artefacts. Lastly, this study did not investigate the interaction effect of simultaneously altering multiple knee marker placements. Future studies should examine the impact of altering several knee markers at once.

5.3. How does this study move the field forward?

The influence of knee marker movement was demonstrated by the coupled workflow modelling results. It has been demonstrated that marker movement, particularly along the anterior-posterior direction, has a significant influence on the tissue mechanical response values computed using a coupled workflow. The study's findings have enabled for a better understanding and interpretation of the potential range of stresses and strains that could exist for specific input values in coupled workflows. For knee marker movement between 0-30mm this study reported that peak maximum stress readings could fluctuate by up to 0.60 MPa and peak shear strain by up to 0.08 %. Wider relative ranges were reported for cumulative stress levels. Overall, the workflow seems to be quite robust to changes in marker placement as changes in FEM knee behaviour due to altered knee marker placement did not exceed the standard error induced by skin movement artefacts (see table 5.1). This, however, also raised the issue that in a clinical setting it would be unclear whether the changes in tissue mechanical response were caused by altered marker placement or skin movement artefacts. This study suggests that when interpreting results from a coupled workflow using skin marker data to describe knee joint motion, a kinematics and tissue mechanical response standard error should be incorporated in the interpretation of the results. Furthermore, factors like ligament representation and insertion location have proven to be crucial factors in determining the knee biomechanics. This shows the importance of correct joint representation for correct simulation of stresses and strains in the cartilage of the knee joint. All things considered, the proposed coupled modelling workflow was able to compute tissue mechanical response values for changed marker placements quickly and with limited knee marker data. Simple musculoskeletal and finite element models were employed for the workflow, enabling simple use and intuitive comprehension of the phenomena. The coupled workflow's ability to produce tissue mechanical response values in the same order of magnitude as workflows employing much more complicated and computationally intensive models is what makes it so valuable.

6

Conclusion

To conclude, coupled modelling workflows have proven to be an emerging modelling technique for research on musculoskeletal disorders like OA. In OA, tissue mechanical response parameters like maximum principal stress and shear strain are thought to play an integral role in cartilage degeneration. To estimate the tissue mechanical response values, coupled workflows come into play. Coupled workflows couple MSM to FEM to estimate tissue mechanical responses from gait analysis data. Variability in marker placement forms one of the major sources of error in gait analysis studies. It, however, is still unknown how the possible error from incorrect marker placement affects coupled workflow results. To study this, the design of a coupled workflow has been realised. Additionally, a sensitivity analysis was performed investigating the influence of marker placement on the tissue mechanical response calculated by the coupled workflow. The coupled workflow has shown to be especially sensitive to anterior-posterior marker movement. This highlights the importance of proper marker placement in gait analysis studies. The workflow has proven to be relatively robust as changes in coupled workflow results due to altered marker placement fell within the expected margin of error caused by skin movement artefacts. This study therefore suggests to incorporate some standard error margin when interpreting coupled workflow results. Such a margin could inform researchers on the possible ranges of stress and strain inside the articular cartilage of the knee and the subsequent onset and progression of OA. Improving FEM design to accommodate for the subject-specific loading imposed by the gait data revealed the sensitivity of the model outcomes to FEM model components and material properties. This confirms that calibration of these parameters is critical and using literature values may not be appropriate. In future research, a coupled modelling workflow that includes subject-specific knee geometry and a larger subject set measured with a fluoroscopic imaging system could pave the way for coupled modelling workflows to be used to help clinical decision-making for musculoskeletal disorders like OA.

References

- [1] Alarcos Cieza et al. “Global estimates of the need for rehabilitation based on the Global Burden of Disease study 2019: a systematic analysis for the Global Burden of Disease Study 2019”. In: *The Lancet* 396.10267 (2020), pp. 2006–2017.
- [2] Bhushan R Deshpande et al. “Number of persons with symptomatic knee osteoarthritis in the US: impact of race and ethnicity, age, sex, and obesity”. In: *Arthritis care & research* 68.12 (2016), pp. 1743–1750.
- [3] Timothy M Griffin and Farshid Guilak. “The role of mechanical loading in the onset and progression of osteoarthritis”. In: *Exercise and sport sciences review* 33 (4 2005), pp. 195–200.
- [4] Xiaogang Wang, Corey P. Neu, and David M. Pierce. “Advances toward multiscale computational models of cartilage mechanics and mechanobiology”. In: *Current Opinion in Biomedical Engineering* 11 (Sept. 2019), pp. 51–57. ISSN: 24684511. DOI: 10.1016/j.cobme.2019.09.013.
- [5] G Kelley Fitzgerald, Sara R Piva, and James J Irrgang. “Reports of joint instability in knee osteoarthritis: its prevalence and relationship to physical function”. In: *Arthritis care & research* 51.6 (2004), pp. 941–946.
- [6] Jesper Knoop et al. “Association of lower muscle strength with self-reported knee instability in osteoarthritis of the knee: Results from the Amsterdam Osteoarthritis Cohort”. In: *Arthritis care & research* 64.1 (2012), pp. 38–45.
- [7] Genevieve Fleeton et al. “Self-reported knee instability before and after total knee replacement surgery”. In: *Arthritis care & research* 68.4 (2016), pp. 463–471.
- [8] Leena Sharma et al. “Knee instability and basic and advanced function decline in knee osteoarthritis”. In: *Arthritis care & research* 67.8 (2015), pp. 1095–1102.
- [9] U-SDT Nguyen et al. “The impact of knee instability with and without buckling on balance confidence, fear of falling and physical function: the Multicenter Osteoarthritis Study”. In: *Osteoarthritis and cartilage* 22.4 (2014), pp. 527–534.
- [10] Farshid Guilak. “Biomechanical factors in osteoarthritis”. In: *Best practice & research Clinical rheumatology* 25.6 (2011), pp. 815–823.
- [11] Friedmar Graichen et al. “Implantable 9-channel telemetry system for in vivo load measurements with orthopedic implants”. In: *IEEE transactions on biomedical engineering* 54.2 (2007), pp. 253–261.
- [12] Benjamin J Fregly et al. “Grand challenge competition to predict in vivo knee loads”. In: *Journal of orthopaedic research* 30.4 (2012), pp. 503–513.
- [13] Liming Shu et al. “Multiscale finite element musculoskeletal model for intact knee dynamics”. In: *Computers in Biology and Medicine* (Nov. 2021), p. 105023. ISSN: 00104825. DOI: 10.1016/j.compbiomed.2021.105023. URL: <https://linkinghub.elsevier.com/retrieve/pii/S0010482521008179>.
- [14] Mickael Fonseca et al. “Impact of knee marker misplacement on gait kinematics of children with cerebral palsy using the Conventional Gait Model—A sensitivity study”. In: *PLoS ONE* 15 (4 Apr. 2020). ISSN: 19326203. DOI: 10.1371/journal.pone.0232064.
- [15] DI Chen et al. “Osteoarthritis: toward a comprehensive understanding of pathological mechanism”. In: *Bone research* 5.1 (2017), pp. 1–13.
- [16] Irene S. Davis and Christopher M. Powers. “Patellofemoral pain syndrome: proximal, distal, and local factors, an international retreat, April 30-May 2, 2009, Fells Point, Baltimore, MD.” In: vol. 40. *Movement Science Media*, 2010. DOI: 10.2519/jospt.2010.0302.
- [17] “Comparison between kinetic and kinetic-kinematic driven knee joint finite element models”. In: *Scientific Reports* 8 (1 Dec. 2018). ISSN: 20452322. DOI: 10.1038/s41598-018-35628-5.

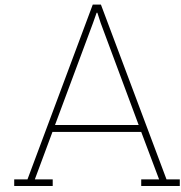
- [18] Satanik Mukherjee et al. "Use of computational modeling to study joint degeneration: a review". In: *Frontiers in Bioengineering and Biotechnology* 8 (2020), p. 93.
- [19] AJ Baliunas et al. "Increased knee joint loads during walking are present in subjects with knee osteoarthritis". In: *Osteoarthritis and cartilage* 10.7 (2002), pp. 573–579.
- [20] KS Halonen et al. "Workflow assessing the effect of gait alterations on stresses in the medial tibial cartilage-combined musculoskeletal modelling and finite element analysis". In: *Scientific reports* 7.1 (2017), pp. 1–14.
- [21] T Miyazaki et al. "Dynamic load at baseline can predict radiographic disease progression in medial compartment knee osteoarthritis". In: *Annals of the rheumatic diseases* 61.7 (2002), pp. 617–622.
- [22] Mimmi K Liukkonen et al. "Simulation of subject-specific progression of knee osteoarthritis and comparison to experimental follow-up data: data from the osteoarthritis initiative". In: *Scientific reports* 7.1 (2017), pp. 1–14.
- [23] Wouter Wilson et al. "Causes of mechanically induced collagen damage in articular cartilage". In: *Journal of Orthopaedic Research* 24.2 (2006), pp. 220–228.
- [24] Emily S Gardinier et al. "Altered loading in the injured knee after ACL rupture". In: *Journal of Orthopaedic Research* 31.3 (2013), pp. 458–464.
- [25] Jason M Konrath et al. "Muscle contributions to medial tibiofemoral compartment contact loading following ACL reconstruction using semitendinosus and gracilis tendon grafts". In: *PLoS One* 12.4 (2017), e0176016.
- [26] Elizabeth Wellsandt et al. "Decreased knee joint loading associated with early knee osteoarthritis after anterior cruciate ligament injury". In: *The American journal of sports medicine* 44.1 (2016), pp. 143–151.
- [27] Bruce S Gardiner et al. "Predicting knee osteoarthritis". In: *Annals of biomedical engineering* 44.1 (2016), pp. 222–233.
- [28] Mika E Mononen et al. "New algorithm for simulation of proteoglycan loss and collagen degeneration in the knee joint: data from the osteoarthritis initiative". In: *Journal of Orthopaedic Research* 36.6 (2018), pp. 1673–1683.
- [29] EK Danso et al. "Comparison of nonlinear mechanical properties of bovine articular cartilage and meniscus". In: *Journal of biomechanics* 47.1 (2014), pp. 200–206.
- [30] Lorenza Henao-Murillo, Keita Ito, and Corrinus C van Donkelaar. "Collagen damage location in articular cartilage differs if damage is caused by excessive loading magnitude or rate". In: *Annals of biomedical engineering* 46.4 (2018), pp. 605–615.
- [31] Lorenzo Chiari et al. "Human movement analysis using stereophotogrammetry: Part 2: Instrumental errors". In: *Gait & posture* 21.2 (2005), pp. 197–211.
- [32] Valentina Camomilla et al. "Methodological factors affecting joint moments estimation in clinical gait analysis: a systematic review". In: *Biomedical engineering online* 16.1 (2017), pp. 1–27.
- [33] Alberto Leardini et al. "Human movement analysis using stereophotogrammetry: Part 3. Soft tissue artifact assessment and compensation". In: *Gait & posture* 21.2 (2005), pp. 212–225.
- [34] Ugo Della Croce et al. "Human movement analysis using stereophotogrammetry: Part 4: assessment of anatomical landmark misplacement and its effects on joint kinematics". In: *Gait & posture* 21.2 (2005), pp. 226–237.
- [35] Daniel L Benoit et al. "Effect of skin movement artifact on knee kinematics during gait and cutting motions measured in vivo". In: *Gait & posture* 24.2 (2006), pp. 152–164.
- [36] AW Zürcher et al. "The Femoral Epicondylar Frame to track femoral rotation in optoelectronic gait analysis". In: *Gait & Posture* 33.2 (2011), pp. 306–308.
- [37] Ewa Szczerbik and Małgorzata Kalinowska. *The influence of knee marker placement error on evaluation of gait kinematic parameters*. 2011. URL: <https://www.researchgate.net/publication/51812506>.

- [38] B Groen et al. "O048 Sensitivity of the OLGA and VCM models to erroneous marker placement in 3D-gait analysis". In: *Gait & Posture* 28 (2008), S34.
- [39] Paul O Bolcos et al. "Identification of locations susceptible to osteoarthritis in patients with anterior cruciate ligament reconstruction: Combining knee joint computational modelling with follow-up T1 ρ and T2 imaging". In: *Clinical Biomechanics* 79 (2020), p. 104844.
- [40] Fabio Galbusera et al. "Material models and properties in the finite element analysis of knee ligaments: a literature review". In: *Frontiers in bioengineering and biotechnology* 2 (2014), p. 54.
- [41] Thomas K. Uchida and Ajay Seth. "Conclusion or Illusion: Quantifying Uncertainty in Inverse Analyses From Marker-Based Motion Capture due to Errors in Marker Registration and Model Scaling". In: *Frontiers in Bioengineering and Biotechnology* 10 (May 2022). ISSN: 22964185. DOI: 10.3389/fbioe.2022.874725.
- [42] David C Ackland, Yi-Chung Lin, and Marcus G Pandy. "Sensitivity of model predictions of muscle function to changes in moment arms and muscle–tendon properties: a Monte-Carlo analysis". In: *Journal of biomechanics* 45.8 (2012), pp. 1463–1471.
- [43] Julien Favre and Brigitte M Jolles. "Gait analysis of patients with knee osteoarthritis highlights a pathological mechanical pathway and provides a basis for therapeutic interventions". In: *EFORT open reviews* 1.10 (2016), pp. 368–374.
- [44] Georgios I Papagiannis et al. "Gait analysis methodology for the measurement of biomechanical parameters in total knee arthroplasties. A literature review". In: *Journal of Orthopaedics* 15.1 (2018), pp. 181–185.
- [45] MATLAB. 9.7.0.1190202 (R2020b). Natick, Massachusetts: The MathWorks Inc., 2020.
- [46] *Explore your biomechanical data in several ways*. URL: <https://biomechanical-toolkit.github.io/mokka/>.
- [47] *OpenSim: Project Home*. URL: <https://simtk.org/projects/opensim>.
- [48] URL: <https://simtk-confluence.stanford.edu:8443/display/OpenSim/Gait+2392+and+2354+Models>.
- [49] Gary T Yamaguchi and Felix E Zajac. "A planar model of the knee joint to characterize the knee extensor mechanism". In: *Journal of biomechanics* 22.1 (1989), pp. 1–10.
- [50] Scott L Delp et al. "An interactive graphics-based model of the lower extremity to study orthopaedic surgical procedures". In: *IEEE Transactions on Biomedical engineering* 37.8 (1990), pp. 757–767.
- [51] Yichen Lu et al. "A comparative study on loadings of the lower extremity during deep squat in Asian and Caucasian individuals via OpenSim musculoskeletal modelling". In: *BioMed Research International* 2020 (2020).
- [52] Steve A Maas et al. "FEBio: finite elements for biomechanics". In: *Journal of biomechanical engineering* 134.1 (2012).
- [53] A Erdemir. "Open Knee (s): Virtual Biomechanical Representations of the Knee Joint". In: *SimTK*, accessed Oct 21 (2017), p. 2017.
- [54] *Rigid connectors*. URL: <https://help.febio.org/docs/FEBioUser-3-7/UM37-Subsection-3.11.2.html>.
- [55] Gustavo A Orozco et al. "The effect of constitutive representations and structural constituents of ligaments on knee joint mechanics". In: *Scientific reports* 8.1 (2018), pp. 1–15.
- [56] A. Esrafilian et al. "EMG-Assisted Muscle Force Driven Finite Element Model of the Knee Joint with Fibril-Reinforced Poroelastic Cartilages and Menisci". In: *Scientific Reports* 10 (1 Dec. 2020). ISSN: 20452322. DOI: 10.1038/s41598-020-59602-2.
- [57] T J A Momersteeg et al. *THE EFFECT OF VARIABLE RELATIVE INSERTION ORIENTATION OF HUMAN KNEE BONE-LIGAMENT-BONE COMPLEXES ON THE TENSILE STIFFNESS*. 1995, pp. 745–752.

- [58] K. S. Halonen et al. "Importance of patella, quadriceps forces, and depthwise cartilage structure on knee joint motion and cartilage response during gait". In: *Journal of Biomechanical Engineering* 138 (7 July 2016). ISSN: 15288951. DOI: 10.1115/1.4033516.
- [59] Nathan Lampen et al. "Finite element modeling with subject-specific mechanical properties to assess knee osteoarthritis initiation and progression". In: *Journal of Orthopaedic Research* (2022). ISSN: 1554527X. DOI: 10.1002/jor.25338.
- [60] Hongqiang Guo et al. "A statistically-augmented computational platform for evaluating meniscal function". In: *Journal of biomechanics* 48.8 (2015), pp. 1444–1453.
- [61] Hongqiang Guo et al. "Reducing uncertainty when using knee-specific finite element models by assessing the effect of input parameters". In: *Journal of Orthopaedic Research* 35.10 (2017), pp. 2233–2242.
- [62] I MARTIN Levy, PA Torzilli, and RF Warren. "The effect of medial meniscectomy on anterior-posterior motion of the knee." In: *JBSJ* 64.6 (1982), pp. 883–888.
- [63] FH Fu and WO Thompson. "Motion of the meniscus during knee flexion". In: *Knee meniscus: basic and clinical foundations*. Raven Press, New York, 1992, pp. 75–89.
- [64] Iliana Loi, Dimitar Stanev, and Konstantinos Moustakas. "Total Knee Replacement: Subject-Specific Modeling, Finite Element Analysis, and Evaluation of Dynamic Activities". In: *Frontiers in Bioengineering and Biotechnology* 9 (Apr. 2021). ISSN: 22964185. DOI: 10.3389/fbioe.2021.648356.
- [65] KM Moerman. *GIBBON: the geometry and image-based bioengineering add-on*. *J. Open Source Software* 3 (22), 506. 2018.
- [66] Jon C Helton and Freddie Joe Davis. "Latin hypercube sampling and the propagation of uncertainty in analyses of complex systems". In: *Reliability Engineering & System Safety* 81.1 (2003), pp. 23–69.
- [67] Ugo Della Croce, Aurelio Cappozzo, and D Casey Kerrigan. "Pelvis and lower limb anatomical landmark calibration precision and its propagation to bone geometry and joint angles". In: *Medical & biological engineering & computing* 37.2 (1999), pp. 155–161.
- [68] A Cappozzo et al. "Position and orientation in space of bones during movement: experimental artefacts". In: *Clinical Biomechanics* 11 (2 1996), pp. 99–100.
- [69] GE Kempson. "Relationship between the tensile properties of articular cartilage from the human knee and age." In: *Annals of the rheumatic diseases* 41.5 (1982), pp. 508–511.
- [70] Olesya Klets et al. "Comparison of different material models of articular cartilage in 3D computational modeling of the knee: Data from the Osteoarthritis Initiative (OAI)". In: *Journal of biomechanics* 49.16 (2016), pp. 3891–3900.
- [71] ED Bonnevie et al. "Chondrocyte death and mitochondrial dysfunction are mediated by cartilage friction and shear strain". In: *Osteoarthritis and cartilage* 24 (2016), S46.
- [72] Shingo Hashimoto et al. "Role of p53 in human chondrocyte apoptosis in response to shear strain". In: *Arthritis & Rheumatism: Official Journal of the American College of Rheumatology* 60.8 (2009), pp. 2340–2349.
- [73] Baddr Shakhsheer et al. "SugarBind database (SugarBindDB): a resource of pathogen lectins and corresponding glycan targets". In: *Journal of Molecular Recognition* 26.9 (2013), pp. 426–431.
- [74] Joseph A Buckwalter et al. "The roles of mechanical stresses in the pathogenesis of osteoarthritis: implications for treatment of joint injuries". In: *Cartilage* 4.4 (2013), pp. 286–294.
- [75] Jacob Benesty et al. "Pearson correlation coefficient". In: *Noise reduction in speech processing*. Springer, 2009, pp. 1–4.
- [76] Ciarán McFadden, Katherine Daniels, and Siobhán Strike. "The sensitivity of joint kinematics and kinetics to marker placement during a change of direction task". In: *Journal of Biomechanics* 101 (Mar. 2020). ISSN: 18732380. DOI: 10.1016/j.jbiomech.2020.109635.
- [77] Richard Baker, Laura Finney, and John Orr. *A new approach to determine the hip rotation profile from clinical gait analysis data*. 1999, pp. 655–667. URL: www.elsevier.com/locate/humov.

- [78] Scott D. Uhlrich et al. "Muscle coordination retraining inspired by musculoskeletal simulations reduces knee contact force". In: *Scientific Reports* 12 (1 Dec. 2022), p. 9842. ISSN: 2045-2322. DOI: 10.1038/s41598-022-13386-9. URL: <https://www.nature.com/articles/s41598-022-13386-9>.
- [79] Steven D. Waldman. "Chapter 15 - Martin Nash: A 21-Year-Old Sprinter With Medial Calf Pain and Bruising". In: *The Knee*. Ed. by Steven D. Waldman. St. Louis (MO): Elsevier, 2022, pp. 204–216. ISBN: 978-0-323-76258-8. DOI: <https://doi.org/10.1016/B978-0-323-76258-8.00015-X>. URL: <https://www.sciencedirect.com/science/article/pii/B978032376258800015X>.
- [80] Hans A Gray et al. "Three-dimensional motion of the knee-joint complex during normal walking revealed by mobile biplane x-ray imaging". In: *Journal of Orthopaedic Research* 37.3 (2019), pp. 615–630.
- [81] "12 Degrees of Freedom Muscle Force Driven Fibril-Reinforced Poroviscoelastic Finite Element Model of the Knee Joint". In: *IEEE Transactions on Neural Systems and Rehabilitation Engineering* 29 (2021), pp. 123–133. ISSN: 15580210. DOI: 10.1109/TNSRE.2020.3037411.
- [82] "New fluoroscopic imaging technique for investigation of 6DOF knee kinematics during treadmill gait". In: *Journal of Orthopaedic Surgery and Research* 4 (1 2009). ISSN: 1749799X. DOI: 10.1186/1749-799X-4-6.
- [83] Per Wretenberg, Dan K Ramsey, and Gunnar Németh. "Tibiofemoral contact points relative to flexion angle measured with MRI". In: *Clinical Biomechanics* 17.6 (2002), pp. 477–485.
- [84] Ruediger von Eisenhart-Rothe et al. "Tibiofemoral and patellofemoral joint 3D-kinematics in patients with posterior cruciate ligament deficiency compared to healthy volunteers". In: *BMC musculoskeletal disorders* 13.1 (2012), pp. 1–8.
- [85] "Tibiofemoral kinematics and condylar motion during the stance phase of gait". In: *Journal of Biomechanics* 42 (12 Aug. 2009), pp. 1877–1884. ISSN: 00219290. DOI: 10.1016/j.jbiomech.2009.05.003.
- [86] Ahmet Erdemir and Scott Sibole. "Open knee: a three-dimensional finite element representation of the knee joint". In: *User's guide, version 1.0* (2010).
- [87] Corinne R. Henak et al. "Specimen-specific predictions of contact stress under physiological loading in the human hip: Validation and sensitivity studies". In: *Biomechanics and Modeling in Mechanobiology* 13 (2 2014), pp. 387–400. ISSN: 16177940. DOI: 10.1007/s10237-013-0504-1.
- [88] Sepehr Ramezani, Joseph M Dranetz, and Matt S Stock. *Validation of Musculoskeletal Models Using Single Degree of Freedom Analysis Skeletal Muscle Plasticity View project Human Musculoskeletal Modeling View project*. URL: <https://www.researchgate.net/publication/346512467>.
- [89] Adam D Sylvester, Steven G Lautzenheiser, and Patricia Ann Kramer. "A review of musculoskeletal modelling of human locomotion". In: *Interface Focus* 11.5 (2021), p. 20200060.
- [90] *OpenSim JAM*. URL: <https://simtk.org/plugins/publications/index.php?type=group&id=1871&pluginname=publications>.
- [91] Robert J Cooper, Ruth K Wilcox, and Alison C Jones. "Finite element models of the tibiofemoral joint: A review of validation approaches and modelling challenges". In: *Medical engineering & physics* 74 (2019), pp. 1–12.
- [92] L Blankevoort et al. *ARTICULAR CONTACT IN A THREE-DIMENSIONAL MODEL OF THE KNEE*. 1991, pp. 1019–1031.
- [93] Jiang Yao et al. "Sensitivities of medial meniscal motion and deformation to material properties of articular cartilage, meniscus and meniscal attachments using design of experiments methods". In: *Journal of Biomechanical Engineering* 128 (3 June 2006), pp. 399–408. ISSN: 01480731. DOI: 10.1115/1.2191077.
- [94] KMDI Manal et al. "The accuracy of estimating proximal tibial translation during natural cadence walking: bone vs. skin mounted targets". In: *Clinical Biomechanics* 18.2 (2003), pp. 126–131.

-
- [95] William R Taylor et al. "On the influence of soft tissue coverage in the determination of bone kinematics using skin markers". In: *Journal of Orthopaedic Research* 23.4 (2005), pp. 726–734.
- [96] *How inverse kinematics works*. URL: <https://simtk-confluence.stanford.edu:8443/display/OpenSim/How+Inverse+Kinematics+Works>.
- [97] *How static optimization works*. URL: <https://simtk-confluence.stanford.edu:8443/display/OpenSim/How+Static+Optimization+Works>.
- [98] Jan Hendrik Naendrup et al. "Influence of knee position and examiner-induced motion on the kinematics of the pivot shift". In: *Journal of Experimental Orthopaedics* 6 (1 Dec. 2019). ISSN: 21971153. DOI: 10.1186/s40634-019-0183-7.



BMM Lab Protocol

Table A.1: BMM laboratory marker placement on anatomical landmarks of both legs

Segment	Abbreviation	Anatomical landmark
Foot	Ankle AnkleMed MT1 MT5 Heel	Ankle Medial ankle Metatarsal 1 Metatarsal 5 Heel
Tibia	SH1 SH2 SH3	Tibial cluster 1 Tibial cluster 2 Tibial cluster 3
Knee	Knee KneeFib KneeMed	Knee Fibular side of the Knee Medial side of the Knee
Femur	TH1 TH2 TH3	Femoral cluster 1 Femoral cluster 2 Femoral cluster 3
Pelvis	ASIS PSIS ICR	Anterior superior iliac Spine (left and right side) Posterior superior iliac Spine (left and right side) Iliac crest (left and right side)
Torso	CLAV STRN Shoulder T1 L5	Clavicle (proximal on sternum, mid between clavicle) Sternum (distal) Shoulder (left and right side) T1 vertebrae L5 Vertebrae

Table A.2: .

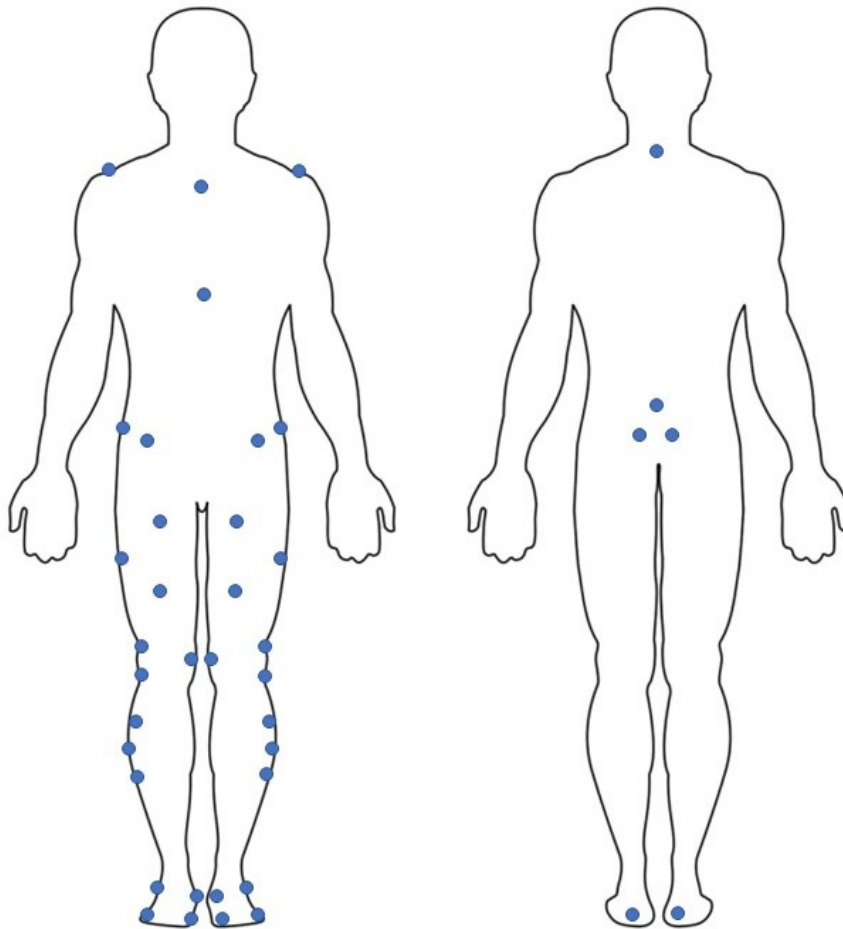


Figure A.1: BMM Lab Marker placement A total of 40 markers were placed on the body to capture the gait kinematics of the subject. Markers were placed on the anatomical landmarks of both sides of the foot (ankle, medial ankle, metatarsal 1, metatarsal 5 and the heel), the tibia (tibial cluster 1, 2 and 3), the knee (knee, fibular side of the knee and medial side of the knee), the femur (femoral cluster 1, 2 and 3), the pelvis (anterior superior iliac spine, posterior superior iliac spine and iliac crest) and the torso (clavicle, sternum, shoulders, T1 and T5).

B

OpenSim Tools

Table B.1: Scale Tool: Scale Factors

Body Name	Measurement(s) Used			Applied Scale Factor(s)		
femur_r	Pelvis X	PelvisX	FemurL	0.984084	0.984084	1.034059
tibia_r	FemurR					1.030686
talus_r	TibiaR					1.063045
calc_n_r	Calc_nRX					0.994451
toes_r	Calc_nRX	Calc_nRX	Calc_nRZ	0.994451	0.994451	0.927405
femur_l	FemurL					1.034059
tibia_l	TibiaL					1.0585051
talus_l	TalusL					0.972097
calc_n_l	Calc_nLX					0.993386
toes_l	Calc_nLX	Calc_nLX	Calc_nLZ	0.993386	0.993386	0.972097
torso	TorsoX	TorsoY	FemurL	0.937578	0.958776	1.034059

Table B.2: Scale Tool: Measurement Set

Measurements	Marker Pairs													
PelvisX	L.ASIS	R.PSIS	R.ASIS	L.PSIS										
FemurL	L.ASIS	L.Knee	L.PSIS	L.KneeMed	L.ASIS	L.KneeMed								
FemurR	R.ASIS	R.Knee	R.PSIS	R.KneeMed	R.ASIS	R.KneeMed								
TibiaR	R.Knee	R.Ankle	R.KneeMed	R.AnkleMed	R.AnkleMed	R.ASIS	R.Ankle	R.PSIS						
TalusR	R.Ankle	R.AnkleMed												
Calc_nRX	R.Heel	R.MT1	R.Heel	R.MT5										
Calc_nRZ	R.AnkleMed	R.Ankle												
TibiaL	L.Knee	L.Ankle	L.KneeMed	L.AnkleMed	L.AnkleMed	L.ASIS	L.Ankle	L.PSIS						
TalusL	R.Ankle	R.AnkleMed												
Calc_nLX	L.Heel	L.MT1	L.Heel	L.MT5										
Calc_nLZ	L.AnkleMed	L.Ankle												
TorsoX	R.Shoulder	R.ASIS	L.Shoulder	L.ASIS	CLAV	T1	L.Shoulder	CLAV	R.Shoulder	CLAV	L.Shoulder	T1	R.Shoulder	T1
TorsoY	L.Shoulder	R.ASIS	R.Shoulder	L.ASIS										

Table B.3: Scale Tool: Static Pose Weights

Marker Name	Weight	Marker Name	Weight	Marker Name	Weight
R.Shoulder	20	R.AnkleMed	2	L.AnkleMed	2
L.Shoulder	20	R.MT1	7.5	L.MT1	7.5
R.ASIS	25	R.MT5	1	L.Heel	1
L.ASIS	25	L.SH1	0.1	L.MT5	1
R.PSIS	5	L.TH2	0.1	CLAV	1
L.PSIS	10	R.Heel	1	L.TH3	0.1
R.Knee	10	L.Knee	20	R.TH3	0.1
R.KneeMed	10	L.KneeMed	10	R.TH2	0.1
R.SH3	0.1	L.Ankle	3	R.TH1	0.1
R.Ankle	3	R.KneeFib	10	L.KneeFib	10
		T1	2	L.TH1	0.1

Table B.4: Inverse Kinematics Tool: Weights

Marker Name	Weight	Marker Name	Weight	Marker Name	Weight
R.Shoulder	3	R.AnkleMed	1	L.AnkleMed	5
L.Shoulder	3	R.MT1	1	L.MT1	5
R.ASIS	10	R.MT5	1	L.Heel	1
L.ASIS	10	L.SH1	0.1	L.MT5	5
R.PSIS	5	L.TH2	0.1	CLAV	0.1
L.PSIS	5	R.Heel	1	L.TH3	0.1
R.Knee	5	L.Knee	5	R.TH3	0.1
R.KneeMed	5	L.KneeMed	5	R.TH2	0.1
R.SH3	0.1	L.Ankle	5	R.TH1	0.1
R.Ankle	1	R.KneeFib	5	L.KneeFib	5
		T1	0	L.TH1	0.1

$$\min_{\mathbf{q}} \left[\sum_{i \in \text{markers}} w_i \left\| \mathbf{x}_i^{\text{exp}} - \mathbf{x}_i(\mathbf{q}) \right\|^2 + \sum_{j \in \text{unprescribed coords}} \omega_j (q_j^{\text{exp}} - q_j)^2 \right]$$

$$q_j = q_j^{\text{exp}} \text{ for all prescribed coordinates } j$$

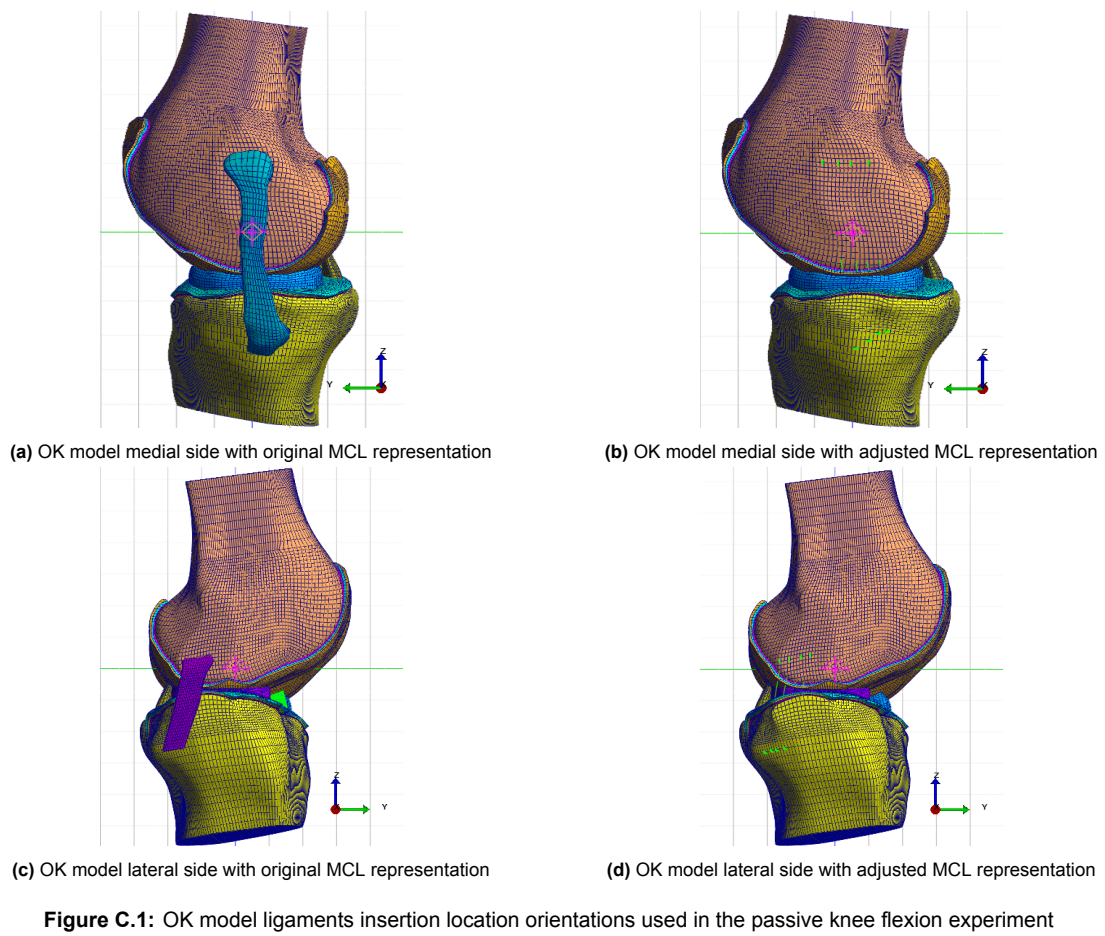
Figure B.1: The weighted least squares problem solved by the IK tool: \mathbf{q} is the vector for joint angles which are solved. $\mathbf{x}_i^{\text{exp}}$ is the experimental position of marker i . $\mathbf{x}_i(\mathbf{q})$ is the position of the corresponding model marker, which is dependent on the joint angle. q_j^{exp} represents the experimental value for coordinate j . marker weights (w_i) and coordinate weight ω_j are specified in the static pose weight file (see table B.3). The above described problem is solved using a general quadratic programming solver. It has a convergence criterion of 0.0001 and a limit of 1000 iterations [96].

$$J = \sum_{m=1}^n (a_m)^p \quad (\text{B.1})$$

Figure B.2: Objective function static optimization: n is equal to the number of muscles in the model. a_m is the activation level of muscle m at a discrete time step. p is a user defined constant which has been set to 2 [97].

C

Ligament insertion location



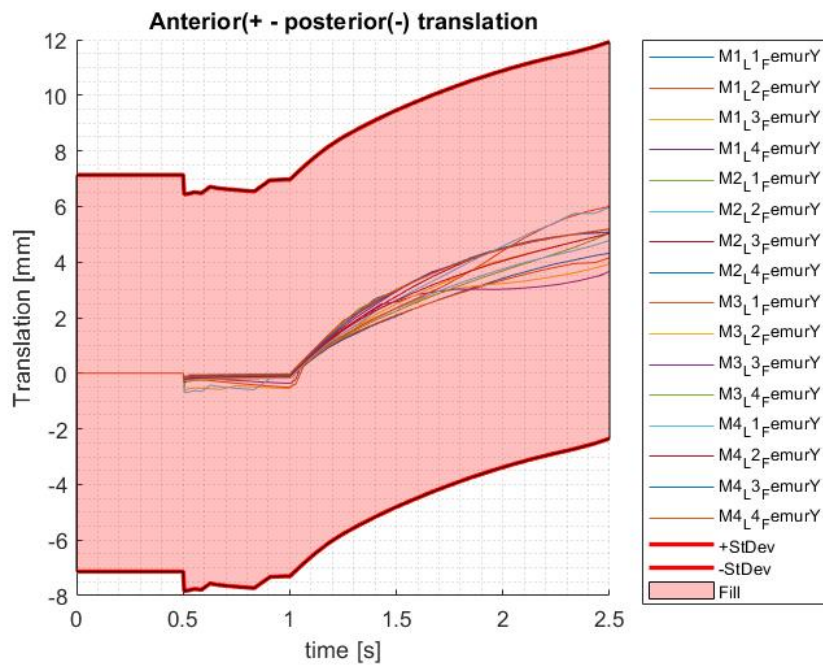


Figure C.2: Anterior-posterior translation of knee joint for different ligament orientation locations. Including visualisation of 4x standard deviation of picked ligament representation (M2L2).

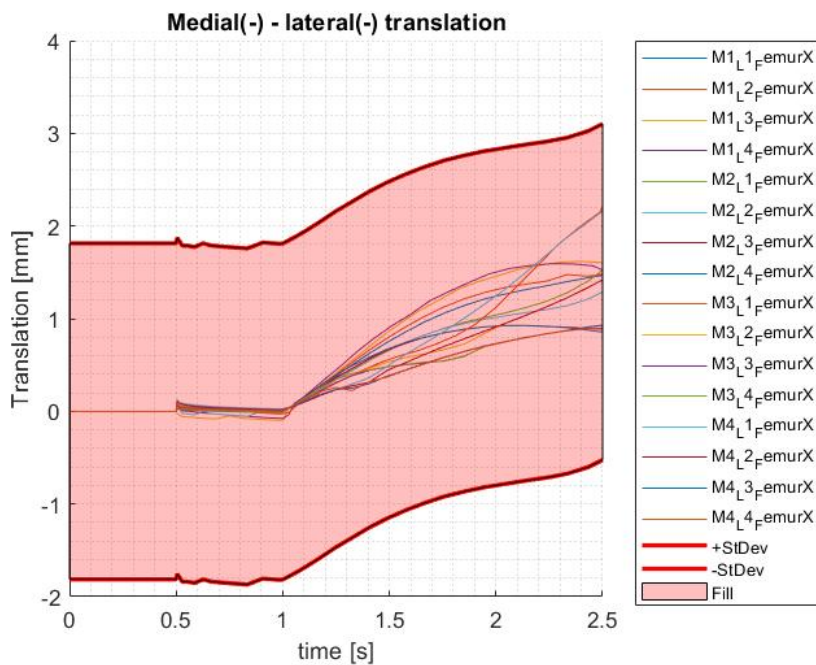


Figure C.3: Medial-lateral translation of knee joint for different ligament orientation locations. Including visualisation of 4x standard deviation of picked ligament representation (M2L2).

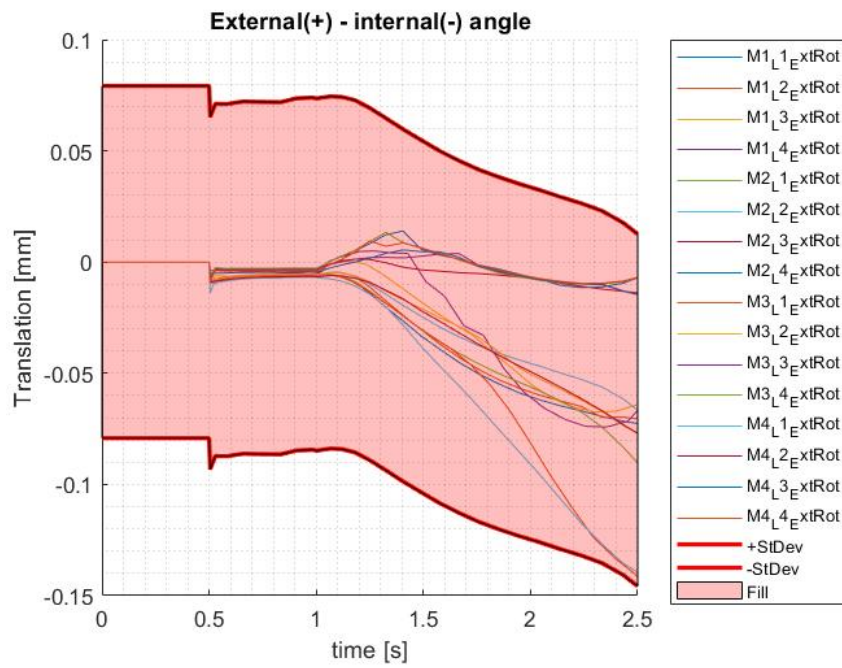


Figure C.4: External-internal rotation of knee joint for different ligament orientation locations. Including visualisation of 4x standard deviation of picked ligament representation (M2L2).

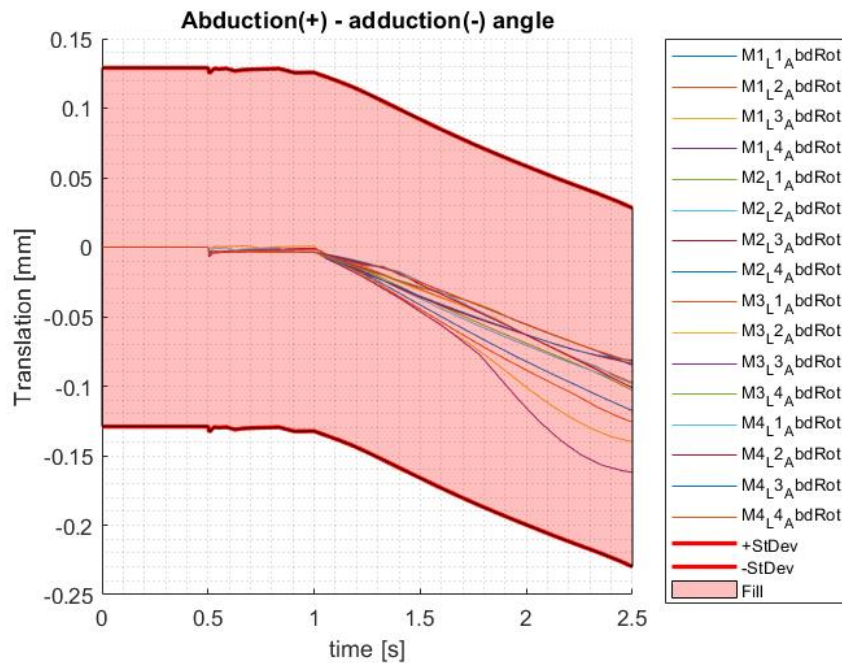


Figure C.5: Abduction-adduction rotation of knee joint for different ligament orientation locations. Including visualisation of 4x standard deviation of picked ligament representation (M2L2).

D

FEM supplementary material

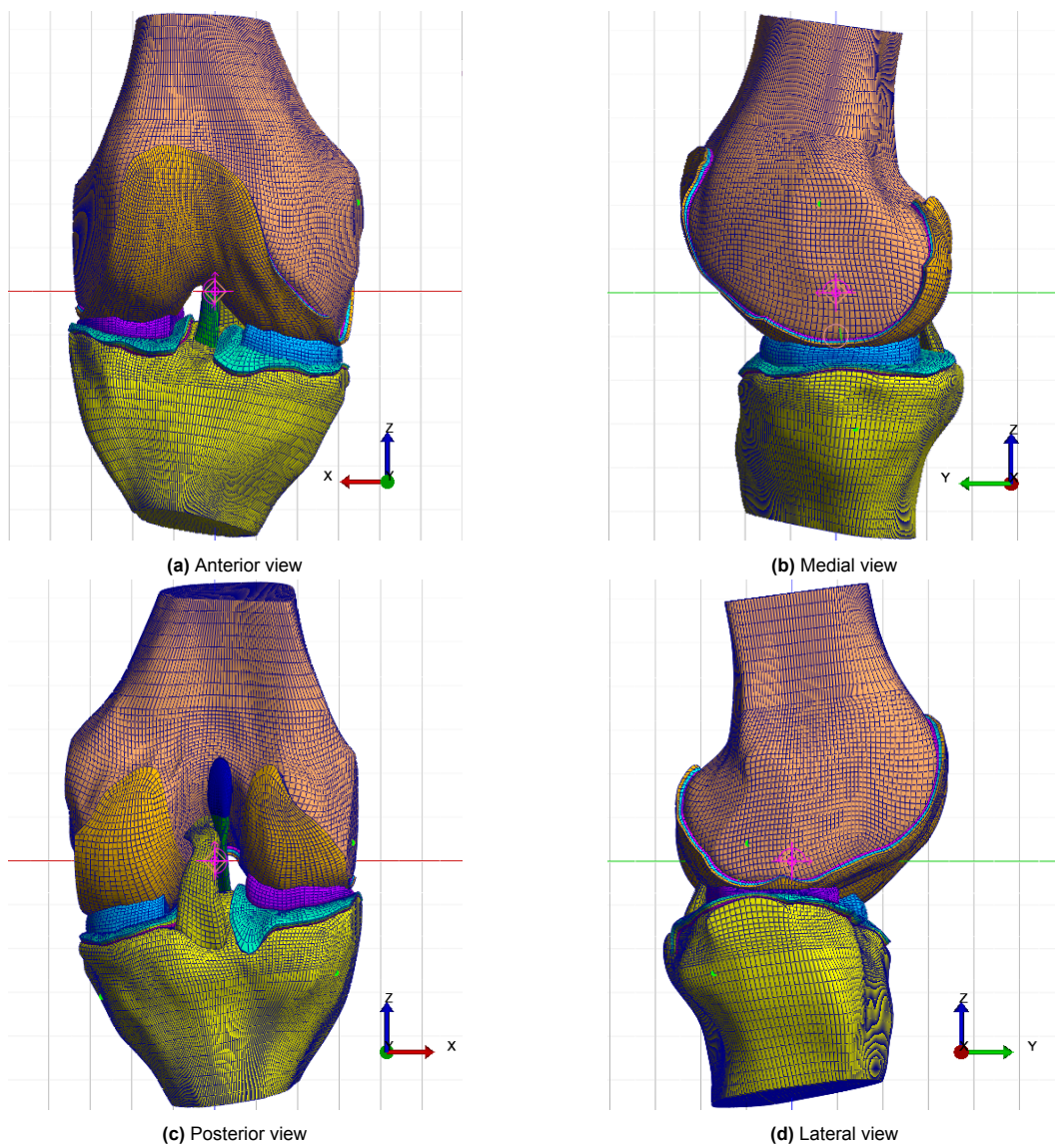


Figure D.1: Altered OK model

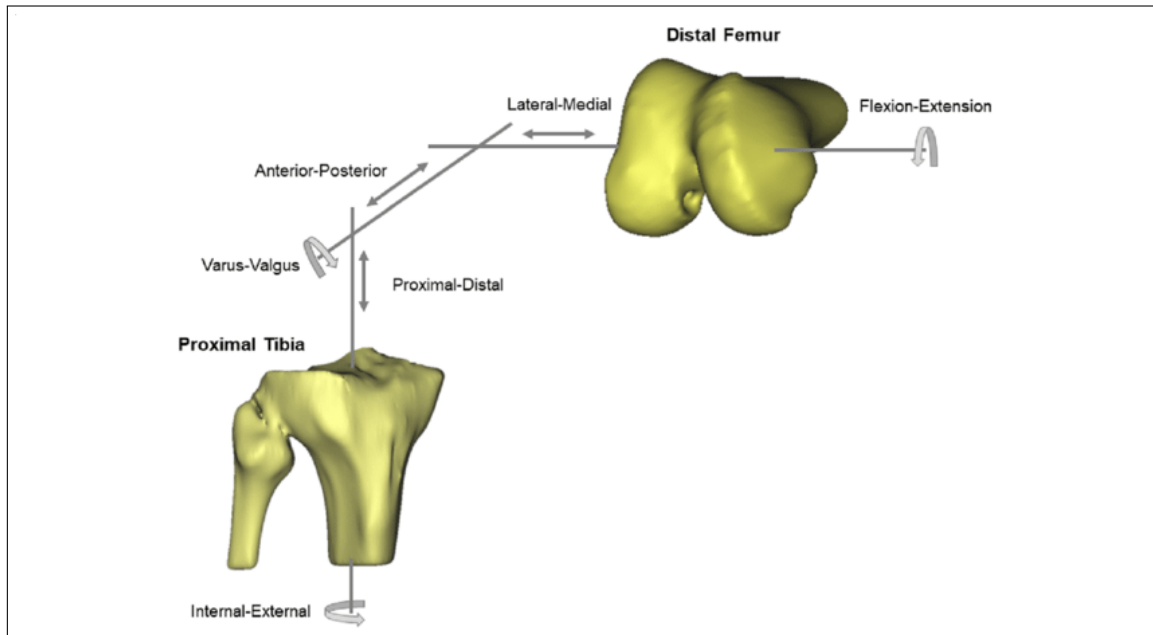


Figure D.2: Grood and Suntay joint coordinate system: coordinate system as used in the OK model. Lateral-medial translation and flexion-extension occurs along the femoral fixed axis, positioned through both femoral epicondyles and as a result perpendicular to the sagittal plane, In FEBio the movement across these DoFs is made possible through the use of Rigid connectors. The rigid cylindrical joint (Femur-ImgLnk1) joint responsible for flexion-extension and lateral-medial translation is positioned along the x-axis. Proximal-distal translation and internal-external rotation occurs along the axis fixed to the tibial shaft, In FEBio movement along this corresponds to the z-axis and is enabled through the movement along the ImgLnk2-Tibia rigid cylindrical joint. Anterior-posterior translation and valgus-varus rotation occurs along the floating axis, this axis defined by the cross product of the femoral and tibial axis and as a result is perpendicular to both body fixed axes. In FEBio this movement is enabled through the ImgLnk1-ImgLnk2 rigid connector which corresponds to movement along the y-axis. The joint origins of all rigid cylindrical joints corresponds to the centers of both the rigid femur and tibia at 0,0,0. [98, 53]

Table D.1: Overview of time settings FEBio simulation

Step	1	4
Analysis type	static	static
Time steps	10	254
Step size	0.05	0.005
Max step size	0.05	0.01
Min step size	0.001	0.0001
Auto time stepper	X	X
Max retries	10	200
Optimal iterations	8	50
Cutback	default	default

Table D.2: Overview of Nonlinear solver FEBio simulation

Step	1	4
Displacement tolerance	0.01	0.01
Energy tolerance	0.1	0.1
Residual tolerance	0	0
Line search tolerance	0.9	0.9
Minimum residual	1e-20	1e-20
Quasi-Newton Method	BFGS	BFGS
Spectral radius	-2	-2
Max reformations	10	100
Max updates	0	0
Reform on diverge	X	X
Reform each timestep	X	X

E

Workflow supplementary material

Latin hypercube sampling of marker placement

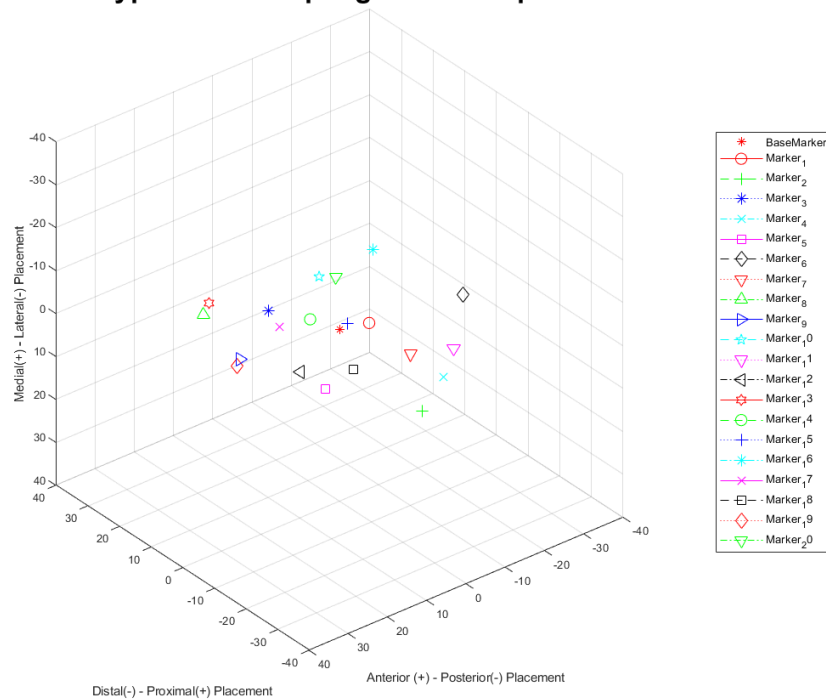
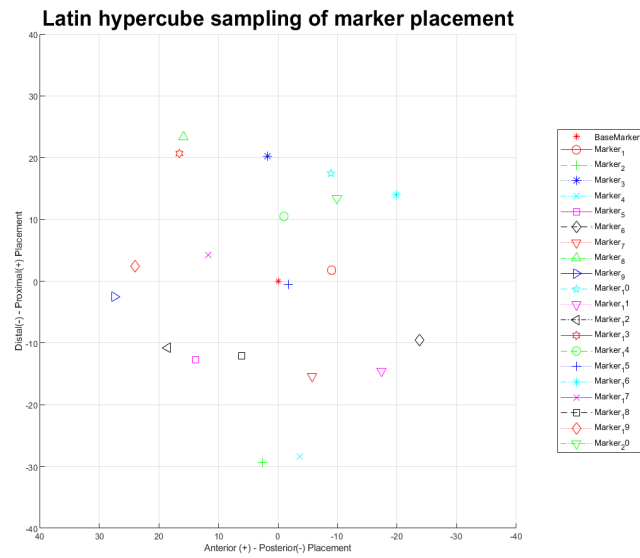
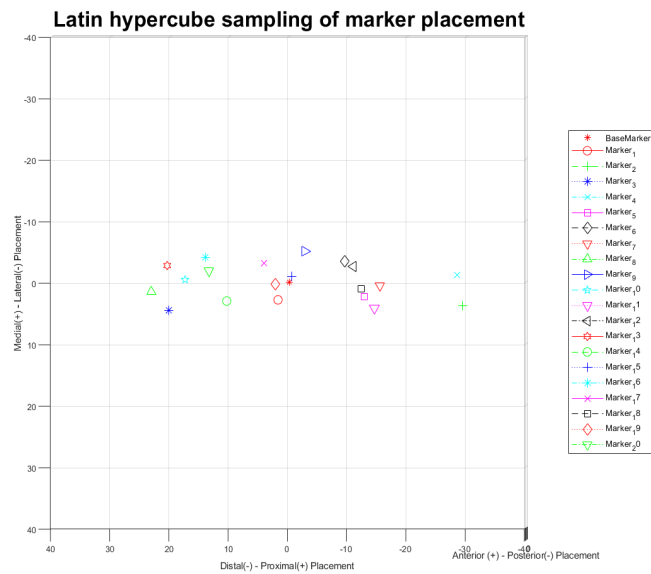


Figure E.1: Overview of knee marker displacements used as input in the workflow. For this specific analysis 20 marker displacements were utilized per knee marker (L.Knee, L.KneeMed, L.KneeFib).

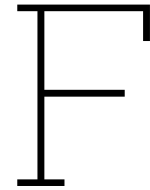


(a) Latin hypercube sampling distribution of marker locations along the distal-proximal, anterior-posterior plane.



(b) Latin hypercube sampling distribution of marker locations along the medial-lateral, distal-proximal plane.

Figure E.2: Latin hypercube sampling distribution of marker locations



Results supplementary material

Correlation: Mean location high stress region	Anterior-Posterior					
Marker placement direction	L.Knee		L.KneeMed		L.KneeFib	
Medial tibial cartilage	<i>r</i>	<i>p</i>	<i>r</i>	<i>p</i>	<i>r</i>	<i>p</i>
Ant-post	0.923	0.000	0.914	0.000	0.598	0.040
Prox-dist	0.249	0.391	0.072	0.776	-0.070	0.829
Med-lat	-0.573	0.032	-0.295	0.818	-0.076	0.815
Lateral tibial cartilage						
Ant-post	0.957	0.000	0.947	0.000	0.732	0.004
Prox-dist	0.473	0.075	0.178	0.467	0.665	0.004
Med-lat	-0.650	0.009	-0.296	0.218	-0.012	0.968
Proximal-distal						
Medial tibial cartilage	<i>r</i>	<i>p</i>	<i>r</i>	<i>p</i>	<i>r</i>	<i>p</i>
Ant-post	0.726	0.002	0.058	0.818	0.264	0.408
Prox-dist	0.255	0.378	-0.190	0.451	0.521	0.083
Med-lat	-0.407	0.149	-0.355	0.148	0.278	0.382
Lateral tibial cartilage						
Ant-post	-0.801	0.000	-0.186	0.446	-0.416	0.158
Prox-dist	0.440	0.884	-0.142	0.561	-0.680	0.011
Med-lat	-0.041	0.100	0.123	0.615	0.014	0.963
Lateral-medial						
Medial tibial cartilage	<i>r</i>	<i>p</i>	<i>r</i>	<i>p</i>	<i>r</i>	<i>p</i>
Ant-post	-0.821	0.000	-0.648	0.004	-0.570	0.053
Prox-dist	-0.456	0.101	-0.167	0.509	-0.322	0.307
Med-lat	0.492	0.074	-0.076	0.763	-0.252	0.429
Lateral tibial cartilage						
Ant-post	-0.912	0.000	-0.827	0.000	-0.734	0.004
Prox-dist	-0.317	0.249	-0.290	0.228	-0.669	0.012
Med-lat	0.513	0.051	0.299	0.213	0.054	0.861

Table F.1: Correlation coefficients (*r*) and corresponding p-values for relationship between marker placement direction and mean location of high stress values which maximum principal stress values exceeding the stress threshold (5 MPa).

Correlation: Mean location high strain region Marker placement direction	Anterior-Posterior					
	L.Knee		L.KneeMed		L.KneeFib	
Medial tibial cartilage	<i>r</i>	<i>p</i>	<i>r</i>	<i>p</i>	<i>r</i>	<i>p</i>
Ant-post	0.905	0.000	0.889	0.000	0.735	0.004
Prox-dist	-0.580	0.044	0.166	0.497	0.330	0.270
Med-lat	0.526	0.023	-0.247	0.308	-0.225	0.460
Lateral tibial cartilage						
Ant-post	0	-	0	-	0	-
Prox-dist	0	-	0	-	0	-
Med-lat	0	-	0	-	0	-
Proximal-distal						
Medial tibial cartilage	<i>r</i>	<i>p</i>	<i>r</i>	<i>p</i>	<i>r</i>	<i>p</i>
Ant-post	-0.546	0.035	0.166	0.006	-0.574	0.040
Prox-dist	-0.337	0.219	-0.336	0.910	-0.111	0.165
Med-lat	0.621	0.013	0.607	0.159	-0.409	0.718
Lateral tibial cartilage						
Ant-post	0	-	0	-	0	-
Prox-dist	0	-	0	-	0	-
Med-lat	0	-	0	-	0	-
Lateral-medial						
Medial tibial cartilage	<i>r</i>	<i>p</i>	<i>r</i>	<i>p</i>	<i>r</i>	<i>p</i>
Ant-post	-0.633	0.011	0.465	0.045	-0.598	0.031
Prox-dist	-0.340	0.215	-0.058	0.815	-0.395	0.182
Med-lat	0.632	0.012	-0.338	0.157	-0.125	0.684
Lateral tibial cartilage						
Ant-post	0	-	0	-	0	-
Prox-dist	0	-	0	-	0	-
Med-lat	0	-	0	-	0	-

Table F.2: Correlation coefficients (*r*) and corresponding p-values for relationship between marker placement direction and mean location of high strain values which maximum principal stress values exceeding the shear strain threshold (0.32%).